Bureau of Safety and Environmental Enforcement
Oil Spill Preparedness Division

Dielectric Fluids Remote Sensing Test
Final Report

February 12, 2026

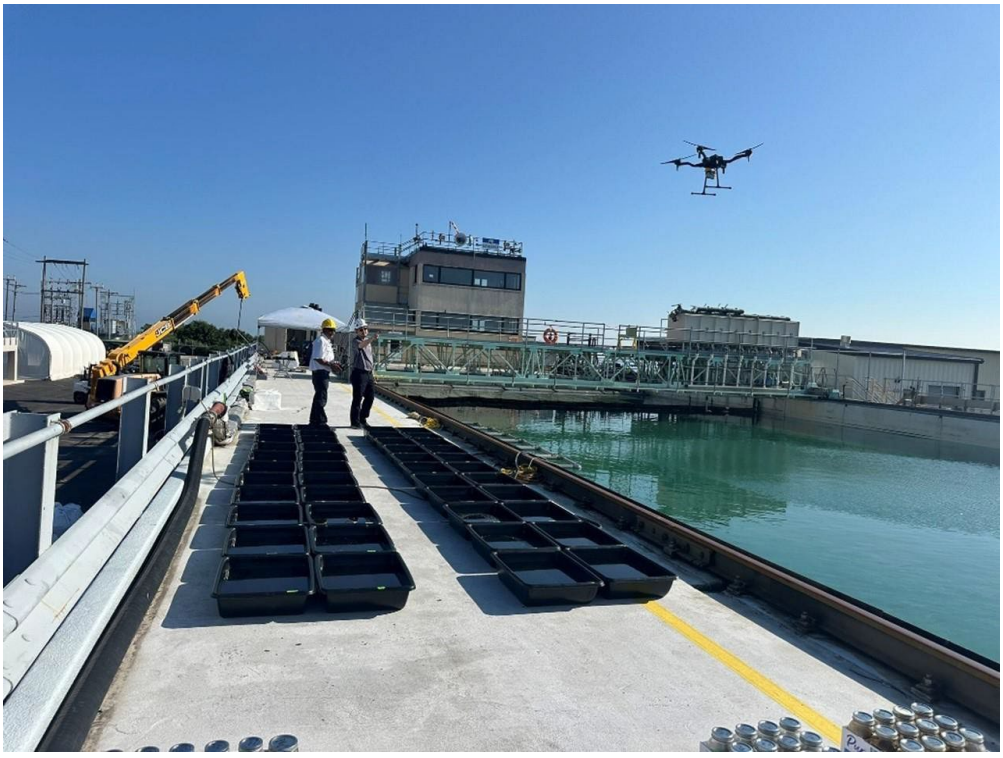

Dielectric Fluids Remote Sensing Testing at Ohmsett on August 2025
(Photo: Water Mapping, LLC, 2025)

Garcia-Pineda, Oscar., Garcia, Diana., and Haces, Francisco.

US Department of the Interior
Bureau of Safety and Environmental Enforcement
Oil Spill Preparedness Division

BSEE OSPD PUBLIC POSTING APPROVAL SHEET

1. **Report Date: (DD-MM-YYYY)**
   26-02-2026

2. **REPORT TYPE: (Interim for peer review, Final, etc.)**
   Final report

3. **START DATE: (DD-MM-YYYY)**
   15/05/2024

4. **END DATE: (DD-MM-YYYY)**
   31-01-2026

5. **TITLE:**
   Dielectric Fluids Remote Sensing Test

6. **CONTRACT/IAA NUMBER:**
   140E0124P0011

7. **OIL SPILL RESPONSE RESEARCH PROJECT NUMBER:**
   1163

8. **PERFORMING ORGANIZATION NAME(S) AND ADDRESS(ES):**

   Water Mapping, LLC.

9. **AUTHOR(S):**
   Oscar Garcia-Pineda ; Diana Garcia; Francisco Haces.

10. **DISTRIBTION/AVAILABILITY STATEMENT (INDICATE PUBLIC AVAILABILIY OR DISTRIBTION LIMIATIONS OF THE REPORT:**

    PUBLIC AVAILABILIY

11. **SUPPLEMENTARY NOTES:**

12. **ABSTRACT:**

The objectives of the project consisted of testing the sensors under a variable set of viewing angles and ambient conditions (illumination and air temperature) to determine operationalization of these sensors for a possible emergency response in case of a spill of DFs into the environment. To meet these objectives, the work was executed as a three-staged test program that moved from controlled target trials to full-scale tank deployments. Initial laboratory testing (first stage) and field-style setups (second-stage) were used to establish sensor behavior over known DF thicknesses, verify calibration and processing routines (including band alignment and thermal temperature conversion), and identify the combinations of viewing geometry and ambient conditions most favorable for detection. These findings were then carried forward into the third-stage Ohmsett campaigns designed to stress-test detection and thickness characterization under realistic outdoor variability (sun angle, irradiance, temperature change through day/night). One of the main challenges of the project was the intrinsic transparency of all DFs, therefore, the Ohmsett tests specifically laid out multiple targets of DF samples of known types and thicknesses.

The results of this project showed that due to the physical and chemical properties of DFs, thermal and multispectral sensors can be used to detect DFs floating over water, however optical/visual sensors where not suitable to neither detect nor characterize DFs. While the near-infrared sensor had a remarkable capacity to detect presence/absence of DFs, the thermal sensors demonstrated their capability to characterize qualitatively and quantitatively their thickness under a range of ambient conditions. The positive results from the Ohmsett experiment shed light towards operationalization of remote sensing mounted on aerial sensors for emergency response operations. The reflectance of

DFs in the near-infrared wavelength shows a contrast of 0.08 reflectance units higher than the clean water under daylight. Due to the physical and chemical properties of DFs to store heat, detection of thicker layers of DFs could be observed even at dark after few hours after sunset using the infrared (thermal) sensor. The significant technical achievement of this work is the development of a sophisticated image processing algorithm. This operationalization tool is distinguished by its ability to process and classify DF thicknesses in near real time, marking a paradigm shift in data processing capacity and establishing a new benchmark for analytical speed critical to inform spill response decision makers.	
13. KEY WORDS/PHRASES: **Dielectric Fluids (DF), Remote Sensing, Ohmsett, Uncrewed Aerial Vehicles (UAVs)**	
14. CONTRACTING OFFICER REPRESENTATIVE: **Jay Cho**	**15. PHONE NUMBER/EMAIL ADDRESS:** **703-787-1525** **Jay.Cho@bsee.gov**
16. APPROVER: (Branch Manager) **Karen Stone**	**17. PHONE NUMBER/EMAIL ADDRESS:** **703-787-1810** **Karen.Stone@bsee.gov**

Dielectric Fluids Remote Sensing Test

Technical Report

Final Report

OSRR #1163

February 12, 2026

Authors:
Oscar Garcia-Pineda, PhD; Diana Garcia; Francisco Haces.
Water Mapping, LLC

Prepared under Award # 140E0124P0011
By: Water Mapping, LLC
1047 Aquamarine Dr., Gulf Breeze, FL 32563

US Department of the Interior
Bureau of Safety and Environmental Enforcement
Oil Spill Preparedness Division

DISCLAIMER

Study concept, oversight, and funding were provided by the US Department of the Interior (DOI), Bureau of Safety and Environmental Enforcement (BSEE), Oil Spill Preparedness Division (OSPD), Sterling, VA, under Contract Number 140E0124P0011. This report has been technically reviewed by BSEE, and it has been approved for publication.

The views and conclusions contained in this document are those of the authors and should not be interpreted as representing the opinions or policies of the US Government, nor does mention of trade names or commercial products constitute endorsement or recommendation for use.

REPORT AVAILABILITY

The PDF file for this report is available through the following sources. Click on the URL and enter the appropriate search term to locate the PDF:

Document Source	Search Term	URL
Bureau of Safety and Environmental Enforcement (BSEE)	Project Number – 1139	https://www.bsee.gov/remote-sensing-test-for-dielectric-fluids
U.S. Department of the Interior Library	Dielectric Fluids Remote Sensing Testing	https://library.doi.gov/uhtbin/cgisirsi/?ps=8L0mpW5uPV/SIRSI/X/60/495/X
National Technical Reports Library	Dielectric Fluids Remote Sensing Testing	https://ntrl.ntis.gov/NTRL/

Sources: a) BSEE (2019), b) DOI [2021], c) National Technical Information Service (2021)

CITATION

Garcia-Pineda O, Garcia D, Haces F. 2025. Dielectric Fluids Remote Sensing Testing. U.S. Department of the Interior, Bureau of Safety and Environmental Enforcement. 111 p. Final Report. Contract No.: 140E0124P0011.

ABOUT THE COVER

Cover image by Water Mapping, LLC. Ohmsett tank during Remote Sensing Study.

ACKNOWLEDGEMENTS

The authors would like to express their gratitude to Dr. Jay Cho, the technical lead at BSEE, for his expert guidance and support throughout this study.

GRAPHICAL ABSTRACT

Near Real-Time Characterization of Dielectric Fluids with Multispectral Remote Sensing

Array of floating targets with transparent Dielectric Fluids at the Ohmsett tank. These targets of 3 different dielectric fluids with a range of thicknesses from 0-1000um are used to study remote sensing technology for its detection.

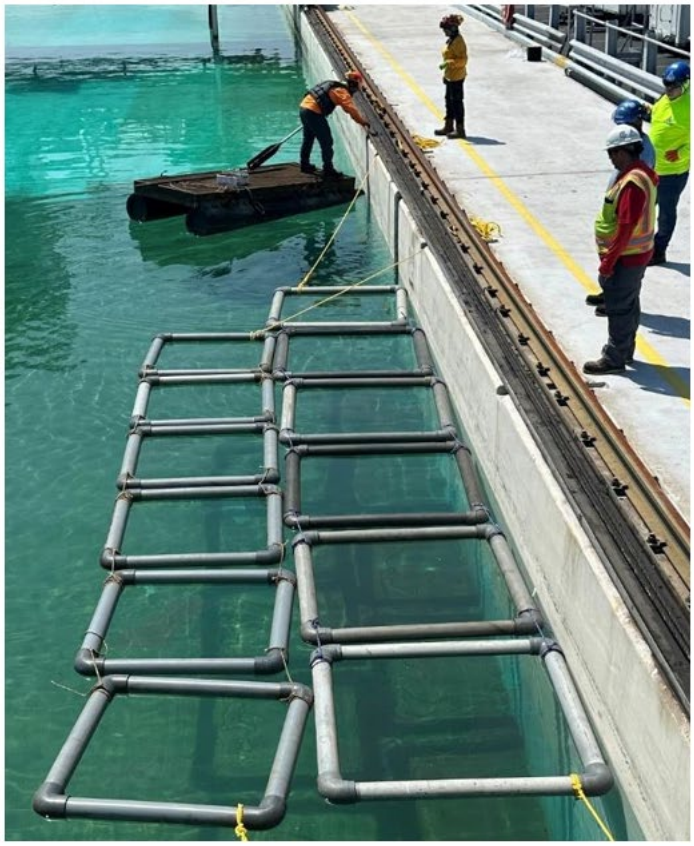

Figure on right, is a *Thickness Classification Map* generated in less than 20 minutes after the aerial image is collected by a UAS rigged with a multispectral sensor. This map is as seen on a mobile device (smartphone) on Google Earth.

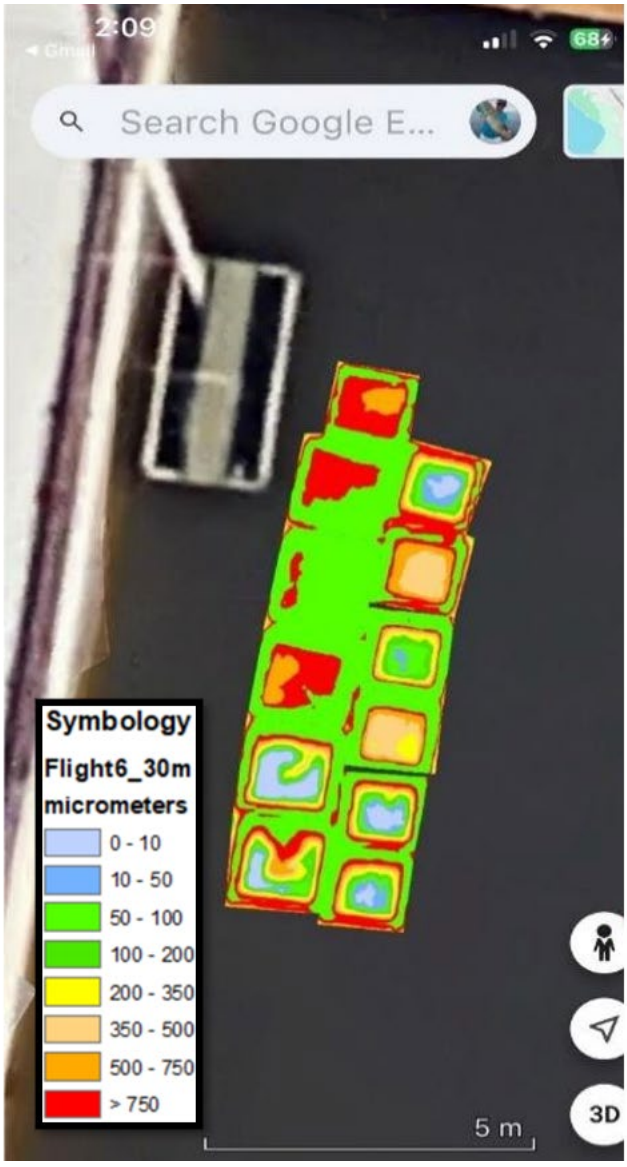

EXECUTIVE SUMMARY

The Bureau of Safety and Environmental Enforcement (BSEE) funded project 140E0124P0011 to Water Mapping, LLC (WM) to conduct research on the capabilities of remote sensing technologies for detecting floating refined hydrocarbons such as Dielectric Fluids (DF) associated with energy harvesting operations on the outer continental shelf. This project consisted of a series of laboratory tests in control setting scenarios at Ohmsett and Water Mapping facilities. To carry out this project, three of the most commonly commercially available DF in the industry were used: Hyvolt, Midel, and FR3. For this project, BSEE acquired a multispectral sensor Altum-PT1 from MicaSense, additionally Water Mapping utilized other infrared, multispectral, and visual sensors. The core mission of this project was to determine under which ambient conditions those sensors could detect presence/absence of floating DFs and at what degree was possible to characterize qualitatively or quantitively the thickness of the floating layer of DF.

The objectives of the project consisted of testing the sensors under a variable set of viewing angles and ambient conditions (illumination and air temperature) to determine operationalization of these sensors for a possible emergency response in case of a spill of DFs into the environment. To meet these objectives, the work was executed as a three-staged test program that moved from controlled target trials to full-scale tank deployments. Initial laboratory testing (first stage) and field-style setups (second-stage) were used to establish sensor behavior over known DF thicknesses, verify calibration and processing routines (including band alignment and thermal temperature conversion), and identify the combinations of viewing geometry and ambient conditions most favorable for detection. These findings were then carried forward into the third-stage Ohmsett campaigns designed to stress-test detection and thickness characterization under realistic outdoor variability (sun angle, irradiance, temperature change through day/night). One of the main challenges of the project was the intrinsic transparency of all DFs, therefore, the Ohmsett tests specifically laid out multiple targets of DF samples of known types and thicknesses.

The results of this project showed that due to the physical and chemical properties of DFs, thermal and multispectral sensors can be used to detect DFs floating over water, however optical/visual sensors where not suitable to neither detect nor characterize DFs. While the near-infrared sensor had a remarkable capacity to detect presence/absence of DFs, the thermal sensors demonstrated their capability to characterize qualitatively and quantitatively their thickness under a range of ambient conditions. The positive results from the Ohmsett experiment shed light towards operationalization of remote sensing mounted on aerial sensors for emergency response operations. The reflectance of DFs in the near-infrared wavelength shows a contrast of 0.08 reflectance units higher than the clean water under daylight. Due to the physical and chemical properties of DFs to store heat, detection of thicker layers of DFs could be observed even at dark after few hours after sunset using the infrared (thermal) sensor. The significant technical achievement of this work is the development of a sophisticated image processing algorithm. This operationalization tool is distinguished by its ability to process and classify DF thicknesses in near real time, marking a paradigm shift in data processing capacity and establishing a new benchmark for analytical speed critical to inform spill response decision makers.

Contents

List of Figures

List of Tables

1. INTRODUCTION

Dielectric materials, hydraulic fluids, and even hydrocarbons in general are used across many energy activities on the U.S. Outer Continental Shelf (OCS), including offshore wind infrastructure, offshore oil and gas facilities, and the subsea power/communication cables and insulated equipment that support offshore operations and grid interconnection. Among these energy industries, offshore wind energy has experienced significant expansion over the last decade, with a worldwide increase in capacity from 2.1 GW in 2009 to 63.2 GW in 2022, and a projected doubling to 177.5 GW by 2027 (Kempel et al, 2014; Roslan et al, 2010). The US has made substantial strides in expanding offshore wind capacity; key developments include federal leasing of offshore areas by the Bureau of Ocean Energy Management (BOEM, which is the only leasing government agency) and the establishment of ambitious offshore wind targets by states such as Massachusetts, New York, New Jersey, and Maryland. Advancements in offshore wind turbine technology and installation techniques have enhanced efficiency and reduced costs, while larger and more efficient turbines have enabled higher electricity generation. Financial incentives such as the Investment Tax Credit (ITC) and Production Tax Credit (PTC) have attracted investment and made offshore wind projects more economically viable. Other offshore renewable energy sources, such as wave, tidal, and ocean current energy, are in the early stages of development and face technical and economic challenges. Thus, offshore wind energy remains the most viable and widely implemented renewable energy source in marine environments, and the development of techniques to study its impacts is crucial for the extraction of offshore energy.

While renewable in nature, offshore wind energy may potentially provide unstudied pollution pathways into marine environments as single offshore windmills could operate from 2,000 to 3,000 gallons of various oils (U.S Department of Energy, 2025). In this context, DFs play a crucial role in offshore wind farms, specifically in the context of power transformers and high-voltage equipment. These fluids serve as electrical insulators and cooling agents, ensuring the reliable and efficient operation of the equipment in harsh offshore environments. However, their presence in marine environments presents a challenge from an environmental fate of transport standpoint. Various types of dielectric fluids are used in offshore wind farms, each with specific characteristics. Mineral oil, a traditional dielectric fluid, has been commonly employed due to its good insulating properties and availability. However, it has limitations in terms of flammability and environmental impact. To address these concerns, synthetic ester-based dielectric fluids have gained prominence. Other emerging options include silicone-based dielectric fluids and natural esters. Silicones offer high thermal stability and fire resistance while exhibiting excellent dielectric properties and can withstand demanding offshore conditions. Natural esters are derived from vegetable oils and have gained attention as environmentally friendly alternatives.

Traditional mineral oil-based fluids pose risks due to their low biodegradability, whereas synthetic esters and silicone-based fluids offer reduced environmental persistence. All dielectric fluids pose various levels of toxicity, which is largely dependent on their specific chemical compositions and environmental factors. The environmental impacts of dielectric fluids in marine environments largely depend on the spill conditions, which cannot be studied under current technical paradigms due to a lack of literature on the assessment of such spills. As such, the feasibility of remote sensing to monitor the accidental and operational release of these dielectric fluids into marine environments remains a crucial and largely unstudied topic in the literature. This

is the core area of contribution of this project.

2. Background: Remote Sensing of floating oils

Remote sensing is the first level of defense for any marine spill response operation. Detecting pollution for monitoring or responding purposes depends on the ability of different sensors to detect the presence/absence of floating oils as pollutants. Therefore, the ultimate goal of this project was to close the gap between the theory and the practical application of commercially available off shelf sensors that responders could use in an operational fashion.

Remote sensing of floating oils and specifically of dielectric fluids in on the Outer Continental Shelf (OCS) is an advanced and interdisciplinary field of research, posing unique challenges from both theoretical and operational standpoints (Klonowski et al., 2003). Although remote sensing of floating hydrocarbons has been widely advanced for active and passive remote sensing technologies, research on the area of remote sensing detection of dielectric oils is almost nonexistent, and this project offers a unique opportunity to resolve crucial understanding of the capacity of different remote sensing technologies to detect DFs. Challenges regarding the detection of dielectric fluid oils to be addressed on this study are based on the properties of the dielectric fluids and its environmental behavior and effects (Lyutikova et al, 2023). According to NOAA oil fact sheets for spill responders, factors between DFs and the environment are summarized herein (Oil Fact Sheets for Spill Responders, 2025).

Physical and chemical properties of Dielectric Fluids

Physical and chemical properties of hydrocarbons (fresh crude, or emulsified) have been widely studied to understand how they can be detected with remote sensing technology. However, differently from hydrocarbons in general, DFs (which many are made from hydrocarbons, particularly mineral and synthetic oils) are complex chemical mixtures containing hundreds of primarily semi-volatile, organic compounds. They are typically stable, chemically inert, and have favorable thermal and dielectric properties. Dielectric fluids are generally characterized by their low to moderate viscosities (<100 cST), which improve flow and flushing; however, some products have higher viscosity at low temperatures.

Environmental Behavior

Dielectric fluids float when released into water and spread quickly into a thin floating layer that is easily dispersed into the water column. Tests in large tanks showed that they can be effectively removed from the water surface using drum and disk skimmers, at rates about 5 times higher than diesel. Their degradation rates vary widely (based on laboratory studies over 10 days): 0% for silicone fluids; 25% for mineral oils; 60% for fluids based on synthetic esters; and 89-99% for fluids based on natural esters (Oil Fact Sheets for Spill Responders, 2025). They are generally colorless and have a weak odor, making them unavoidable by wildlife. For similar reasons, these oils may be difficult to detect when spilled on the water surface or when stranded on shorelines.

Environmental Effects

Dielectric fluid spills can cause the smothering of biological resources, which is considered its most severe hazard. Dielectric fluids may also cause bird mortality by hypothermia from matted feathers. Greater risks to birds may result from large aggregations in the proximity of the spill. Mineral oils, silicone fluids, and ester-based fluids have low to very low water solubility aquatic toxicity, and bioaccumulation potential; therefore, mortality of aquatic resources (fish, invertebrates and seaweed) is unlikely (Oil Fact Sheets for Spill Responders, 2025). Products based on light petroleum distillates will have physical and fate properties based on their chemical composition. Environmental hazard may be attributed primarily to the additives used in these products. The effects of low dissolved oxygen concentration may be a concern for highly biodegradable dielectric fluids, particularly for releases to shallow or isolated water bodies. There is little fate, environmental and toxicological information regarding spills of these fluids in freshwater and marine environments.

3. Problem Statement

As the offshore energy industry continue to expand, and many of the activities on the Outer Continental Shelf (OCS) involve dielectric fluids (oil platforms, wind energy industry, mineral harvesting, etc) detection of this hydrocarbon refined byproduct becomes crucial. These fluids, essential for efficient power equipment operation, hold significant implications for the environment. It is imperative to develop methods for assessing dielectric fluid spills in offshore infrastructure.

Remote sensing has the potential to allow us to study spills that are presently not observable. The potential ecological impacts and regulatory considerations notwithstanding, accurately quantifying the extent of such spills remains a challenge as wind turbines can use thousands of gallons of oils depending on size, for example a single 14-15 MW turbine would require 1800 to 3500 liters of DF to operate (Garret et al, 2023) therefore, this project brings forth a convergence of environmental science, technology, and policy-making.

Investigating the feasibility and accuracy of remote sensing techniques to monitor dielectric fluid spills contributes not only to our understanding of the environmental impact but also empowers decision-makers with actionable insights to mitigate the impact of the spill.

4. Research Design and Project Stages

Since the objectives for this research encompass determining the operational feasibility of using multispectral sensors to detect DF in emergency response, the selected approach is based on the experience gained from the multiple previous studies of oil/ice/water remote sensing research conducted previously at Ohmsett (Garcia et al., 2019) and CREEL (Garcia et al., 2022). These studies have resulted in a deep understanding on the implementation of remote sensing technologies for the detection of floating oil for arctic and temperate waters. The practical and operational results obtained from these studies have proved invaluable in the field, enabling the use of remote sensing to respond to oil spills under a broad range of environmental and climate conditions including arctic and temperate environments.

The overall research design is summarized herein. In ***Stage 1*** of this project (described in Section 4.1), a laboratory assessment of the provided DFs was performed to establish baseline physical behavior relevant to remote sensing, including qualitative appearance, viscosity, and emulsion stability, and to confirm that controlled thickness targets could be produced reliably. Following this bench-scale characterization, the ***Stage 2*** (Section 4.2) conducted controlled target trials using containers with known DF thicknesses to evaluate detectability across visual (RGB), multispectral (with emphasis on near-infrared and red-edge bands), and thermal imagery under varying ambient illumination and temperature conditions. These controlled trials were then scaled to full-size testing in the ***Stage 3*** (Section 4.3) at the Ohmsett facility across multiple campaigns, where DF targets of known thickness were deployed both along the tank perimeter ("totes") and as larger floating in-tank targets to better represent uneven surface distributions. Throughout the Ohmsett campaigns, imagery was collected repeatedly across different times of day and environmental conditions, with concurrent measurements of incoming irradiance to contextualize contrast variability. Collectively, this phased approach progressed from bench-scale to real-world validation, enabling evaluation of DF presence/absence detection and the development of qualitative and quantitative thickness characterization workflows.

5. First Stage: Laboratory-scale Assessment

This first stage established baseline physical behavior of the three dielectric fluids (DFs) prior to field-scale remote sensing trials. The goal was to document visually observable properties (e.g., color and transparency), compare relative viscosity, and assess emulsion behavior that could influence how DF signatures appear in multispectral and thermal imagery. Bench-scale mixing tests were used to evaluate emulsion stability across multiple water-to-DF ratios, providing early insight into whether emulsions persist long enough to be operationally relevant. These observations also confirmed that targets with consistent thicknesses could be prepared repeatedly for the subsequent staged testing under sensor-based data collection.

Three Dielectric Fluids (DF) were received from BSEE for testing at Ohmsett during stages 2 and 3 of this project. These DFs are Cargil-FR3, Midel-7131, and Hyvolt. Figure 1 below shows the aspects of the three DFs; it is important to point out that Midel and Hyvolt samples provided were previously dyed by BSEE for previous experiments carried out at Ohmsett.

FR3	Midel	Hyvolt
		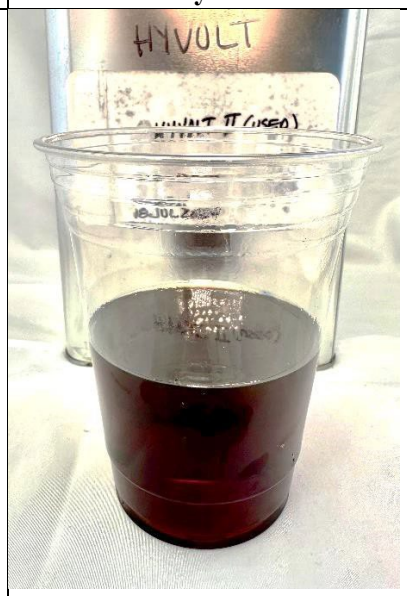
From Cargil SpecSheet: Cargill FR3® fluid is a renewable, biobased natural ester dielectric coolant for use in distribution and power class transformers where its unique fire safety, environmental, electrical, and chemical properties are advantageous. (According to manufacturer's claims)	From Midel SpecSheet: The MIDEL family of transformer fluids comprises MIDEL eN 1215, MIDEL eN 1204 and MIDEL 7131.The "eN" prefix denotes natural esters, which are formulated using renewable base oils from different seed crops, whilst MIDEL 7131 is a synthetic ester fluid. All MIDEL fluids are fully/readily biodegradable.. (According to manufacturer's claims)	From Hyvolt SpecSheet: This dielectric fluid is produced from a hydrotreated naphthenic oil to meet the specification requirements defined by CSA C50-14 Class A, Type II and IV. HyVolt products have very low pour points and excellent oxidation stability. (According to manufacturer's claims)
Color: ASTM 0.5	Color: ASTM 0.5	Color: ASTM 0.5
Viscosity @ 40C: 32-34	Viscosity @ 40C: 29	Viscosity @ 40C: 8.4

Figure 1. DF tested during the Remote Sensing experiment.

The three DFs show clear differences not only on the visual aspect (color and transparency) but also on its viscosity, which are important physical properties for the remote sensing detection. Even though the three spec sheets from the manufacturer state the same ASTM color of 0.5 there is a clear difference among the three types of DFs mostly caused by the dye used previously by BSEE. However, this coloration would not affect our results due to our experiment design which focuses on the joint use of temperature and multispectral sensors, and as such coloration or aspect (how it looks) of the DF would not affect their thermal properties.

In a qualitative way, DFs can be described as follows:

FR3	Midel	Hyvolt
Transparency: Clear	Transparency: Medium	Transparency: Dark
Color: Light Green	Color: Red	Color: Dark Brown
Viscosity: Low	Viscosity: Medium	Viscosity: High

One of the first tests conducted consisted of observing the viscosity properties of each of the DF for the creation of emulsions. An example of emulsion results is shown in Figure 2. Emulsions were tested with ratios of 50:50, 70:30, 30:70 (Salt Water/DF). For the emulsion process, were three low speed blenders at 2000 rpm were employed for a total of 1 minute (each DF) mixing a total volume of 1L of emulsion. In all cases, the aspect (color) and viscosity of the DF emulsions changed significantly from its original.

FR3	Midel	Hyvolt
		
Qualitative Aspects:	Qualitative Aspects:	Qualitative Aspects:
Color: White with viscosity like 'Milk'	Color: light brown with viscosity like 'Coffee cream'	Color: Brown with viscosity like 'Honey'
Emulsification: Very stable	Emulsification Highly unstable	Emulsification: Medium unstable

Figure 2. DF emulsified tested during the Remote Sensing experiment

The emulsion process generated surprising results for all cases of Water/DF mixtures. FR3 DF generated highly stable emulsions that stayed mixed for hours before showing signs of separation. The Midel and Hyvolt emulsifications were very unstable and separated quickly. As more water was added on the mixture (increasing the emulsification ratio Water/DF) the stability of the emulsion increased making the mixture last longer. However, in all cases, DFs change their physical aspect drastically from semi-transparent to colored.

6. Second Stage: Remote sensing testing

This second stage transitioned from bench-scale characterization to controlled remote sensing trials using known DF thickness targets. A UAS-mounted sensor suite (visual/RGB, multispectral, and thermal) was used to evaluate detectability and contrast across surfaces and backgrounds that approximate operational clutter. Targets of DF on floating water were prepared in containers at multiple thicknesses, allowing repeatable comparisons of spectral response and thermal behavior under changing illumination and ambient temperature conditions. Results from these controlled trials were used to refine acquisition and processing methods before scaling to the full-size Ohmsett campaigns.

For this experiment Visual, Thermal, and Multispectral sensors were mounted on a UAS. To observe the contrast with multiple features besides the DF and emulsions, the experiment was set on a concrete parking lot at Water Mapping facilities and created targets of DF on containers with multiple thicknesses as shown in Figure 3. Vegetation and rocks were present close by to provide standard remote sensing targets for further analysis.

Thicknesses in Micrometers

FR3	MIDEL	HYVOLT
0	0	0
10	10	10
50	50	50
100	100	100
200	200	200
500	500	500
750	750	750
1000	1000	1000
3000	3000	3000
5000	5000	5000
Emulsion 1	Emulsion 1	Emulsion 1
Emulsion 2	Emulsion 2	Emulsion 2

Figure 3. DF array with multiple thicknesses and emulsions.

Examples of the full resolution imagery collected by the Multispectral MicaSense Altum PT1 (sensor acquired for this experiment) is shown in Figure 4 using the R-G-B channels for true color.

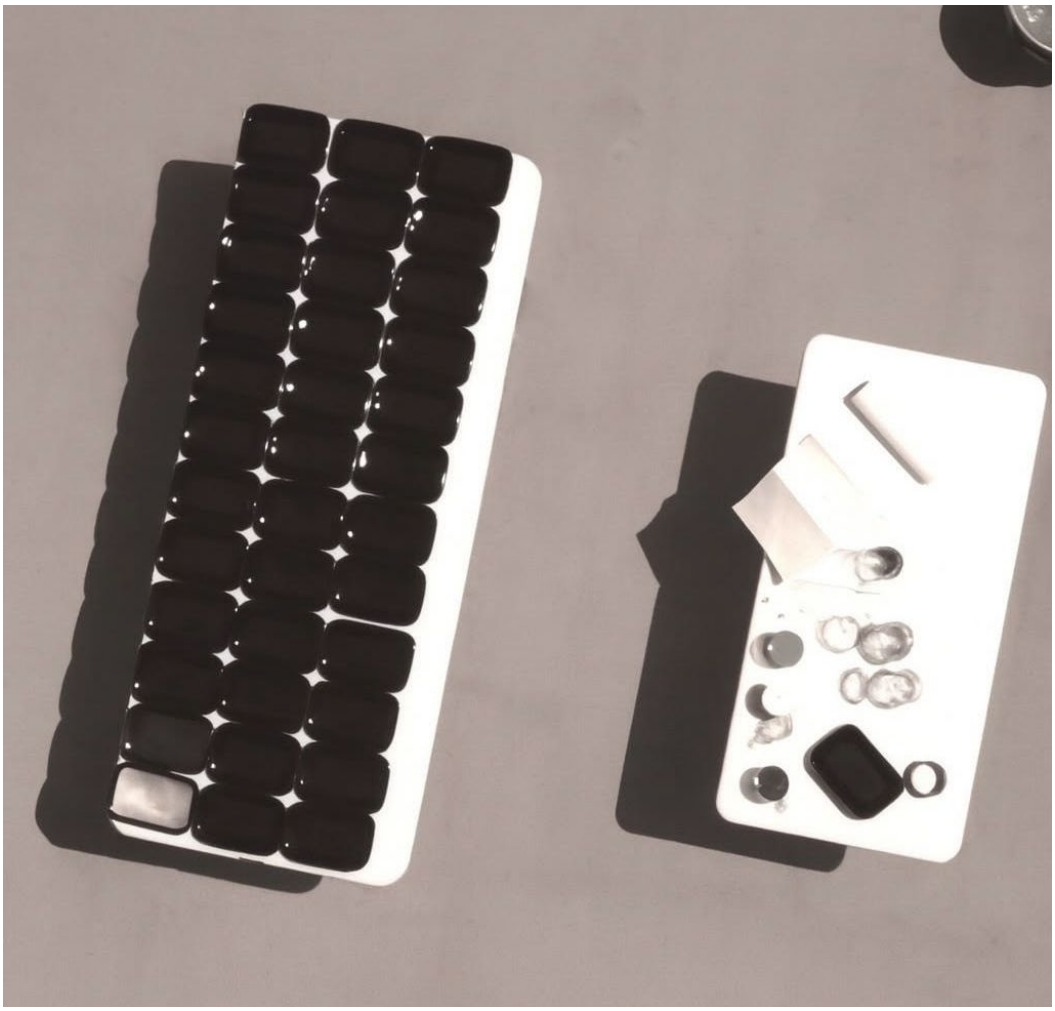

Figure 4. Experiment setup. Visual-RGB image collected at 40ft altitude from a UAS with the MicaSense Altum PT1.

The multispectral bands of the Altum PT cover the spectrum shown in Figure 5. These bands are named Blue, Green, Red, RedEdge, Near-Infrared, and Infrared. The UAS employed to carry the Altum-PT1 sensor is an Astro-Max from Freefly-systems. It is important to point out that this UAS complies as a government approved Blue-list drone.

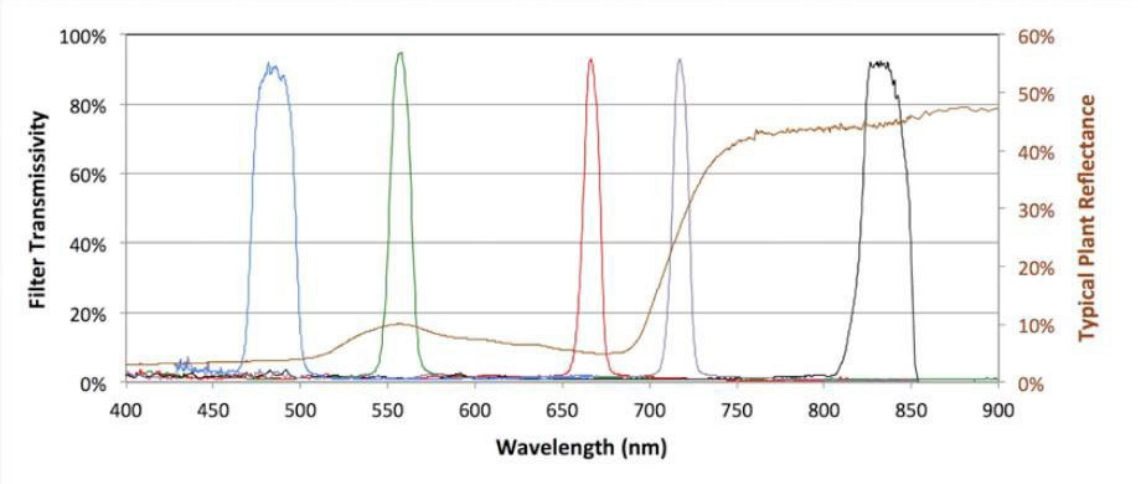

Band Number	Band Name	Center Wavelength (nm)	Bandwidth FWHM (nm)
1	Blue	475	20
2	Green	560	20
3	Red	668	10
4	Near IR	840	40
5	Red Edge	717	10

Figure 5. Multispectral bands of the sensor PT1. In addition to these 5 bands, the sensor collects a full panchromatic (visual) and thermal image.

The PT1 sensor allows the collection of all the bands at the same snapshot. Independent bands of multispectral images collected are shown in Figure 6.

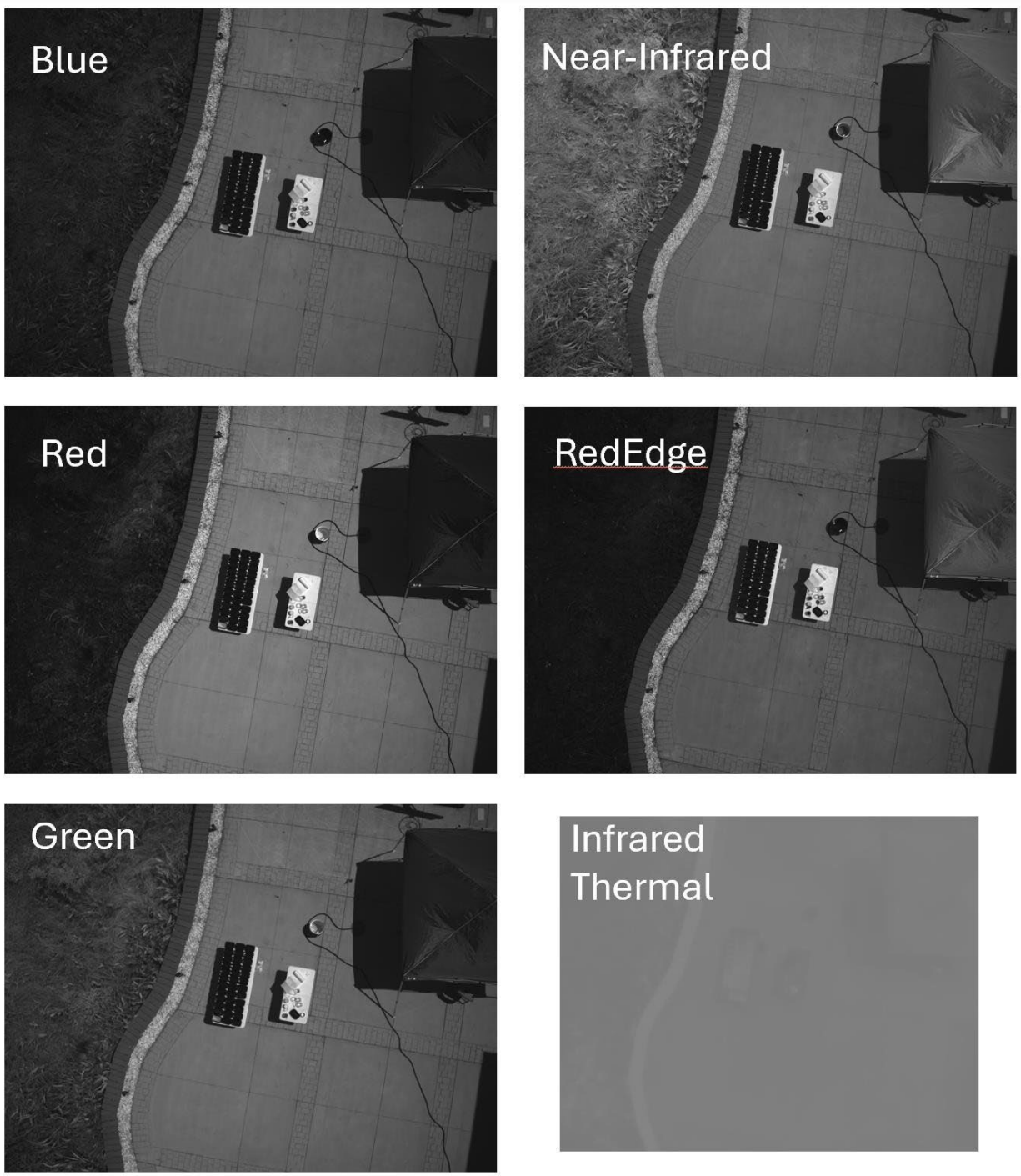

Figure 6. Multispectral bands collected by the PT1 sensor, presented as collected in grayscale. The brighter the color on the image the higher reflectance value for that given wavelength. Note how the reflectance of the vegetation or tent changes among the wavelengths.

7. Image processing workflow:

Processing the imagery from the PT1 sensor requires a custom-made workflow. Each individual band is acquired with its own lens and sensor. It was found that although minimal, there is an offset among the independent bands that needed to be rectified. This stage has been crucial to achieve the goals of the overall project. The PT1 thermal sensor was tested by acquiring images over multiple targets in the ground during variable illumination and weather conditions, this was achieved by imaging the same object at different times of the day and at different altitudes. Capturing the same object at different locations withing the field of view allowed us to quantify the offset among bands in addition to thermal and reflectance changes due to variability of the incoming sun light. These tests were repeated multiple times from sunrise to sunset. The thermal sensor is radiometrically calibrated and obtains temperature data on each pixel of the imagery. These pixel values are represented as Kelvin degrees multiplied by 100 (Figure 7). A simple arithmetic operation is used to convert these to Fahrenheit or Celsius degrees (Figure 8).

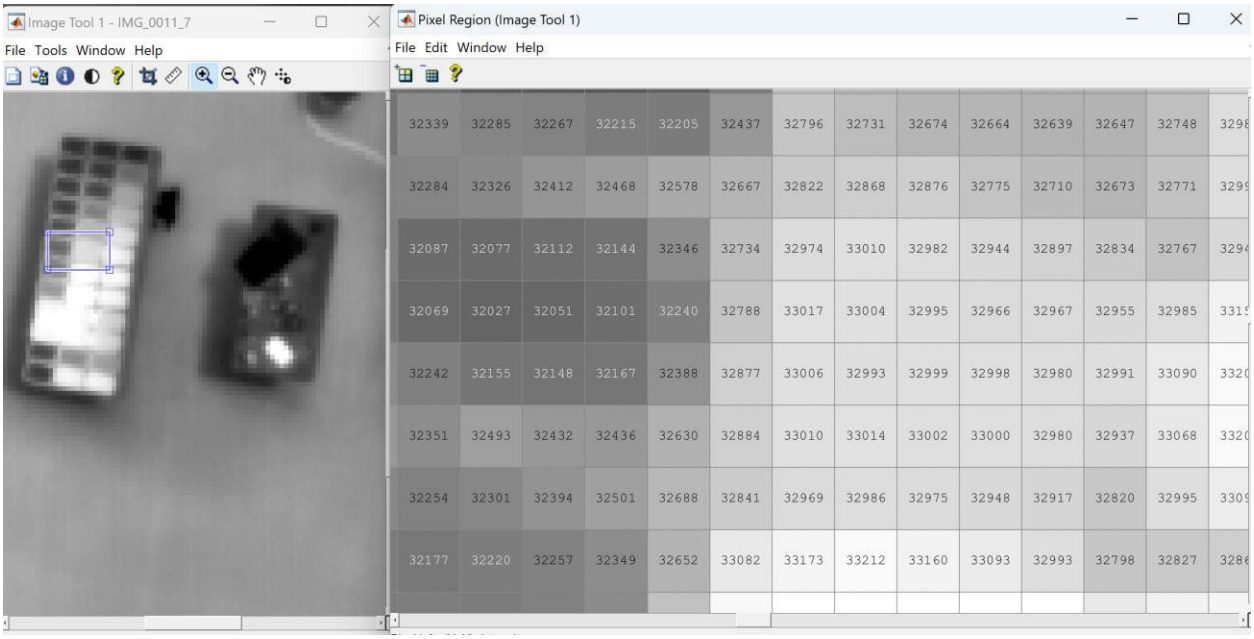

Figure 7. Pixel values represented as Kelvin Degrees multiplied by 100.

The workflow requires the image processing algorithm to have this routine of temperature value conversion automatically. The objective is to generate maps of temperature data where each pixel represents a finite number of Celsius degrees. This enabled us to perform classification of targets based on temperature values. The code ingests the multiple thermal images collected during a flight survey and performs the two tasks of georeferencing-projection and temperature conversion in an automated fashion.

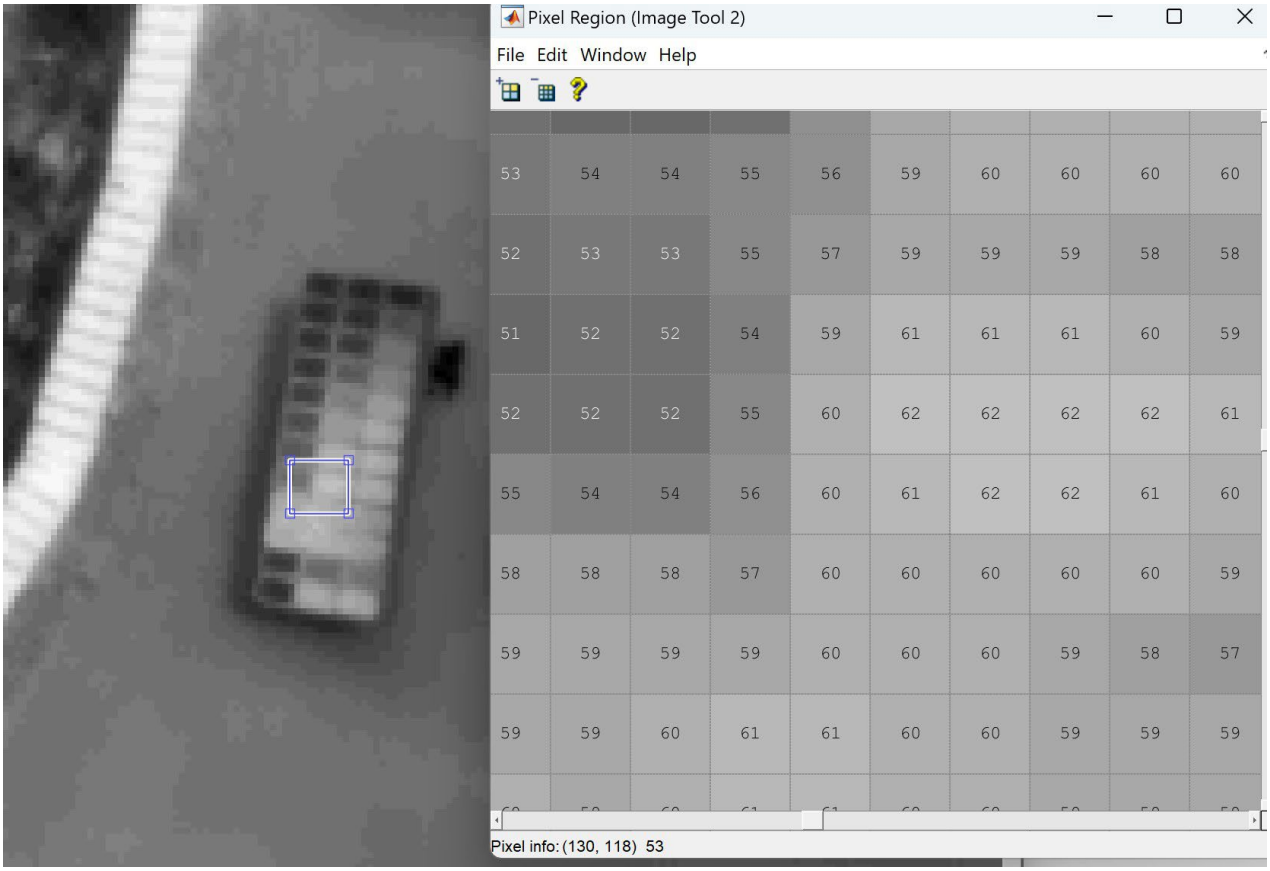

Figure 8. Thermal imagery, converted pixel values to Celsius degrees.

Data was collected under a wide range of temperature and illumination conditions including dark at night (few hours after sunset). While night imaging can have marginally (non-significant) different illumination conditions due to varying moon phases, the vast majority of luminance variation comes from different solar incidence angles during the day. The workflow described above allowed us to analyze the imagery and extract temperature data of the DF targets with multiple thicknesses. The next section shows the results of a variety of observations spreading over a 24°C variability of ambient temperatures. Each analysis shows how the different DF temperatures vary with the thickness of the fluid.

Temperature readings were collected to characterize the thermal contrast as thickness increases under multiple ambient conditions. See Appendix B with the temperature data collected during this test.

8. Thermal analysis

The initial stage of this project consisted of testing the new PT1, and visual-thermal sensors and defining a data workflow for image processing and analysis. The tests were successful, and data was acquired, processed, and analyzed over multiple targets of DF with different thicknesses under a variety of illumination and temperature conditions during day and night. The first conclusion is that DFs are not fully transparent, and some (FR3) can generate stable emulsions that change the aspect (color and viscosity) of the DF. This indicates that the multispectral bands could be used to differentiate between emulsified and non-emulsified DF. A larger scale test was then carried out at Ohmsett with larger quantities of emulsified DF.
The second and most important conclusion at this point is the observation of temperature increases as the DF thickness increases (direct correlation). The graphs below show the range of temperature values that were observed during the experiment for each of the DF.

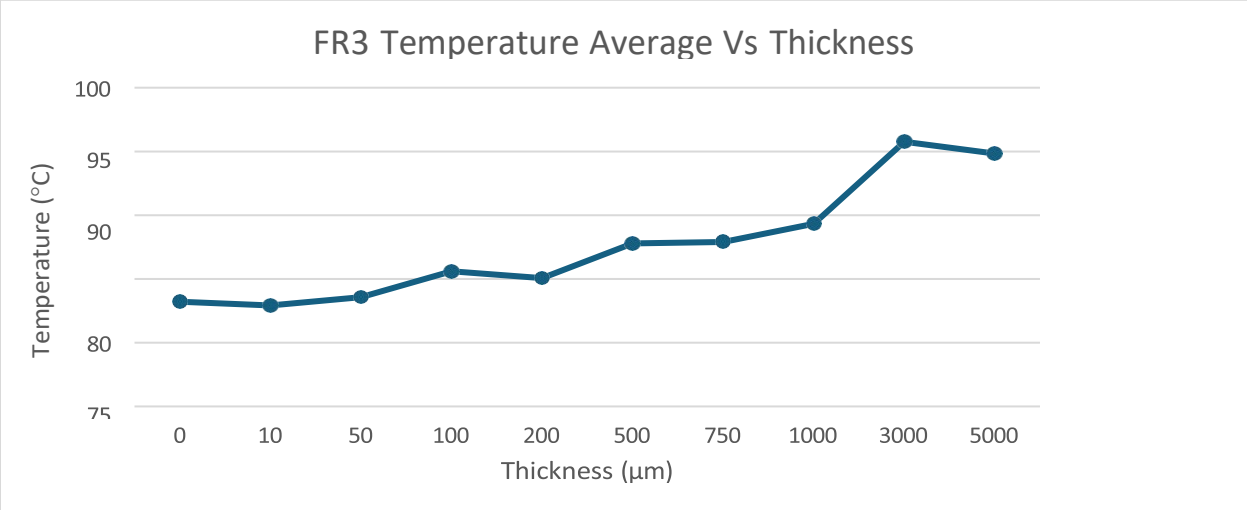

Figure 9. These graphs show the FR3 temperature range along the different thickness at different times of the day (above) and average temperatures throughout the day (below)

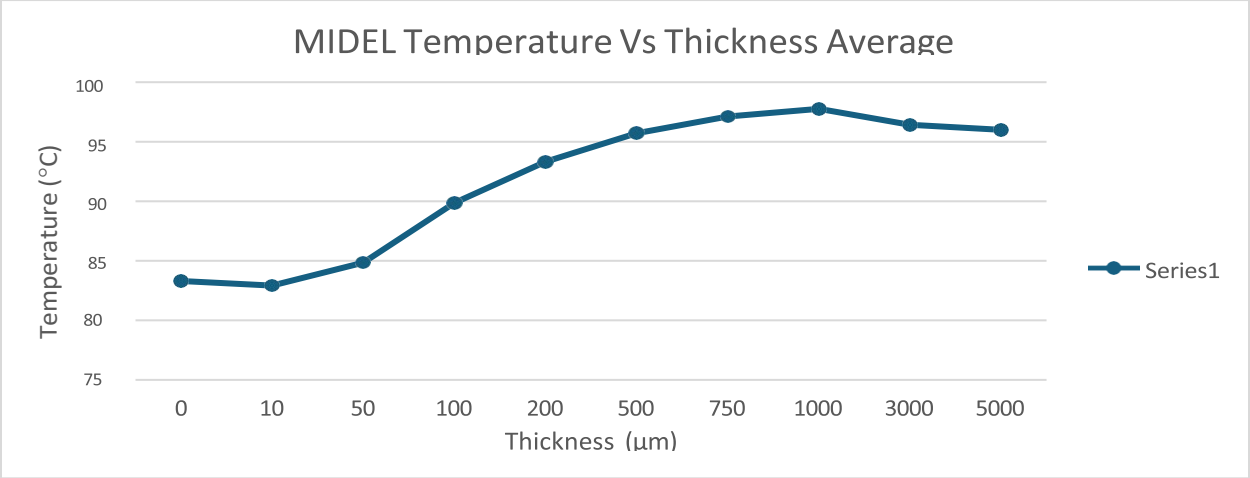

Figure 10. These graphs show the MIDEL temperature range along the different thickness at different times of the day (above) and average temperatures throughout the day (below)

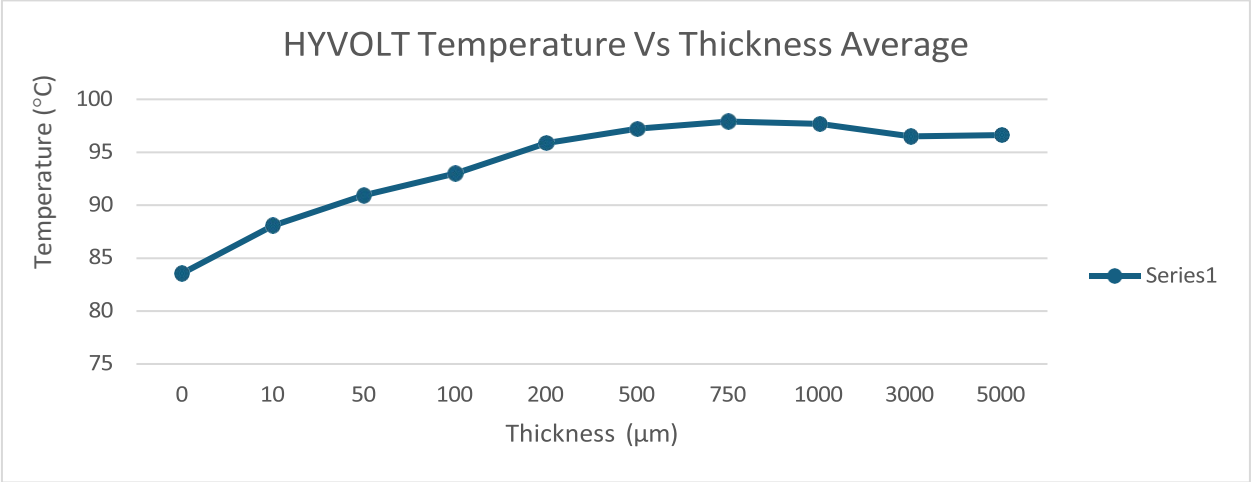

Figure 11. These graphs show the HYVOLT temperature range along the different thickness at different times of the day (above) and average temperatures throughout the day (below)

These results shows that the different physical properties among the DFs are significant to their remote sensing. These requires generating different sets of equations to derive the thickness of the oil. This is a hypothesis that was demonstrated during the Ohmsett experiments.

9. Third Stage: OHMSETT experiments

During the weeks of September 16-20. 2024 and the following year from August 17-21, 2025 , Water Mapping worked alongside the Ohmsett team to conduct the experiment of remote sensing of Dielectric Fluids (DF) at the Ohmsett facility. These experiments consisted of setting multiple

targets with different thicknesses of 3 different DF outside and inside the Ohmsett tank. Figure 12 shows the setting of the targets of DF on plastic containers placed outside the tank.

Figure 12. Setting up the DF thickness targets outside the tank. In total 46 plastic containers were used. All the plastic containers were filled with the same volume of water, then known amounts of DF were added to generate a variety of DF thickness layers.

The DFs utilized were FR3 Cargil, Midel, and Hyvolt as shown in Figure 13.

Figure 13. DF samples. From left to right: Fr3 Cargil, Midel, and Hyvolt. It is important to note that for this test, the DF Midel utilized was previously Dye with red coloration.

Targets of DF thicknesses were deployed in the plastic containers ranged as:

1) No DF (just water)
2) 10 um
3) 50 um
4) 100 um
5) 150 um
6) 200 um
7) 350 um
8) 500 um
9) 750 um
10) 1000 um
11) 2000 um
12) 3000 um

Sensors were installed on top of the building adjacent to the Ohmsett tank as shown in Figure 14.

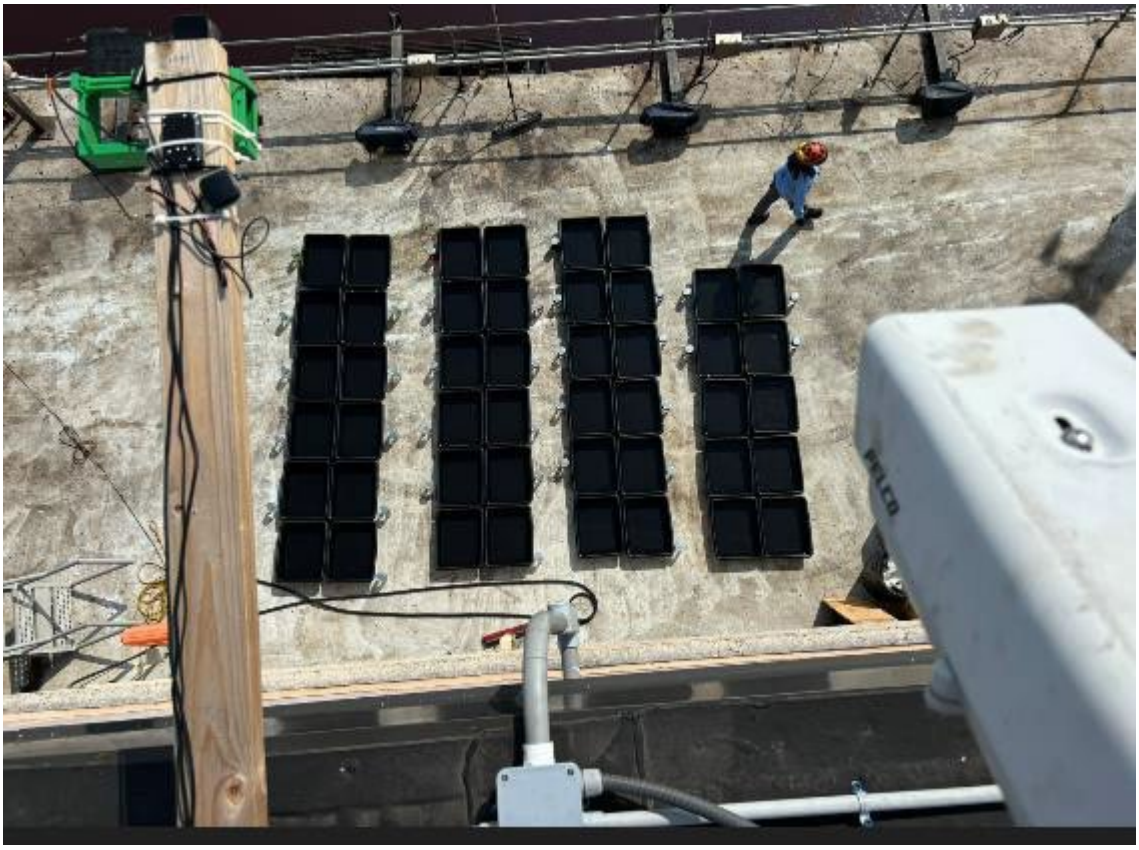

Figure 14. Sensors mounted on the bracket included the multispectral MicaSense Rededge, Thermal Flir Duo-Pro-R, and the Flir Vue-Pro. An up-looking sensor that recorded the incoming light for the calibration of the multispectral imagery was also installed and used. The up-looking sensors measures the radiance and sun angle that hits the DF targets.

In addition to the DF targets, 6 targets were added with crude hydrocarbon as a reference with HOOPS crude oil. A schematic representation of the layout of the DF targets thickness is shown in Figure 15.

2000	3000
750	1000
350	500
150	200
50	100
0	10

FR3

2000	3000
750	1000
350	500
150	200
50	100
0	10

MIDEL

2000	3000
750	1000
350	500
150	200
50	100
0	10

HYVOLT

9	10
7	8
5	6
3	4
1	2

TARGET of REFERENCE

Figure 15. Configuration of targets outside the tank. The numbers inside the FR3, Midel, and Hyvolt rectangles correspond to thicknesses of DF in microns. The targets of reference correspond to multiple thicknesses of Hoover Offshore Oil Pipeline System (**HOOPS)** crude oil.

Inside the tank, 12 rectangles were set (4 for each DF) with multiple volumes of DF. The objective of the larger squares (1 and 1.5 square meters) was to replicate a more realistic (but known) uneven distribution of the floating DF inside each square.

Figure 16. Floating targets inside the Ohmsett tank.

A crane was utilized to support a metal bracket with all the sensors mounted on it. Imagery was collected over the targets at different days and times under different ambient conditions (Figure 17).

Figure 17. Collection of imagery over the squares using the sensors mounted on the crane. In this case there were overcast (cloudy) conditions. All the environmental variables were recorded associated with the remote sensing data.

10. Data Acquisition

The sensors were set to collect data at multiple intervals to assure they record a progression of changes on the targets under different ambient conditions. Sensors used are shown in Figure 18 below.

Multispectral 1	Multispectral 2	Visual-Thermal HD	Thermal
a) 	b) 	c) 	d) 

Figure 18, Array of sensors utilized for the detection of dielectric fluids. From Left to Right: a) MicaSense Rededge-M. b) MicaSense Altum PT. c) Flir Dual Pro-R and d) Flir Vue Pro-R.

A full directory and catalog of all the data collection is included on Appendix 1 at the end of this report. As a summary, there were collected in total:

a) 150 multispectral images over the targets on plastic containers
b) 477 thermal images over the targets on plastic containers
c) 71,487 multispectral images over the floating targets on the Ohmsett tank
d) 8,406 thermal images over the floating targets on the Ohmsett tank

In addition to the remote sensing imagery, an up-looking radiometer was setup on top of the Ohmsett building to measure the incoming irradiance from the illumination conditions at the times of snapshots from the sensors. The purpose of this sensor was to associate how incoming irradiation from the sun affects the detection of the targets by the multispectral and thermal sensors set inside and outside of the tank.

Variables recorded included:

1) Total spectral irradiance
2) Horizontal-Vertical irradiance
3) Scattered irradiance
4) Solar elevation
5) Solar azimuth
6) Total incoming flux

The recorded ambient illumination data was associated with the imagery as the examples shown on Table 1.

Table 1. Records of illumination conditions associated with each of the images collected.

Date	Time	File Name	Spectral Irradiance	Horizontal Irradiance	Direct Irradiance	Scattered Irradiance	Solar Elevation	Solar Azimuth	Type	LUX Phone	Thermal Image
9/16/2024	15:19	IMG_0003_1	79.70	61.30	89.80	0.00	0.75	3.90	Totes	125,000	20240916_152008_R
9/17/2024	12:11	IMG_0006_1	37.93	36.57	23.34	19.42	0.83	3.68	Totes	200,000	20240917_121211_R
9/18/2024	10:09	IMG_0009_1	20.01	12.17	20.32	0.00	0.64	2.21	Squares	55,000	20240918_100936_R
9/18/2024	10:49	IMG_0036_1	26.56	29.40	16.26	18.29	0.75	2.42	Squares	68,000	20240918_105401_R
9/18/2024	15:09	IMG_0021_1	39.99	27.18	36.75	3.74	0.69	3.99	Squares	120,000	20240918_150956_R
9/19/2024	8:24	IMG_1202_1	43.26	28.64	69.21	0.69	0.42	1.92	Squares	37,000	20240919_082457_R
9/19/2024	10:10	IMG_3402_1	37.34	26.44	37.86	0.88	0.74	2.41	Squares		20240919_102109_R

11. Image Processing

Nearly 80,000 images multispectral images were collected from the DF targets inside and outside the tank from a wide range of illumination and temperature conditions. All the imagery was analyzed digitally using Matlab image processing tools to review radiometry (temperatures) and reflectance values of the multiple spectral bands. This section contains examples of some cases where significant variation on reflectance and thermal values was observed. Matlab routines were coded to extract pixel values from within the totes to calculate minimum, maximum, and average temperature values for each target.
Images and cases included on this section are some of the most representative samples collected under various illumination conditions that showed from low (very limited) contrast to high contrast for discerning the targets and additional relevant cases are included on Appendixes 1 and 2. Next section shows a summary of the range of data collections as follows:

Case 1: Low contrast of temperatures for DF targets in plastic containers (outside tank)
Case 2: Moderate contrast of temperatures for DF targets in plastic containers (outside tank)
Case 3: Low contrast of temperatures for floating DF targets (inside Ohmsett tank)
Case 4: Moderate contrast of temperatures for floating DF targets (inside Ohmsett tank)
Case 5: High contrast of temperatures for floating DF targets (inside Ohmsett tank)
Case 6: High contrast of temperatures for floating DF targets (inside Ohmsett tank)
Case 7: Very high contrast of temperatures for floating DF targets (inside Ohmsett tank)

For each case image collection, the Matlab routine allows extraction of temperatures for all of the thicknesses (inside the container or the floating square) which are summarized on the tables and graphs. The point of these graphs is to visualize the variation of thermal radiation vs DF thickness under the given illumination and ambient temperature conditions.

Case 1: Very low thermal contrast: Image Name: 20240916_152008_R

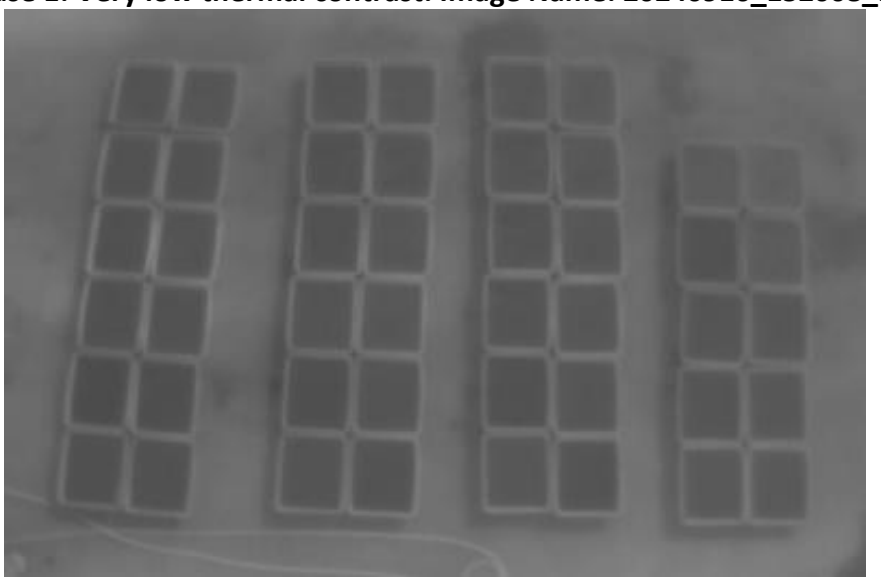

Thickness (µm)	FR3 MAX (°C)	FR3 MIN (°C)	FR3 AVG (°C)	MIDEL MAX (°C)	MIDEL MIN (°C)	MIDEL AVG (°C)	HYVOLT MAX (°C)	HYVOLT MIN (°C)	HYVOLT AVG (°C)
WATER	24	22.9	23.3	25.9	24.3	24.8	27.1	25.2	25.9
10	24.6	23.3	23.7	25.7	24.4	24.8	26	24.5	25
50	23.9	21.6	22.2	24.2	22.6	23.1	25	23.4	23.9
100	25.4	22.4	22.9	26.1	24.3	24.9	26.8	24.9	25.4
150	24.1	22.9	23.4	25.5	24.4	24.8	26.9	25.1	25.7
200	25.1	23.5	24.2	27.1	25	25.8	27.8	25.1	25.7
350	26	22.1	23.6	25.1	23.5	24.1	25.9	24.2	24.9
500	27	24.3	24.9	26.5	25	25.6	26.5	24.8	25.6
750	25.2	23.6	24.1	25.3	23.2	23.9	27	24.3	25
1000	25.3	23.8	24.2	29.3	24.3	25.2	26.9	24.9	25.8
2000	26	23.9	24.5	25.7	24.2	24.7	26.9	24.9	25.8
3000	26.5	24.7	25.2	27.6	25.3	25.9	28.1	26.4	26.9

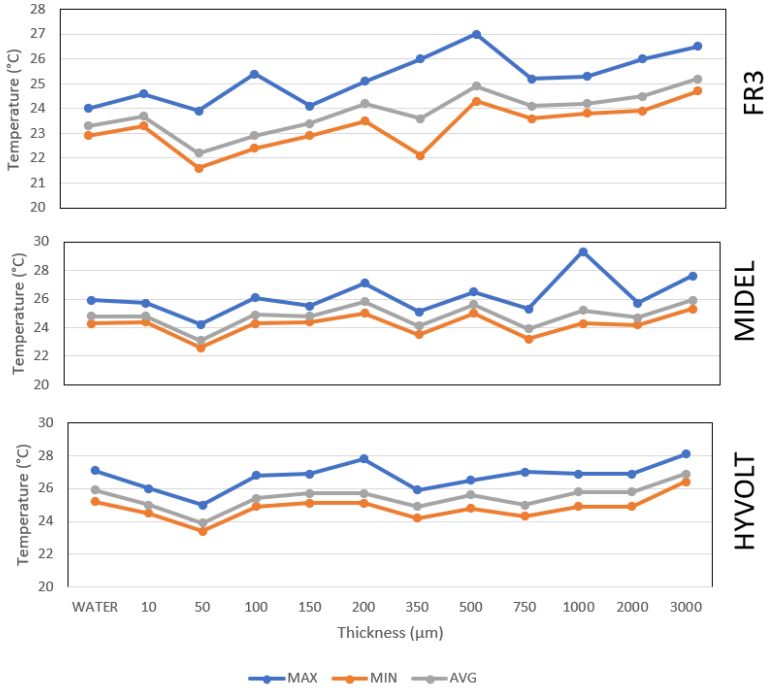

Case 2: Moderate Thermal Contrast: Image Name: 20240917_121211_R

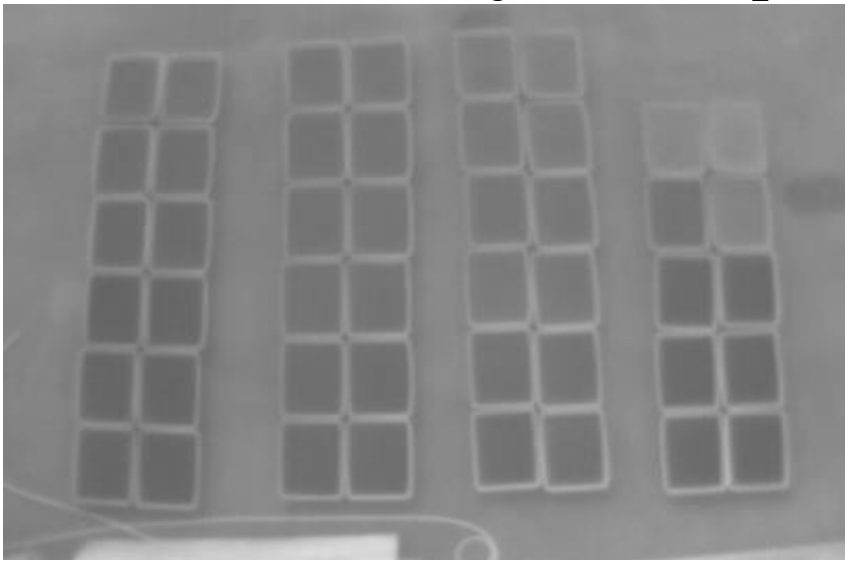

	FR3			MIDEL			HYVOLT		
Thickness (µm)	**MAX (°C)**	**MIN (°C)**	**AVG (°C)**	**MAX (°C)**	**MIN (°C)**	**AVG (°C)**	**MAX (°C)**	**MIN (°C)**	**AVG (°C)**
WATER	27.5	25.8	26.4	27.2	25.8	26.3	30.5	27.5	28.1
10	27.8	25.9	26.4	28.9	27.2	27.7	29.1	27.9	28.4
50	27.3	25.8	26.3	28.7	27.2	27.6	30.1	28	28.5
100	27.5	24.6	26.2	28.4	27.1	27.5	30.6	28	28.6
150	27	25.6	26.1	28.8	28	28.3	30.2	29	29.4
200	27.1	25.8	26.3	29.8	27.9	28.3	30.5	28.6	29.3
350	27.8	26.6	27	29.2	27.9	28.3	29.8	28.5	28.9
500	27.6	26.7	27.1	29.2	28.3	28.6	30.5	28.5	29.1
750	29.8	27	27.6	29.1	27.9	28.3	30.4	29	29.4
1000	28.6	27.1	27.7	29.6	28.2	28.6	30.7	29.3	29.8
2000	29.9	27.7	28.4	30.5	28.3	28.9	30.8	29.1	30
3000	29.7	28.1	28.6	31.3	28.7	29.2	31.2	30.1	30.6

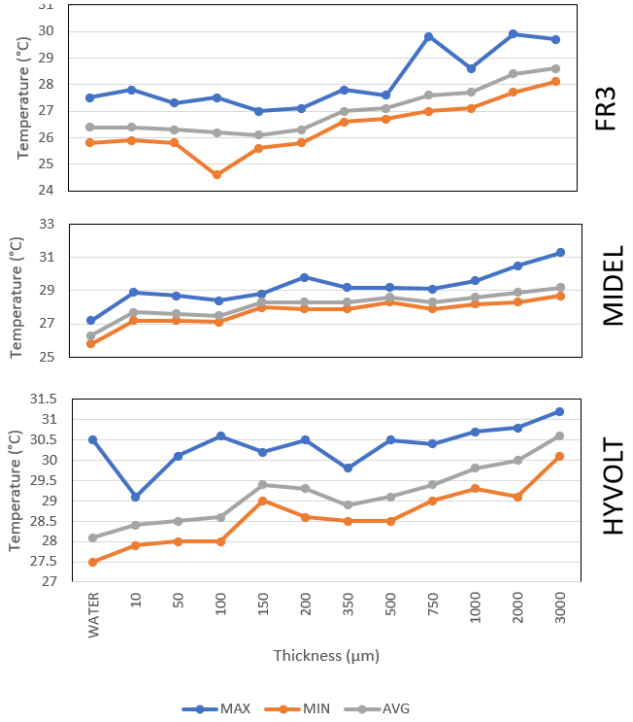

Case 3: Low thermal contrast inside the tank: Image Name: 20240918_100936_R

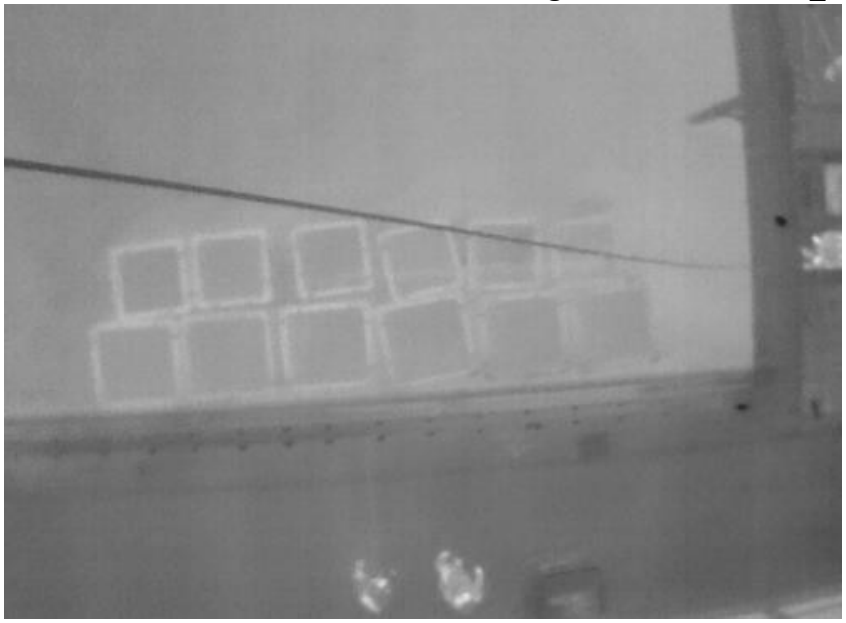

	FR3			MIDEL			HYVOLT		
Thickness (µm)	MAX (°C)	MIN (°C)	AVG (°C)	MAX (°C)	MIN (°C)	AVG (°C)	MAX (°C)	MIN (°C)	AVG (°C)
50	24.6	22.3	23.9	24.6	23.5	23.9	24	23.4	23.77
200	24.5	23.8	24.2	24.5	23.9	24.2	24.3	23.6	23.9
500	24.2	23.5	23.9	24.3	23.6	23.9	24.1	23.5	23.8
1000	24.3	23.5	23.9	24.3	23.6	23.9	24.1	23.6	23.9

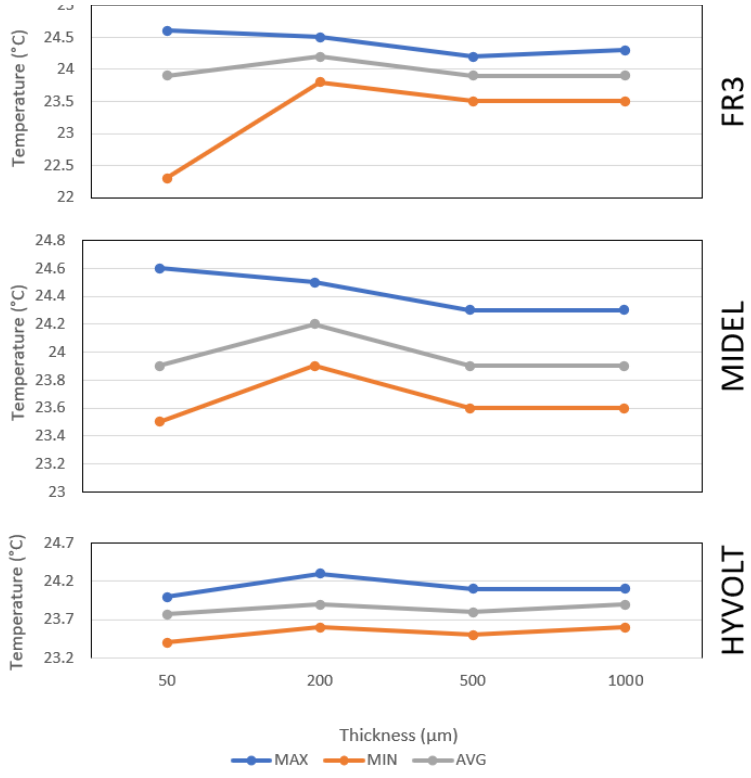

Case 4: Moderate Thermal Contrast inside the tank: Image Name: 20240918_105401_R

	FR3			MIDEL			HYVOLT		
Thickness (µm)	MAX (°C)	MIN (°C)	AVG (°C)	MAX (°C)	MIN (°C)	AVG (°C)	MAX (°C)	MIN (°C)	AVG (°C)
50	25.1	24.1	24.5	25	24.3	24.6	24.8	24.1	24.4
200	25	24.3	24.6	25.2	24.3	24.6	24.9	24.3	24.6
500	24.9	24.1	24.5	25	24.4	24.7	25	24.3	24.6
1000	24.9	24	24.4	25.1	24.3	24.6	25	24.4	24.7

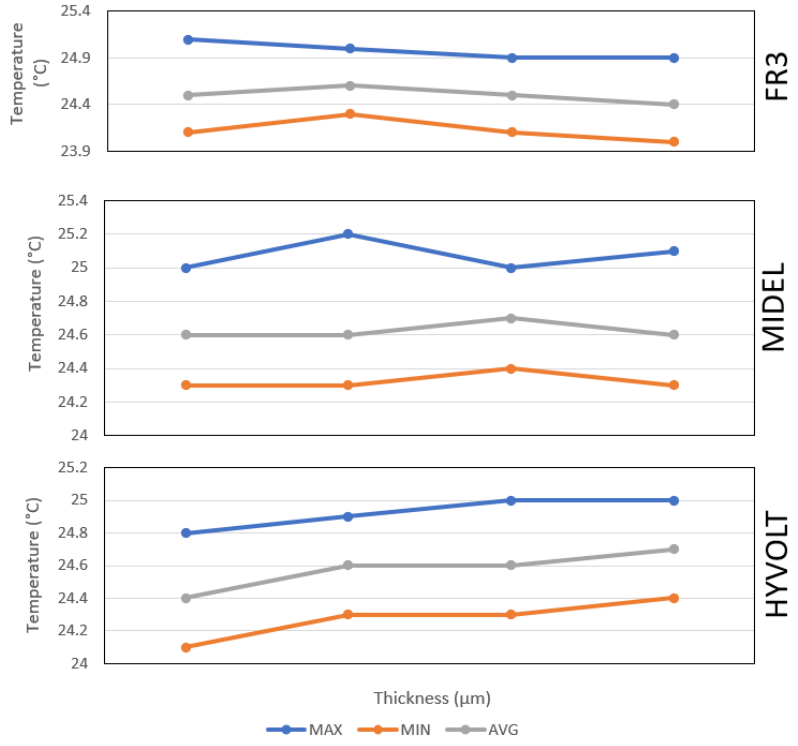

Case 5: High Thermal Contrast Inside the Tank: Image Name: 20240918_150956_R

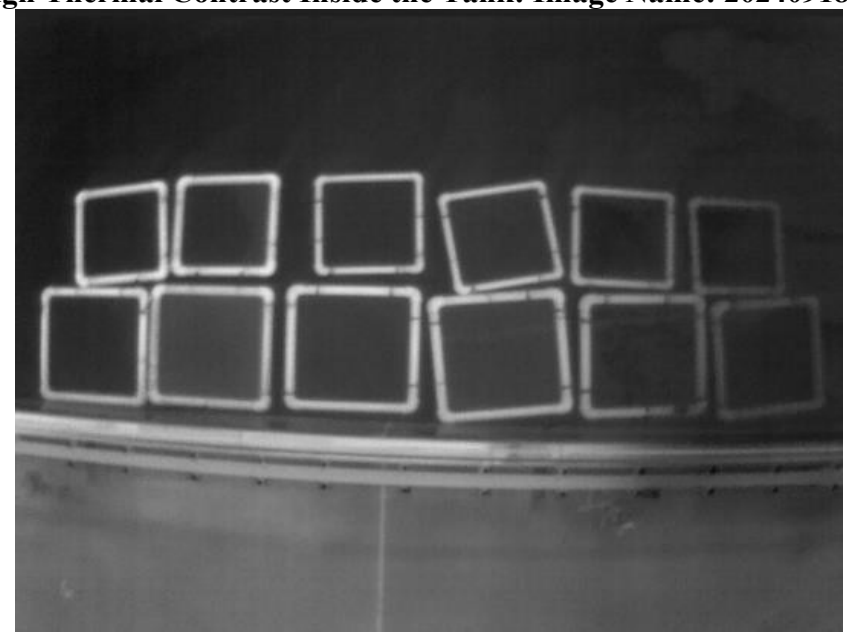

	FR3			MIDEL			HYVOLT		
Thickness (µm)	MAX (°C)	MIN (°C)	AVG (°C)	MAX (°C)	MIN (°C)	AVG (°C)	MAX (°C)	MIN (°C)	AVG (°C)
50	25.1	23.3	23.9	25.2	24.2	24.6	26.1	23.3	24
200	24.4	23	23.7	25.4	24.3	24.8	25.4	24	24.6
500	25.1	23.7	24.3	25.6	24.7	25.1	25.3	23.8	24.4
1000	24.6	23.3	23.8	25.9	24.7	25.3	26.7	25.1	25.7

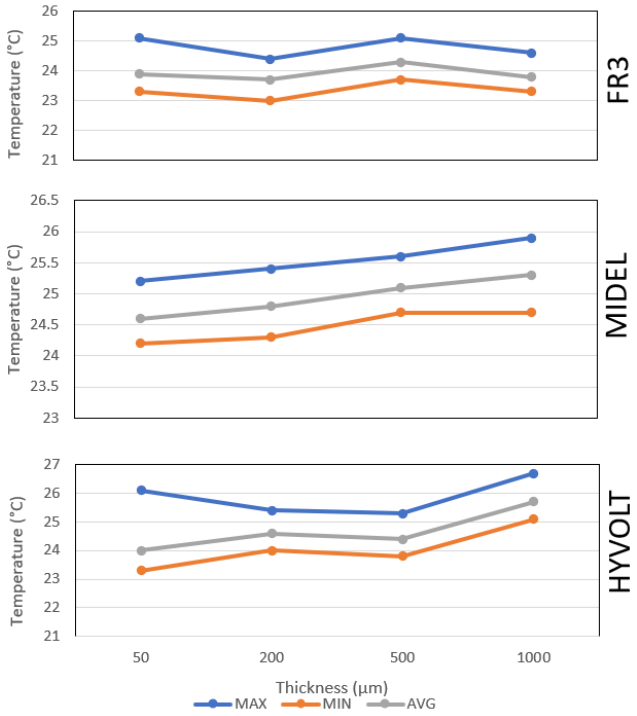

Case 6: High Thermal Contrast Inside the Tank: Image Name: 20240919_082457_R

	FR3			MIDEL			HYVOLT		
Thickness (µm)	MAX (°C)	MIN (°C)	AVG (°C)	MAX (°C)	MIN (°C)	AVG (°C)	MAX (°C)	MIN (°C)	AVG (°C)
50	23.8	22	22.6	23.6	22.6	23.1	23.8	22.2	22.9
200	23.3	22.2	22.7	24.5	22.5	23.1	24.3	22.4	23.1
500	23.2	21.9	22.4	23.7	22.8	23.2	24.4	22.4	23
1000	23	21.8	22.3	24.3	22.6	23.1	24.3	22.8	23.2

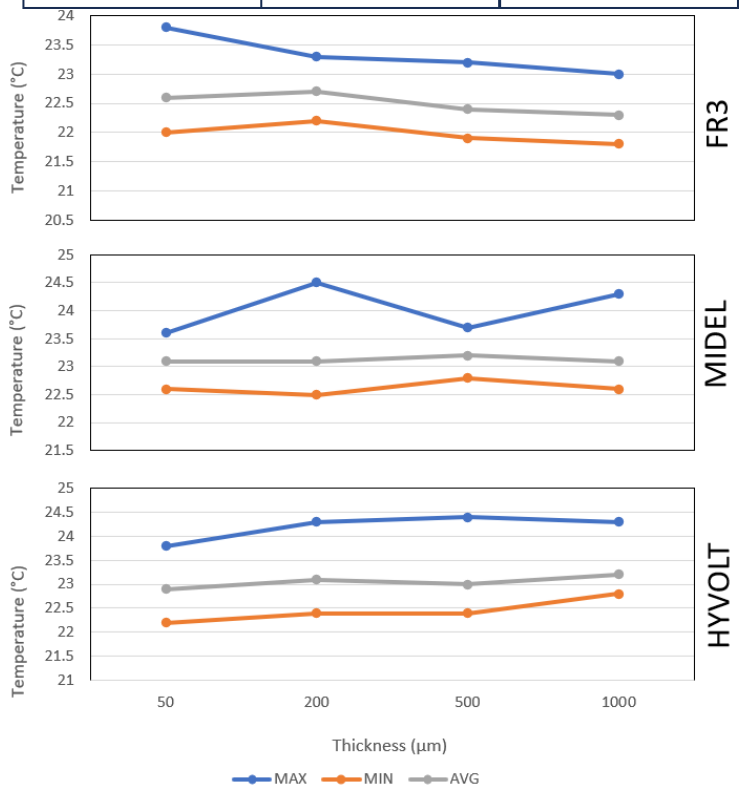

Case 7: Very High Thermal Contrast Inside the Tank: Image Name: 20240919_102109_R

	FR3			MIDEL			HYVOLT		
Thickness (µm)	**MAX (°C)**	**MIN (°C)**	**AVG (°C)**	**MAX (°C)**	**MIN (°C)**	**AVG (°C)**	**MAX (°C)**	**MIN (°C)**	**AVG (°C)**
50	24.3	21.8	22.7	25.3	22.9	23.4	24.1	21.8	22.4
200	24.9	22.4	23	25.1	23	23.4	25.7	23.4	24.1
500	25.9	22.7	23.4	26.8	23.4	24.7	27.9	22.9	24.7
1000	25.8	22.4	23.3	26.8	23.7	25.2	30.1	27	28

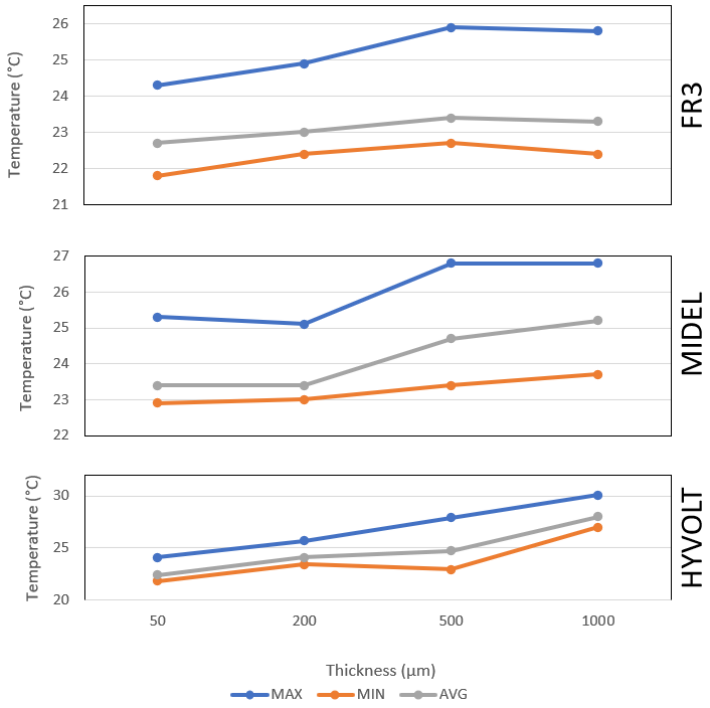

12. Thermal Imagery Contrast

A filtering/conversion routine was applied on the thermal imagery where a multicolor palette was added. The filter assigns colors on the temperature values of the pixels given the range of temperatures of the DF. The emissivity on the sensor was set at 95%. The algorithm was set to read the minimum temperature detected over water targets and the maximum temperature over DF targets. Then a standard deviation is applied on the data and the color palette is assigned on the data. This allows to visualize a thermal contrast on the multiple targets inside the tank by applying a fitting equation for all DFs at the same time. These cases shown below display a range from low to high contrasts on the thicknesses of the DF depending on the time (illumination conditions) and radiation received from the sun. The output of this algorithm reveals features that would be normally undetected if one just use the raw thermal data, however this method would not allow to distinguish between DF types. Therefore, it would be imperative to know what type of DF it is being imaged to get the thickness information calculated quantitatively with minimum errors possibly.

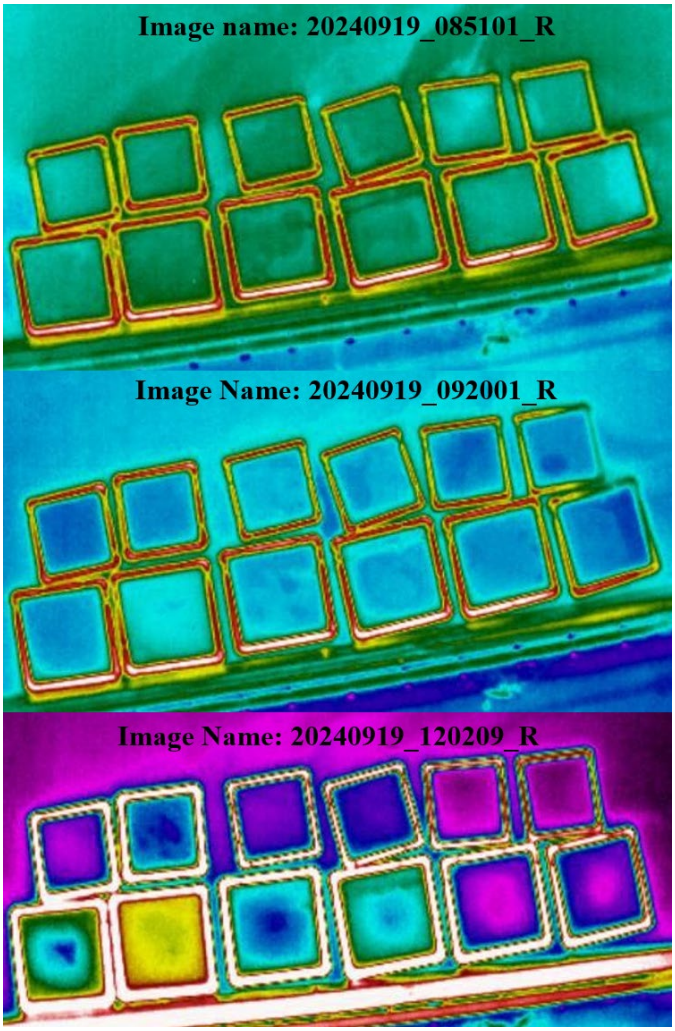

Figure 19. Conversion of temperature values for qualitative interpretation of thickness.

The image on top was collected on September 19 at 08:51 hrs. Middle image was collected approximately 30 minutes later 09:20, and bottom image was collected about 3 hours later at 12:02 hrs (same day). This algorithm allows to stretch temperature values and detect floating DF with some level of qualitative classification of thickness. As sun radiation peaks at noon the heat storage properties of the DF allows the visual distinction of thicker from thinner layers of DF. Additional images were sampled and can be found on Appendix C

13. Multispectral Altum-PT Imagery

The Altum-PT sensor was used over the targets on the tank. This sensor was acquired by BSEE particularly for this experiment. This sensor shows a great advantage over its predecessor the MicaSense RedEdge. The radiometric resolution has much higher signal to noise ratio, and the spatial resolution is four times higher than the MicaSense. This superiorresults in much finer and detailed imagery. It also captures thermal and panchromatic bands that allowe implementation of various algorithms of the multispectral bands (Figure 20).

BLUE	GREEN	RED	NearIR	REDEDGE	PANCHRO	LWIR
			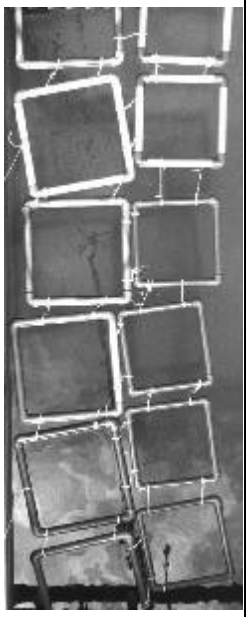	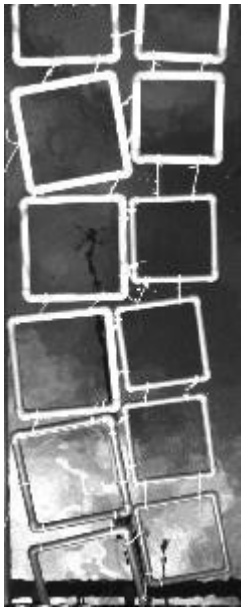	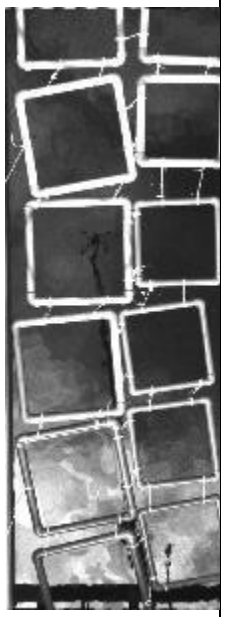	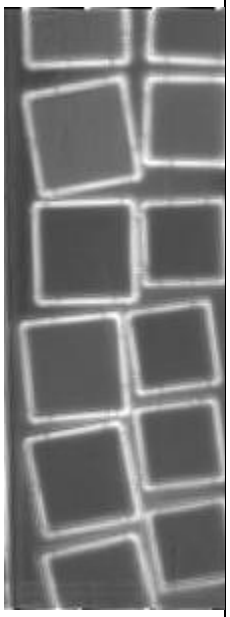

RED+GREEN+BLUE	LWIR (jet)	BLUE+RED+NearIR	GREEN+RED+NearIR	BULE+REDEDGE+NearIR		
	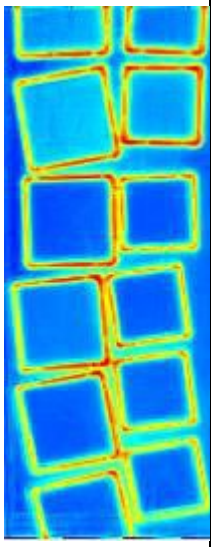	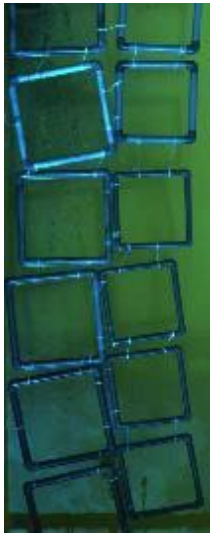				

Figure 20. Altum PT imagery and algorithm outputs.

The MicaSense RedEdge sensor was also used over the targets set on the plastic containers. An example of the 5 multispectral bands is shown in Figure 21.

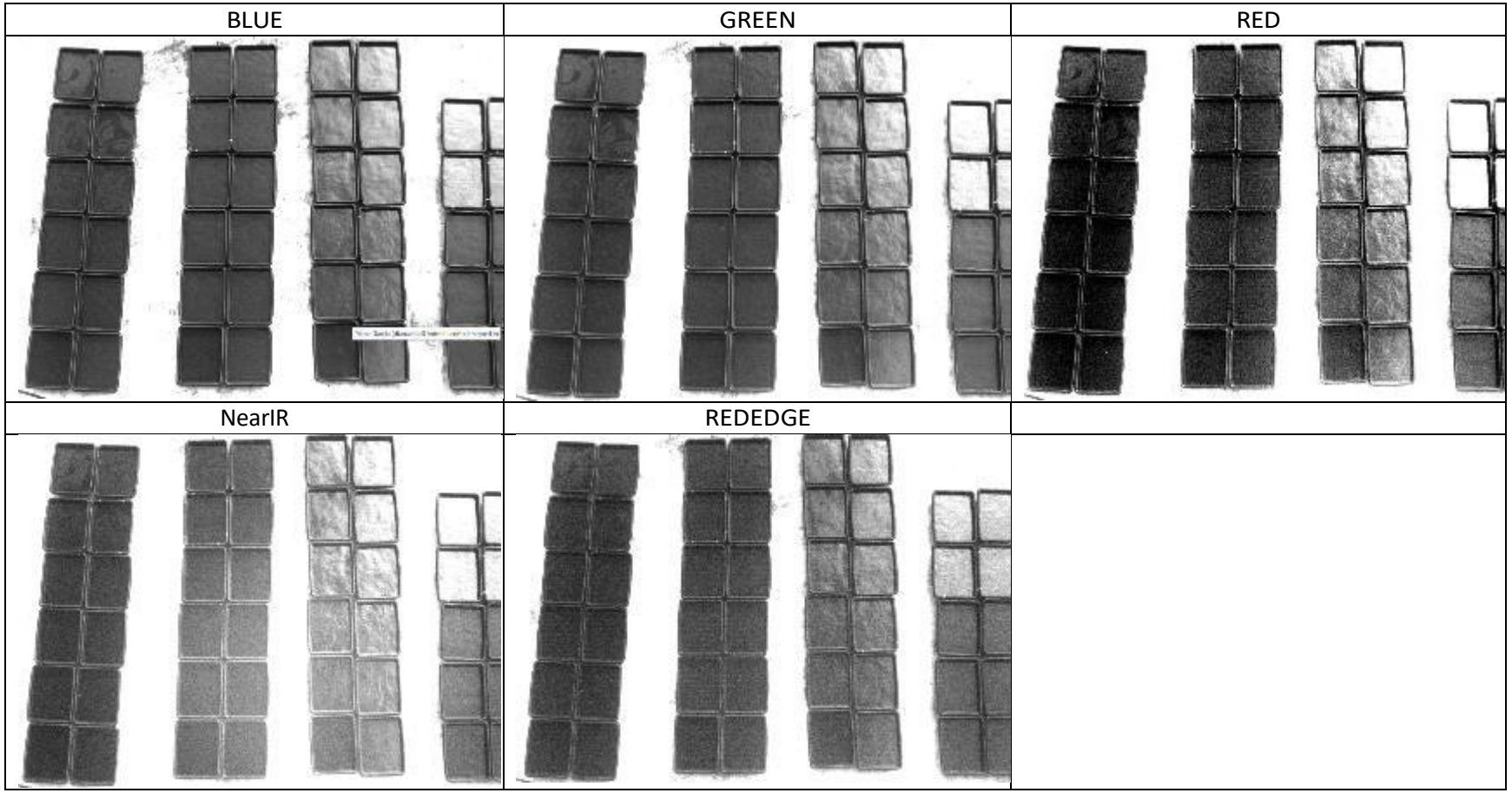

Figure 21. Multispectral bands of the MicaSense collected over the plastic container targets on 09/17/2024 12:11 pm

For the experiment inside the tank, volumes of DF were added to increase the thickness of the targets. The first set of targets were for 50, 200, 500, and 1000 um of each of the DF. The second set of targets were 100, 500, 1000, 2000 um of each of the DF. Next are examples from the first and second sets of targets.

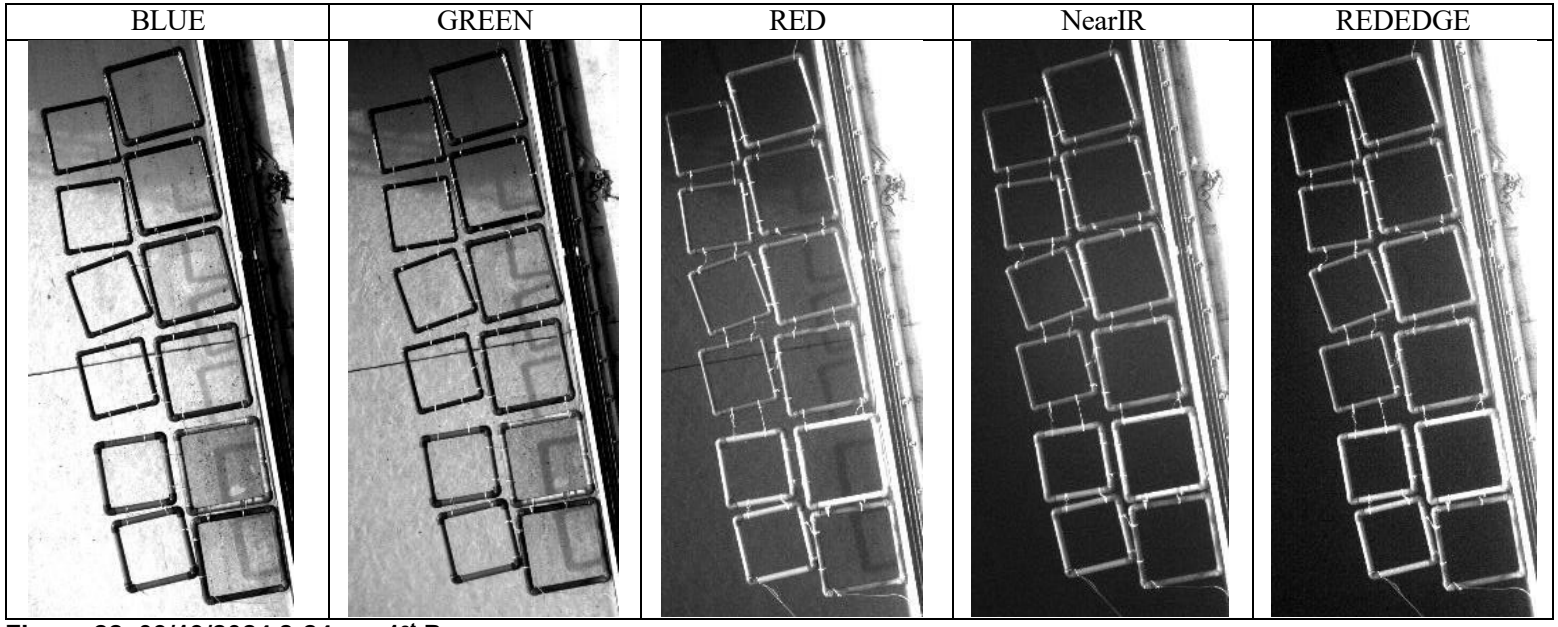

Figure 22. 09/19/2024 8:24 am 1st Pour

BLUE	GREEN	RED	NearIR	REDEDGE
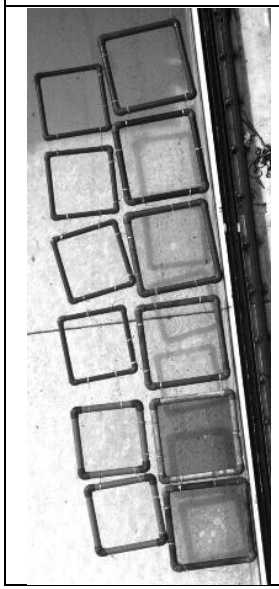	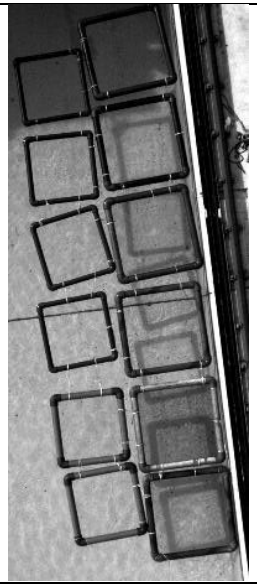	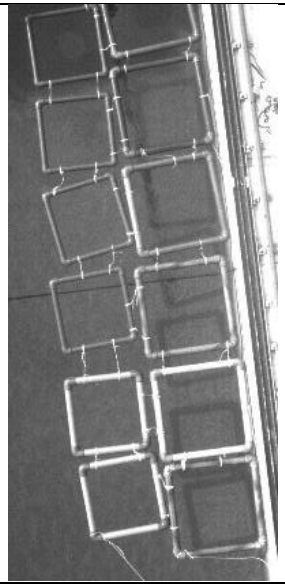	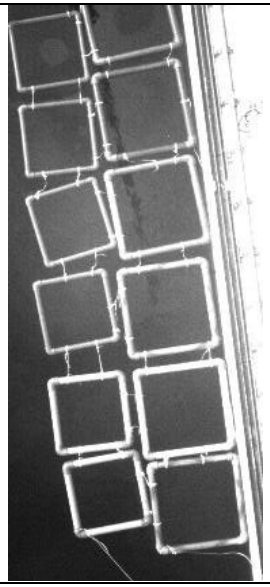	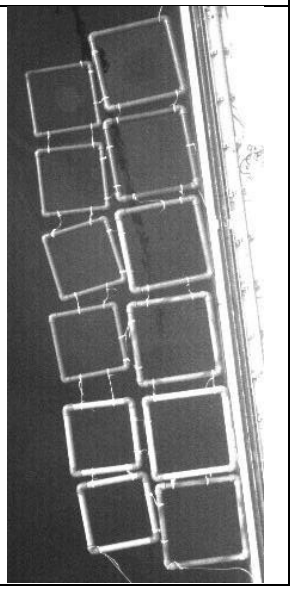

Figure 23. 09/19/2024 2:20 pm 2nd Pour

14. Results and Discussion

A total of 80,520 visual, multispectral, and thermal images were acquired over the targets set at Ohmsett. A summary of the imagery catalog is shown on table 2.

Table 2. Summary of image catalog

Sensor	Inside Tank	Outside tank
FLIR DUO	4,209	14
FLIR VUE	4,197	463
MICASENSE	71,312	150
MICASENSE ALTUM	175	0
TOTAL	79,893	627

Analysis of the imagery indicates that there are positive results for both multispectral and thermal sensors for the detection of DF. As expected, visual imagery (RGB) is not effective for monitoring or detecting DF; however, the Near Infrared channel of the Altum PT sensor shows capacity for detecting presence/absence of floating DF.

By applying normalization and filtering of the multispectral imagery, it was discovered that DF generate a surfactant effect that is detectable on the Near-Infrared imagery as shown in Figure 24 below. While DF is totally invisible under the visual spectrum, the near-infrared shows potential for utilizing this channel for detecting the presence (or absence) of the DF.

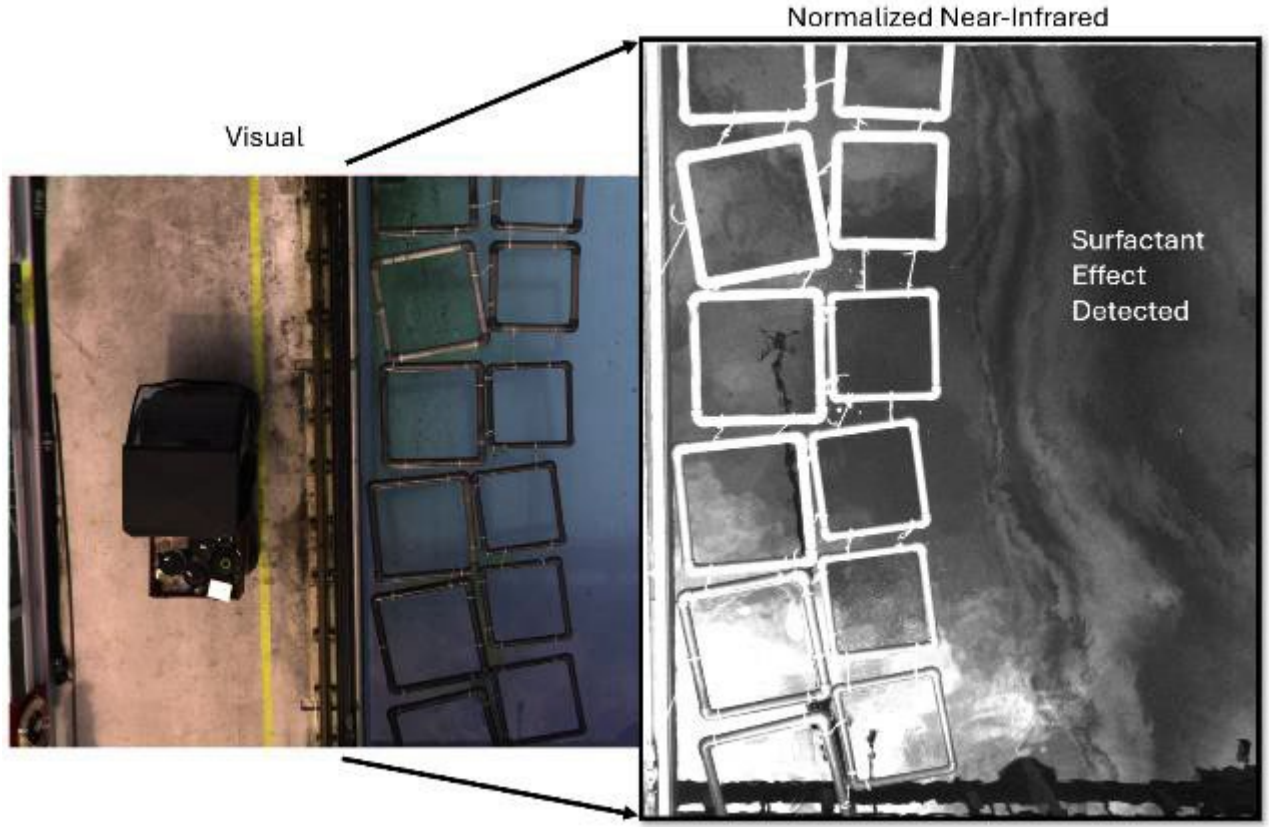

Figure 24. Image Normalization and filtering

While a relationship between the reflectance value of the NIR and the thickness of DF could not be found, this channel consistently worked for detecting the presence of DF. In other words, the reflectance values of the pixels for DF targets with different thickness did not show a consistent variability, however, all of the pixels where there was presence of DF had reflectance values higher than clean water targets (without any DF). These reflectance values vary depending on the sun angle, however in all cases, clean water targets had lower reflectance of the NIR channel than targets with any volume (and thickness) of DF.

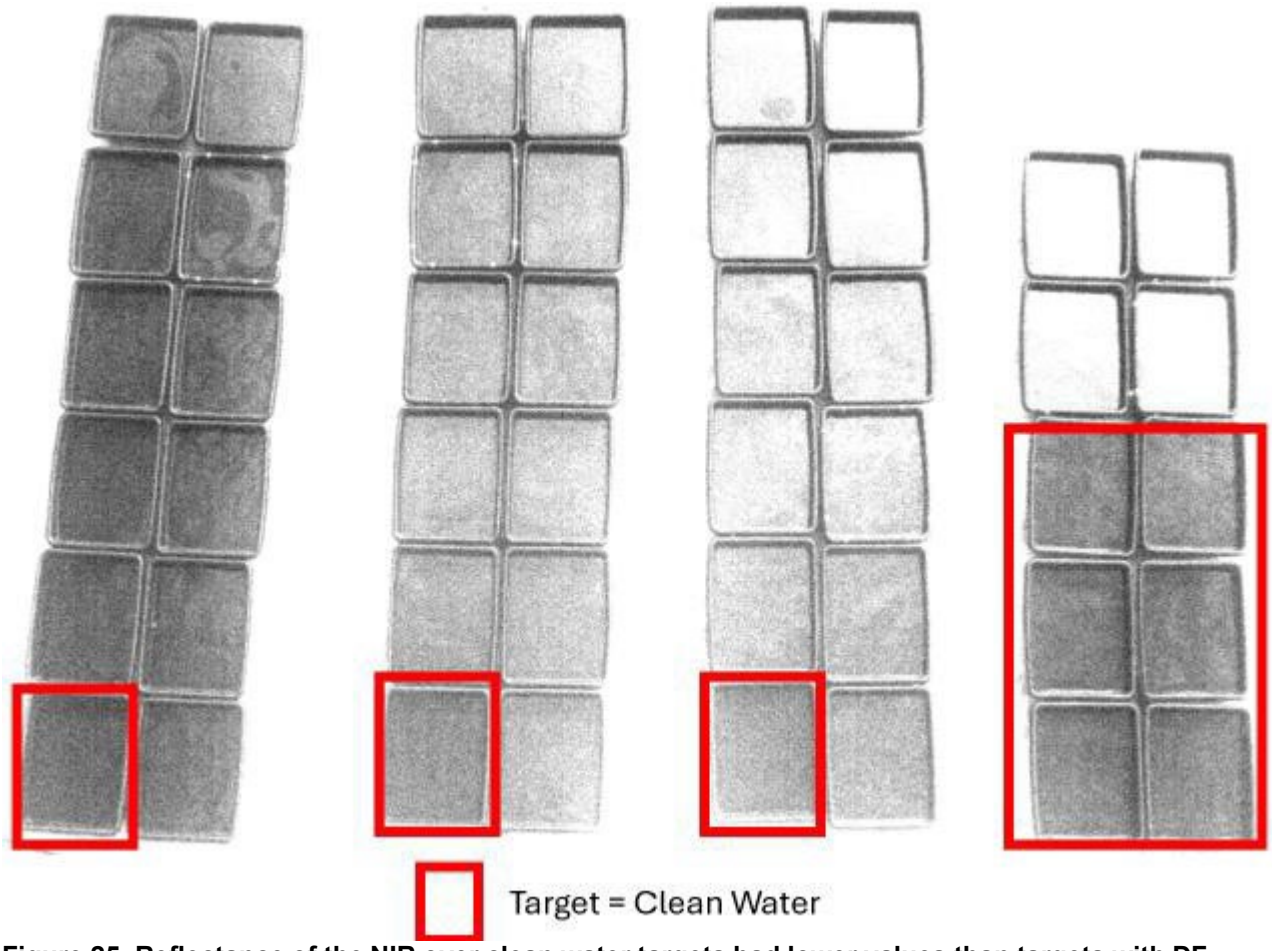

Figure 25. Reflectance of the NIR over clean water targets had lower values than targets with DF.

The Altum-PT1 sensor demonstrated to have a remarkable signal to noise ratio compared to the MicaSense RedEdge. Figure 26 below shows the comparison of the two sensors NIR channel. The spatial resolution 4 times higher on the Altum-PT also helped to identify a higher level of detail on the floating DF.

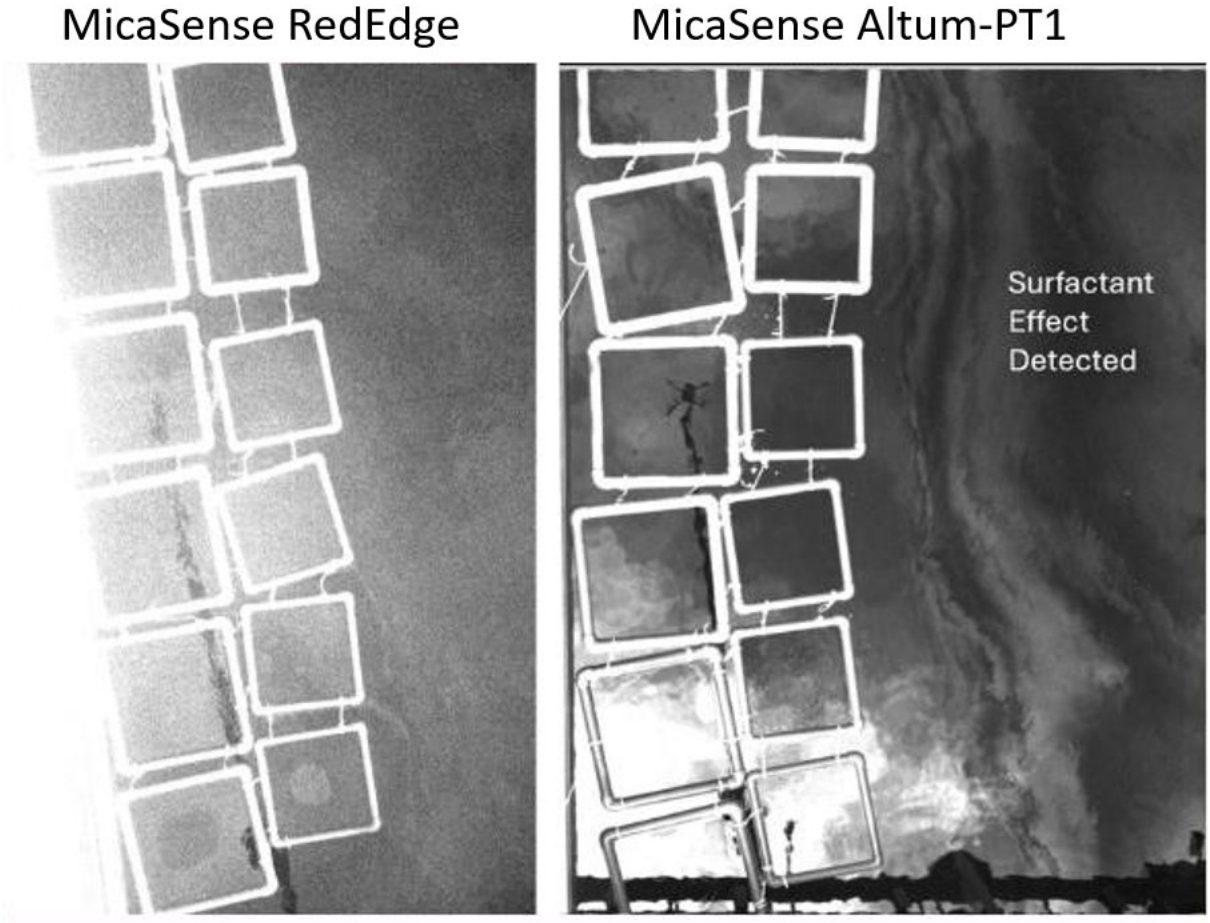

Figure 26. Near-Infrared channel comparison between the MicaSense RedEdge and the Altum-PT.

The reflectance of DFs in the near-infrared wavelength shows a contrast of 0.08 reflectance units higher than the clean water under daylight. Due to the physical and chemical properties of DFs to store heat, detection of thicker layers of DFs could be observed even at dark after few hours after sunset using the infrared (thermal) sensor.

By combining the channels RedEdge, Red, and Near-Infrared from the Altum-PT it's possible to generate an algorithm that produces a false composite color image that shows the contrast of the floating DF more distinctively as shown of Figure 27 below.

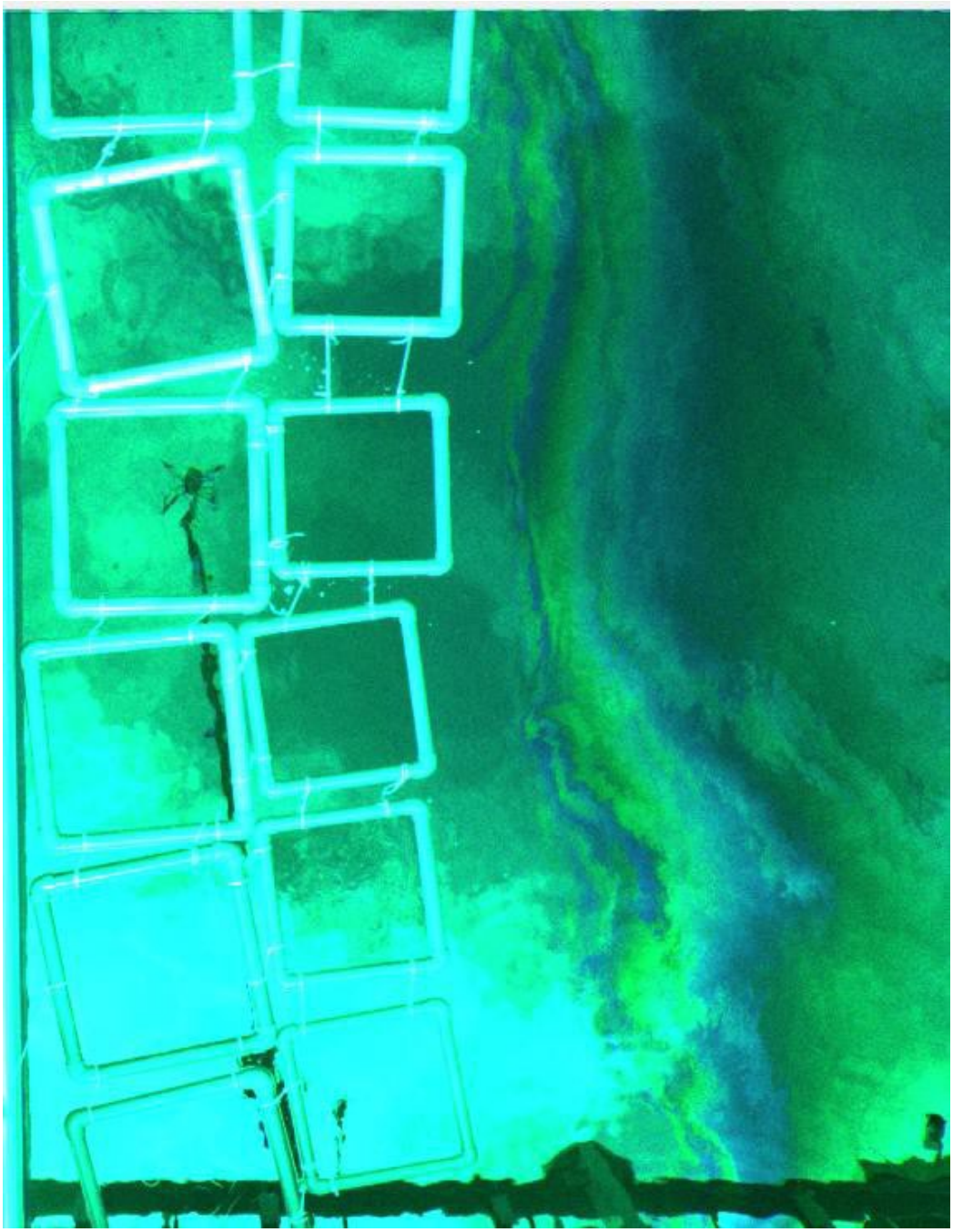

Figure 27. False composite color for detection of floating DF

It would require to conduct more data acquisition to understand the limits of detections for the Near-Infrared wavelength to discern presence/absence of DF. The strong reflectance caused by the sun glint at the bottom of Figure 27 is caused by a specular reflection of the incoming light. To avoid this artifact, optimal viewing angles in which the boundary between DF and water

exists would have to be studied.

15. Detection of DF Thickness with Thermal Sensors

The potential of thermal sensors for detection of DF is clearly demonstrated using the Altum PT. It was found in most cases a direct correlation between the increase of temperature as the thickness of the DF increases. Detection of thicknesses on thermal sensors is affected by the incoming irradiance absorbed by the DF. In other words, the temperature of the DF will be affected not only by the level of incoming light present at the moment of the snapshot and detected from the thermal sensor, but also by the heat stored by the DF over time. This was demonstrated with the thermal images captured at night and also due to a variability on the incoming light during the day due to cloudy conditions that did not impact he emissivity of the DF targets.

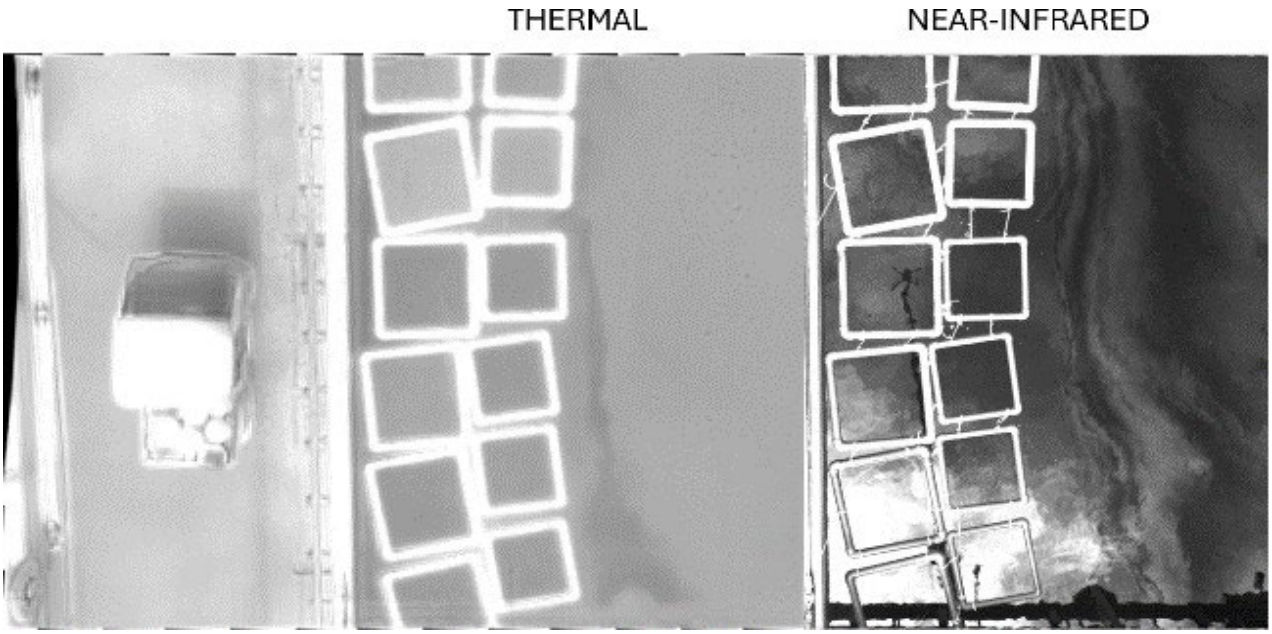

Figure 28. Thermal and Near Infrared comparison

The infrared sensor captured the variability among the three different DFs to store heat. By combining the Near Infrared band and the Thermal sensor images, its possible to produce an algorithm to display a color scale of the thickness of the three different DFs. The figure below shows the value of utilizing these multispectral bands on the Altum-PT combined to reveal not only the presence of the DF but also the relative (qualitative) thickness. By contrast, this figure shows the panel on the left a visual (RGB) image of the targets where none of the floating DFs can be discerned, and the panel on the right shows the output of the multispectral algorithm where a color palette can be used to identify the increase in DF thickness.

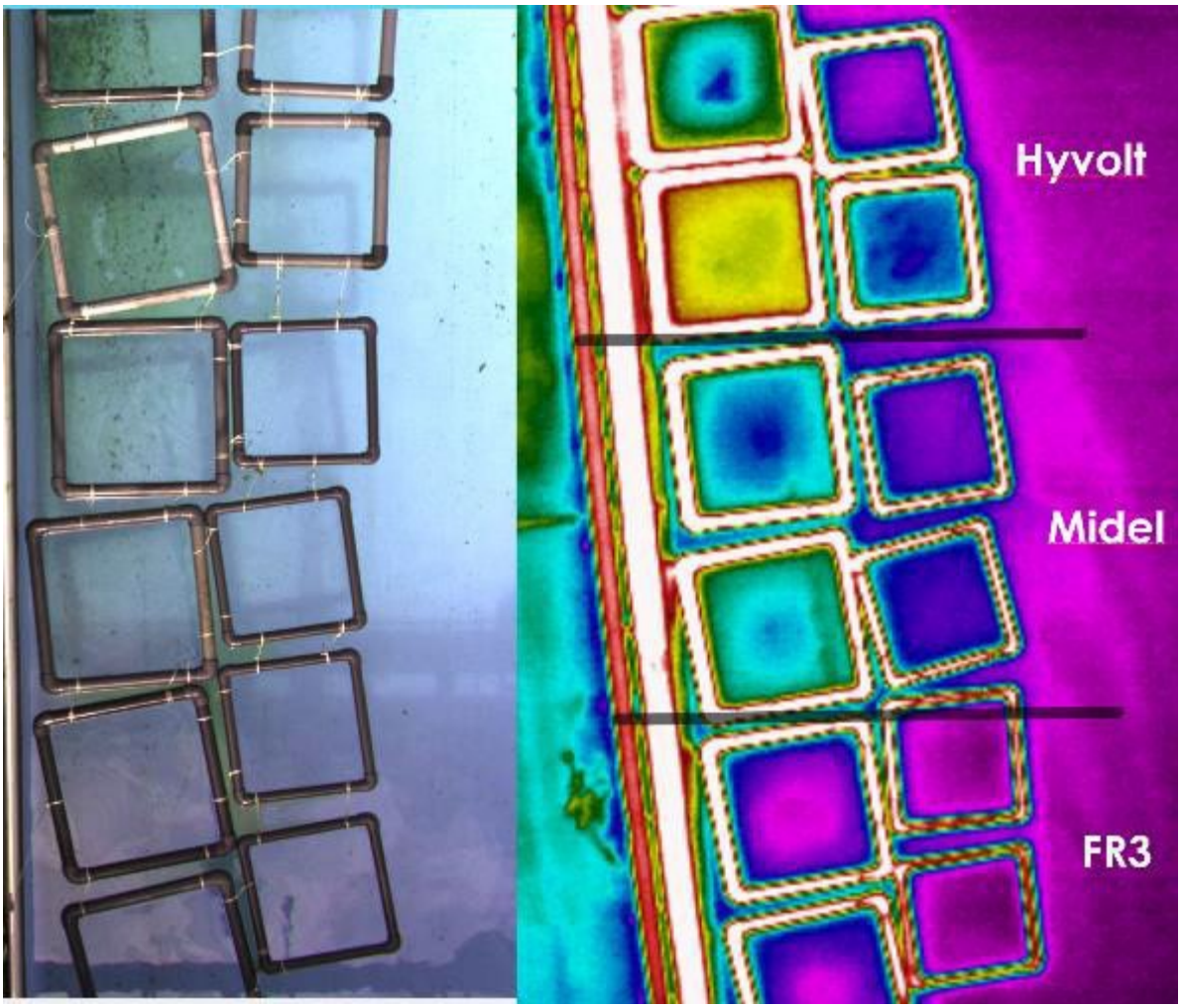

Figure 29. Left panel is the visual image of the targets. Right panel is the multispectral algorithm that associates a color scale with the thickness of DF.

This experiment demonstrates the importance capacity of DF to store/dissipate heat, and how one could use this property to estimate thickness. The analysis from the temperatures obtained by the study on the plastic containers shows that different logarithm equations should be applied to the temperature values to transform the pixels from temperature and reflectance to thicknesses.

Figure 30 below is a sequence of thermal images collected over the targets in the tank spaced by several hours difference with the same targets and shows a progression on the increment of the temperatures of the DFs as the incoming radiation from the sun also increases. The panel on the top was collected at 9:10 a.m., the middle approximately one hour later at 10:24 a.m., and the bottom and 11:33 a.m.

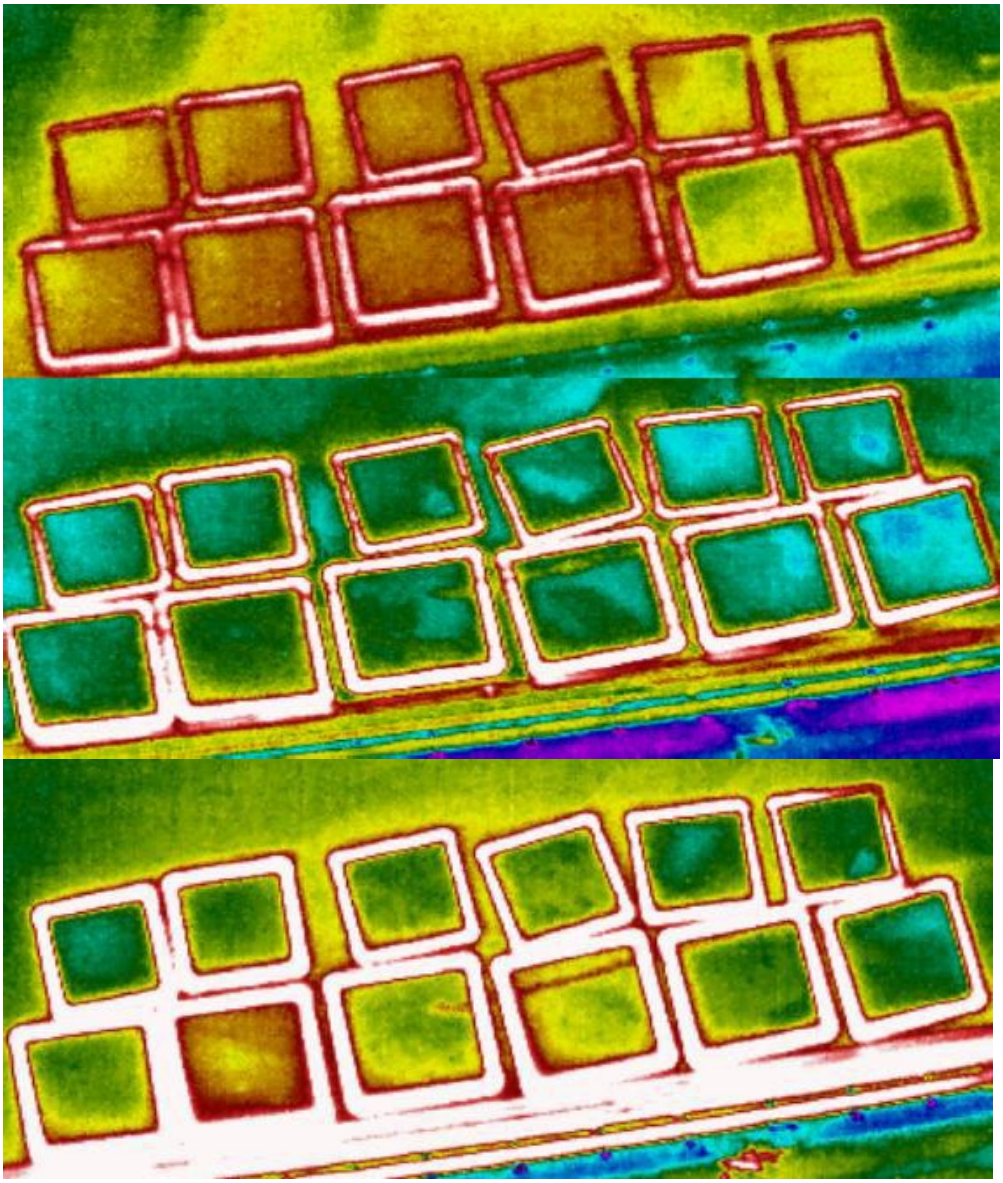

Figure 30. Algorithm outputs from different times (different illumination and sun radiation conditions). In order to convert the temperatures of the targets to thicknesses one will have to apply the corresponding equations obtained from the plastic containers experiment depending on the temperature of the water (outside the targets) and applicable for each of the 3 types of DFs.

In other words, the conversion from reflectance and temperature values will be affected by the type of DF and also by the incoming sun radiation. The corresponding equation needs to be selected based on the range of temperature from the surrounding water. For example, Figure 31 shows a set of equations for a range of temperatures between 80°F and 96°F.

CARGIL FR3	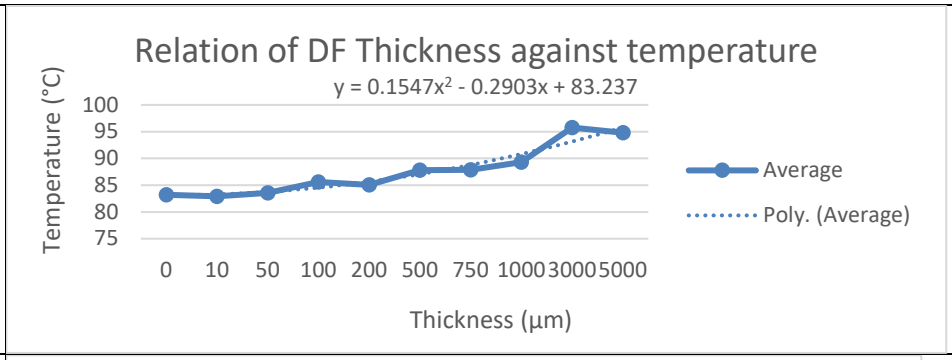
MIDEL	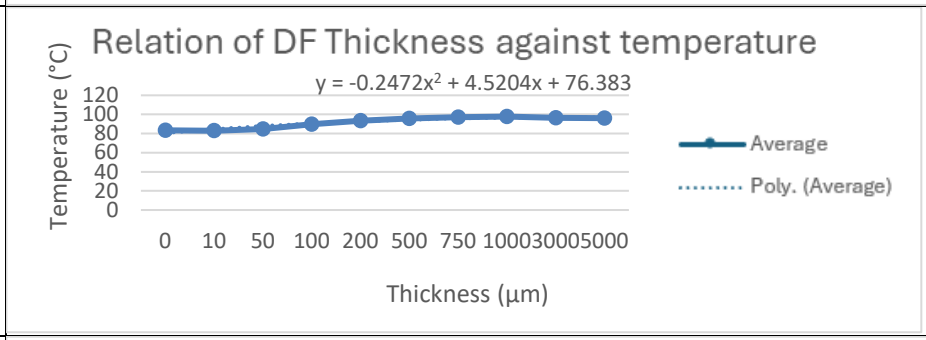
HYVOLT	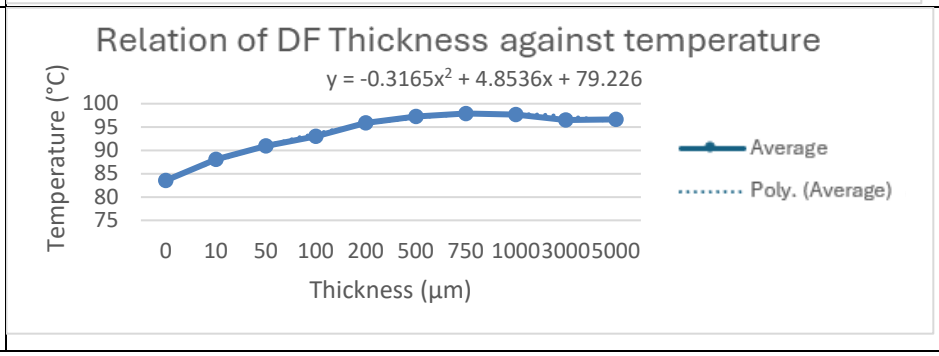

Figure 31. **Set of equations for converting Near-Infrared and Thermal output to thickness values.**

By applying the equations shown in Figure 31 to the temperature values captured on the thermal image, the pixel values are then converted to thicknesses in micrometers.

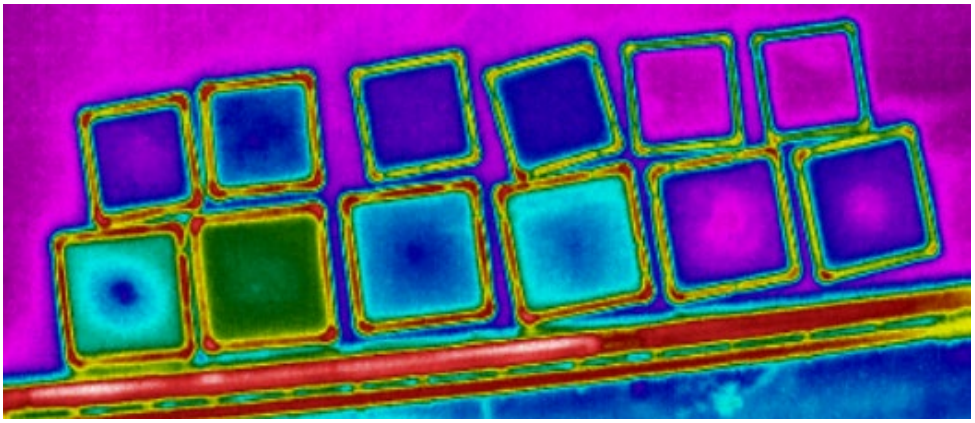

Figure 32. **Highest contrast of temperatures observed among the thicknesses. Equations used to convert temperature to thickness values are shown on the equations below.**

DF thickness values in micrometers can be obtained by applying the conversion equations for each of the DF. This technique normalize the thickness values of DF even if different DF types were imaged at the same time (or captured on the same image).

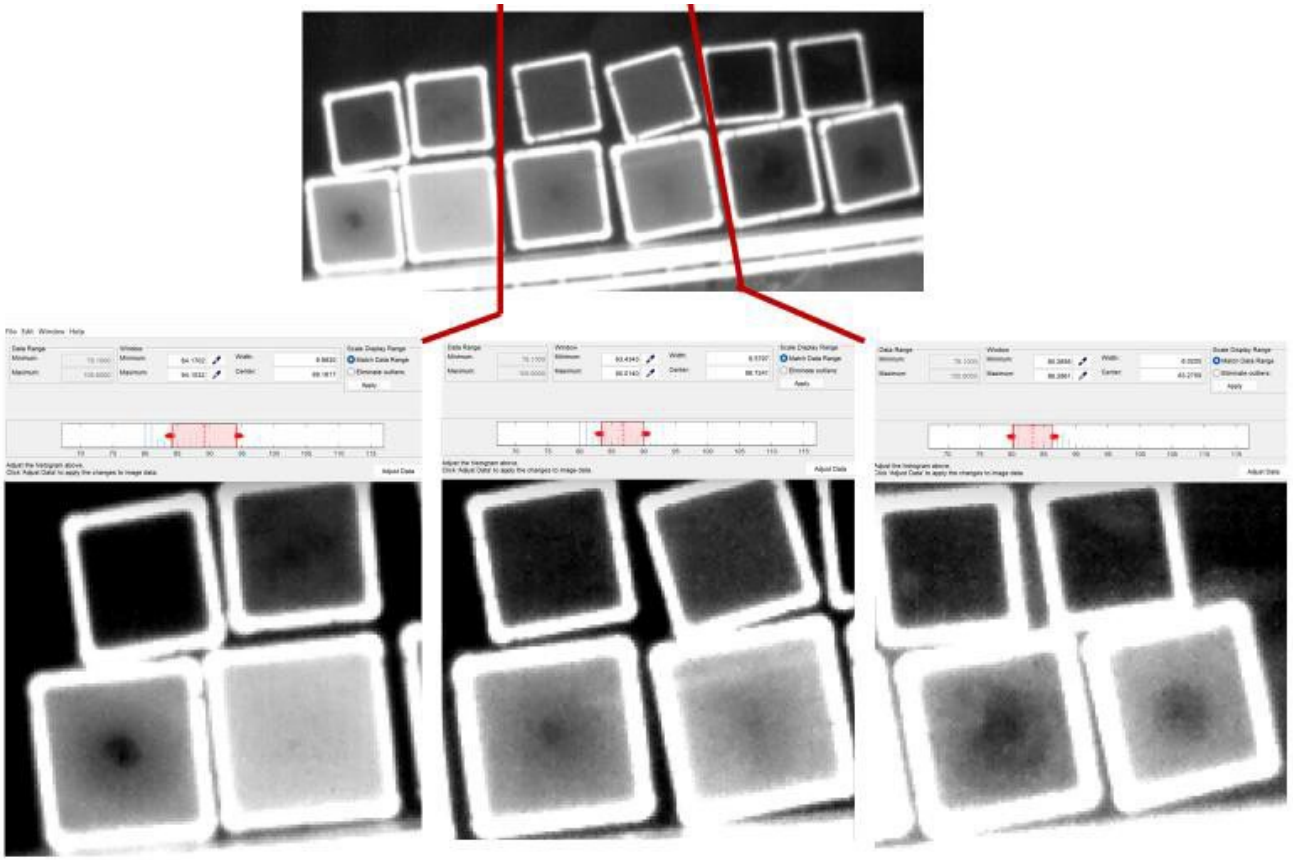

Figure 33. **Conversion from temperature values to thickness values in microns.**

Application of the transformation equation equalizes the thicknesses of the DFs. For these subsets of images, the brighter the pixel the thicker it is, and the 3 sets of thicknesses in the targets of the different DFs are now relatively the same regardless of the temperature. The goal of transforming the thermal images to quantitative thickness values will be difficult without knowing the type of DF. Further work is needed to experiment under a wider set of ambient temperature and illumination conditions to build a full catalog of environments. Another identified factor playing a role on the heat storage of the DFs is a timing effect of the incoming radiation; heat storage affects how quickly a surfactant equalizes in temperature with the surrounding environment.

An analysis on the continuity of the thermal values over time was conducted on each of the thickness targets, and it was identified that the presence of clouds affecting the incoming radiation affects largely the amount of heat stored in the DFs. The goal of transforming the thermal images to quantitative thickness values will be difficult without knowing the type of DF. It would also need to run an experiment much longer under a wider set of ambient temperature and illumination conditions to build a full catalog of environmental factors. It was identified that another factor playing a role on the heat storage of the DFs is a timing effect of the incoming radiation. An analysis on the continuity of the thermal values over time on each of the thickness targets was conducted, and it was identified that the presence of clouds affecting the incoming radiation affects largely the amount of heat stored in the DFs. These graphs represent a time series of the temperatures of each target over time. The ambient temperature (air temperature around the Ohmsett tank) does not change up/down as drastically as the temperature stored by the DFs as shown in these graphs below. This effect is caused by the passing clouds that produce the sun radiation to be intermittent over the floating DF which demonstrate the remarkable capacity of these fluids to store/dissipate heat.

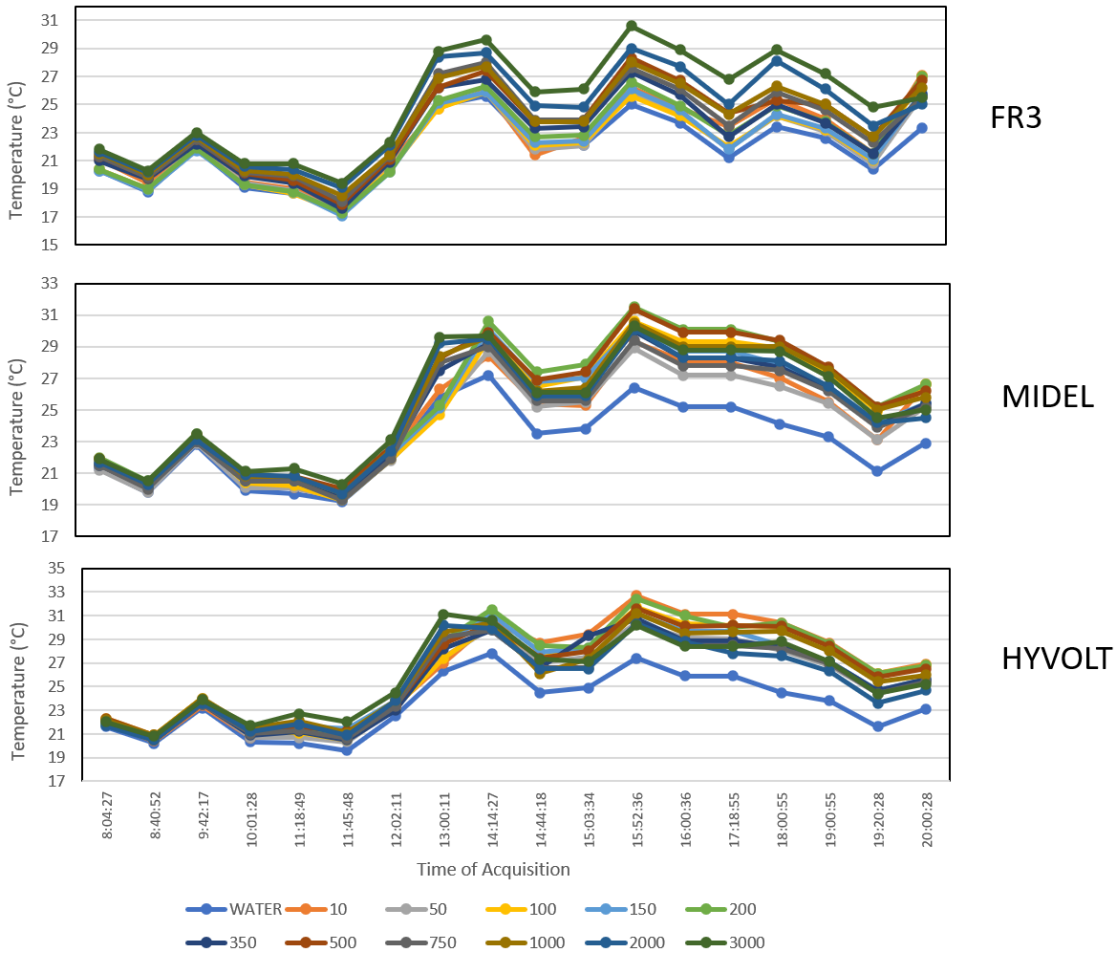

Figure 34. **Measurement of temperature values of 3 DF types and thicknesses from 0 to 3000um over time.** All temperature values vary up/down simultaneously over time (regardless of the thickness or DF type) mostly due to interruption of the sun radiation caused by the intermittence passage of clouds.

The range of temperatures per DF is summarized on table 3:

Table 3. Range of Temperatures

Dielectric Fluid	Minimum (°C)	Maximum (°C)
Hyvolt	19.6	33.7
Midel	18.8	31.4
Cargil	17.3	30.5

The variability observed on the timelapse graphs demonstrates that there is a time component on the heat storage of the DF, where the temperature of the DF will be depending on the incoming radiation of the sun over time and not only at the time of the imagery collection snapshot. Further work is necessary to understand the timing of the heat storage to convert the temperature values to thicknesses more accurately in a quantitative fashion. However, this study suggests that the Hyvolt Dielectric Fluid is more efficient at storing heat than both Midel and Cargil.

16. Results from first week of Ohmsett testing in 2024

Ohmsett testing was successful to demonstrate that the multispectral remote sensing of Dielectric Fluids can be used to detect not only presence/absence of DFs but also the relative (qualitative) thickness of the targets. The near-infrared channel on the Altum-PT sensor was capable of discerning when targets had or not dielectric fluid. An algorithm combining the near-infrared and the thermal bands on the Altum-PT was utilized to generate an output where one can clearly identify the areas of the targets where thicker layers of DF are present.
An example of a qualitative classification of the DF thickness is shown below in Figure 35. Here it was combined the near-infrared and the thermal bands to generate a matrix that is then multiplied by the equation previously shown in Figure 31. Then a color palette was applied to represent the different thickness values in a qualitative output. By doing this, all the target pixels are now converted to DF thicknesses in micrometers. This model algorithm can be used to characterize the thickness and volumes of DF in a range.

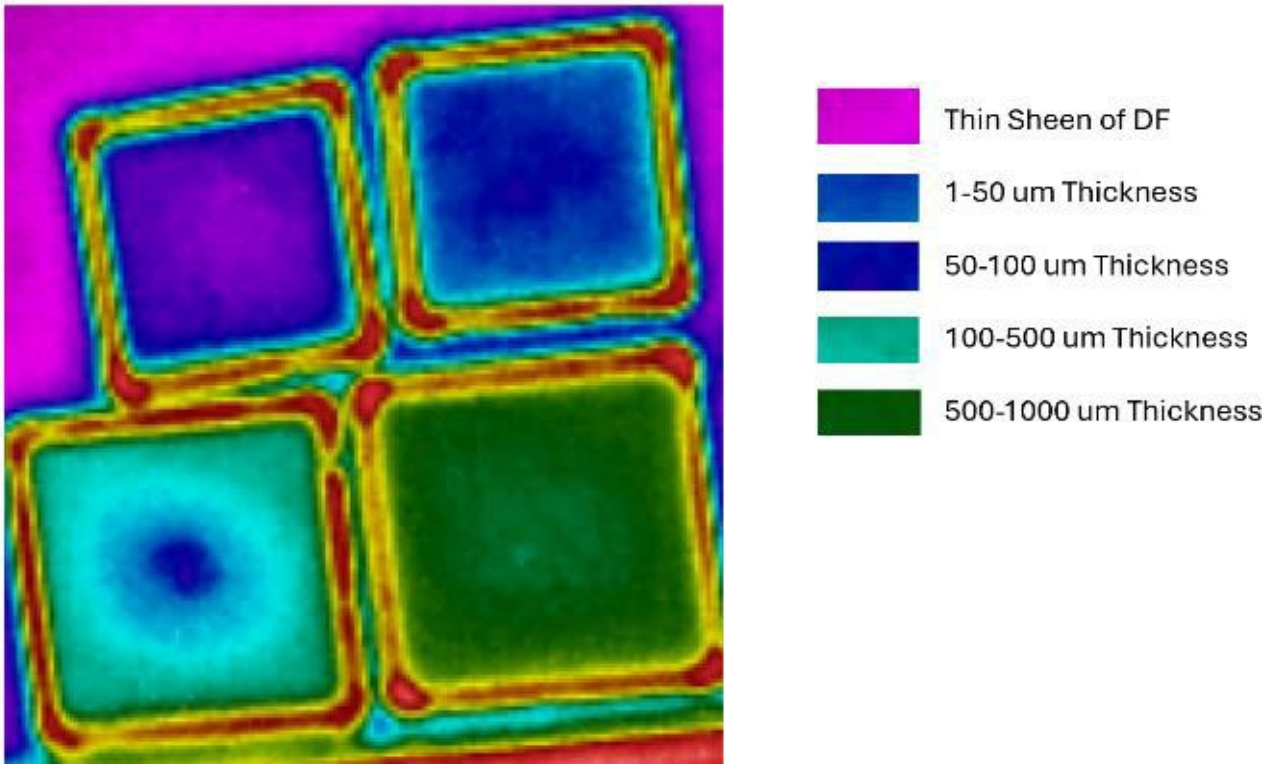

Figure 35. Quantitative output from the algorithm that calculates DF thicknesses.

To pursue the quantitative classification of the thickness will be to have information regarding not only about the temperature of the water without DF, but also about the incoming solar radiation and the type of DF under analysis. A quantitative classification would be ideal for estimating the total volumes of oil concentration per area, however from an emergency response operation perspective a simple qualitative evaluation of the thickness of the floating DF could be very informative

An example of a qualitative classification is shown in Figure 36. In this case a linear representation of the color is applied to the thickness range assignments.

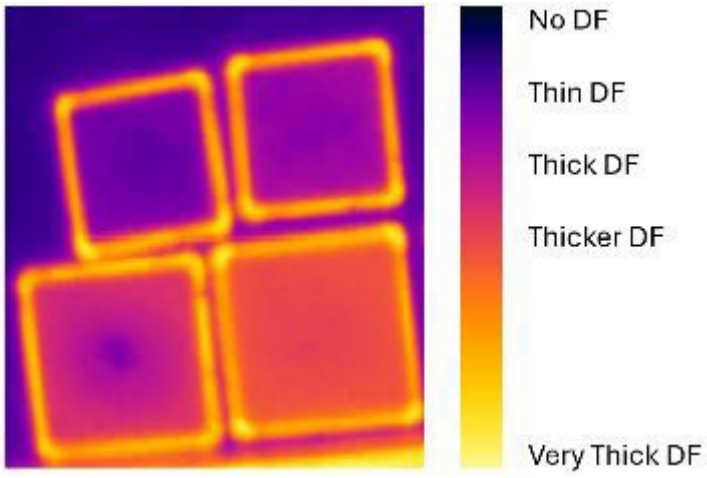

Figure *36.* Qualitative Classification of DF thicknesses.

17. Ohmsett Testing August 2025

The main objective for this week of testing was to demonstrate the implementation of the algorithms in our system to perform near-real time quantitative classifications of the DFs. From August 11-15 Water Mapping carried out the Ohmsett experiment for remote sensing of dielectric fluids using UAS. This experiment consisted of the setup of multiple targets with various thickness for the 3 dielectric fluids under research (Midel, FR3, and Hyvolt) to measure remote sensing properties of the different dielectric fluids. Targets were placed on the side of the tank with thicknesses ranging from 0 to 3000um. These targets were used to measure reflectance and temperatures from the sensor Altum-PT mounted on the UAS (Figure 37). Floating targets inside the tank were placed with a range of thicknesses from 50 to 1000um as shown in Figure 38.

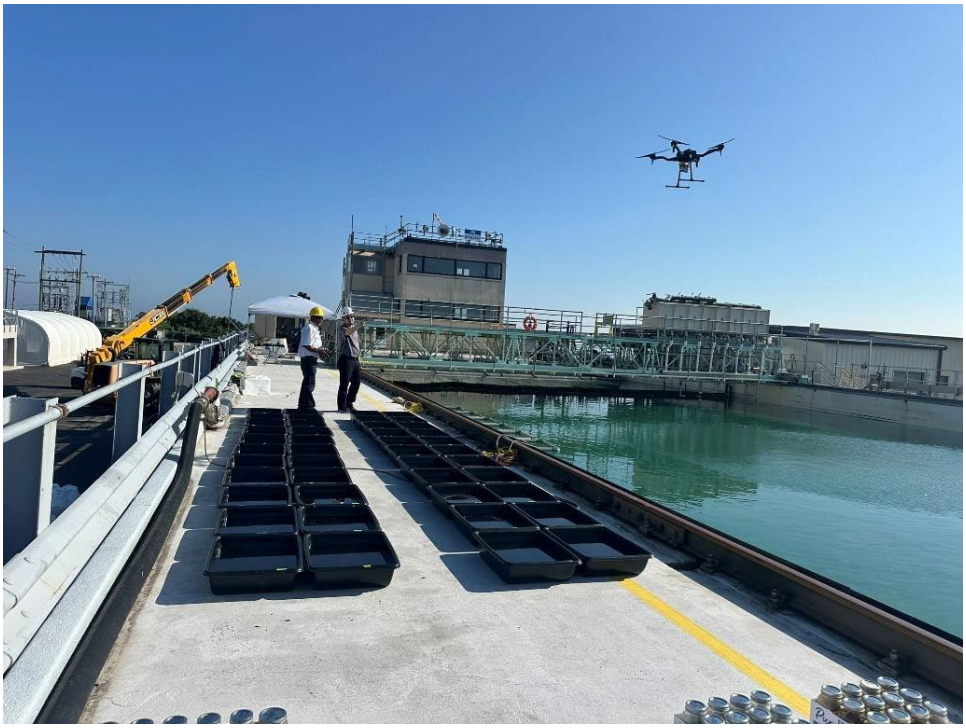

Figure *37.* Setup of dielectric fluid targets with known thicknesses on the side of the Ohmsett tank.

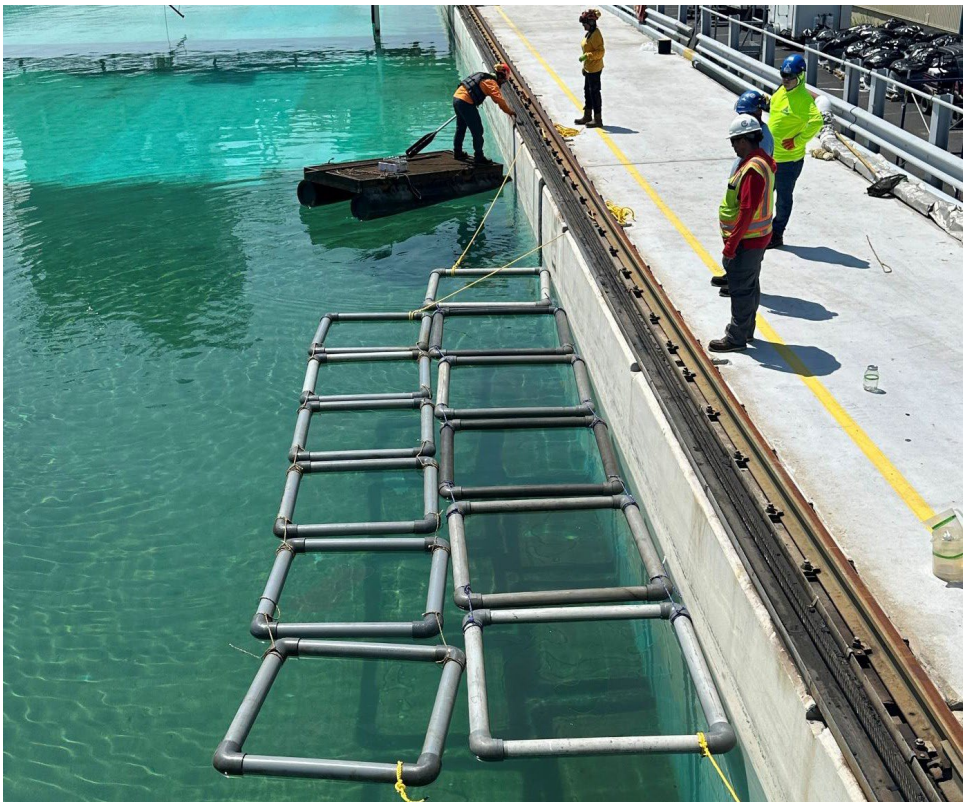

Figure *38.* Floating targets inside the tank.

Thicknesses of the targets on the plastic containers and inside the tank (floating) were set as displayed on Figure 39.

DECK TOTES

HYVOLT	MIDEL	FR3	HOOPS
0	0	0	0
10	10	10	10
50	50	50	50
100	100	100	100
150	150	150	150
200	200	200	200
500	500	500	500
750	750	750	750
1000	1000	1000	1000
2000	2000	2000	2000
3000	3000	3000	3000

Thicknesses in plastic containers (um)

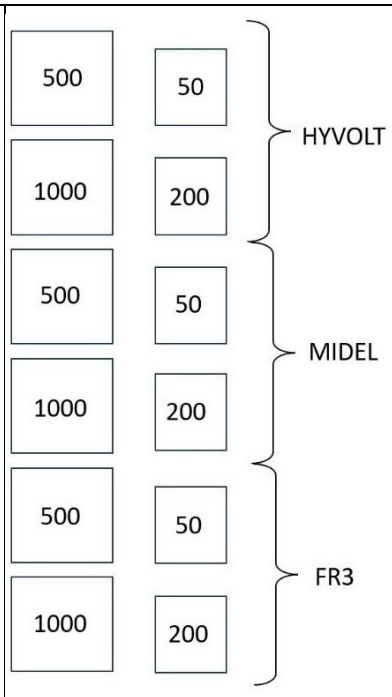

Thicknesses in floating targets (um)

Figure *39.* Thicknesses (in micrometers) of Targets on plastic containers

A UAS with the multispectral sensor was deployed for a total of 33 flights as shown in Table 4.

Table 4. Flights deployed with the multispectral sensor

FLIGHT #	DATE	TIME	TARGET
001	8/11/2025	9:50	Test before oil
002	8/11/2025	10:59	Test before oil
003	8/11/2025	12:15	Oil on Tank (squares)
004	8/11/2025	13:13	Oil on Tank (squares)
005	8/11/2025	14:09	Squares and Totes
006	8/11/2025	14:37	Squares and Totes
007	8/11/2025	15:00	Squares and Totes
008	8/12/2025	8:01	Squares and Totes
009	8/12/2025	8:31	Squares and Totes
010	8/12/2025	9:02	Squares and Totes
011	8/12/2025	10:03	Squares and Totes
012	8/12/2025	11:05	Squares and Totes
013	8/12/2025	12:08	Squares and Totes
014	8/12/2025	14:20	Squares and Totes
015	8/12/2025	14:56	Squares and Totes
016	8/13/2025	8:04	Squares and Totes
017	8/13/2025	9:03	Squares and Totes
018	8/13/2025	9:58	Squares and Totes
019	8/13/2025	11:07	Change Squares to oil
020	8/13/2025	12:07	Squares
021	8/13/2025	13:40	Squares
022	8/13/2025	14:30	Squares
023	8/13/2025	15:08	Squares
024	8/13/2025	16:03	Squares
025	8/13/2025	17:05	Squares
026	8/13/2025	17:59	Squares
027	8/13/2025	18:30	Squares (thunderstorm)
028	8/14/2025	8:00	Squares (after storm)
029	8/14/2025	9:03	Squares
030	8/14/2025	9:53	Squares
031	8/14/2025	10:44	Mike photos
032	8/14/2025	13:32	Clean tank (south side)
033	8/14/2025	13:40	Dropped oil on south of the tank

For each flight temperatures and reflectance of targets were measured from the imagery collected from the multispectral sensor with the format shown in table 5:

Table 5. Flight temperatures and reflectance of targets

Drone Settings	Humidity 50%	Emmisivity .95	Target field set at 25m		Data Set 1 Image Altitude 40M	

All data is metric except wind speed is MPH

Flight #	Time	Air Temp	Water Temp	Rail Temp	Concrete Temp	Wind	HyVolt 50 µm
2	10:59	26.1					
3	12:15	27.2	25	39	36.3	7	28.5
4	13:13	27.8	27.5	35.9	38.4	10	27.6
5	14:09	27.8	26.6	32.4	36.3	14	26.2
6	14:37	27.8	27.4	37.7	38.8	14	28.2
7	0.625	28.3	27.5	39.3	38.7	15	28.6

Flight #	HyVolt 200 µm	HyVolt 500 µm	HyVolt 1000 µm	Midel 50 µm	Midel 200 µm	Midel 500 µm	Midel 1000 µm	FR3 50 µm	FR3 200 µm	FR3 500 µm	FR3 1000 µm
2											
3	29.2	31.3	33	28.5	28.9	29.8	30.06	28.6	28.6	29	29.1
4	28.8	31.6	33.6	27.8	28.7	30.2	31	26.9	27.2	27.4	28.1
5	28	30.9	32.6	26.7	27.9	29.2	29.7	25.4	25.2	25.7	25.6
6	30.5	33.2	34.8	28.8	30.3	31.8	32.4	28.2	28.2	28.5	28.4
7	30.3	32.8	33.8	28.7	30.2	30.9	31.6	27.2	27.4	27.6	27.9

Over 1000 UAS multispectral images were collected during the experiment. An example of thermal imagery data is shown in Figure 40. For this example, temperature ranges for all targets are from 10 to 57 Celsius degrees.

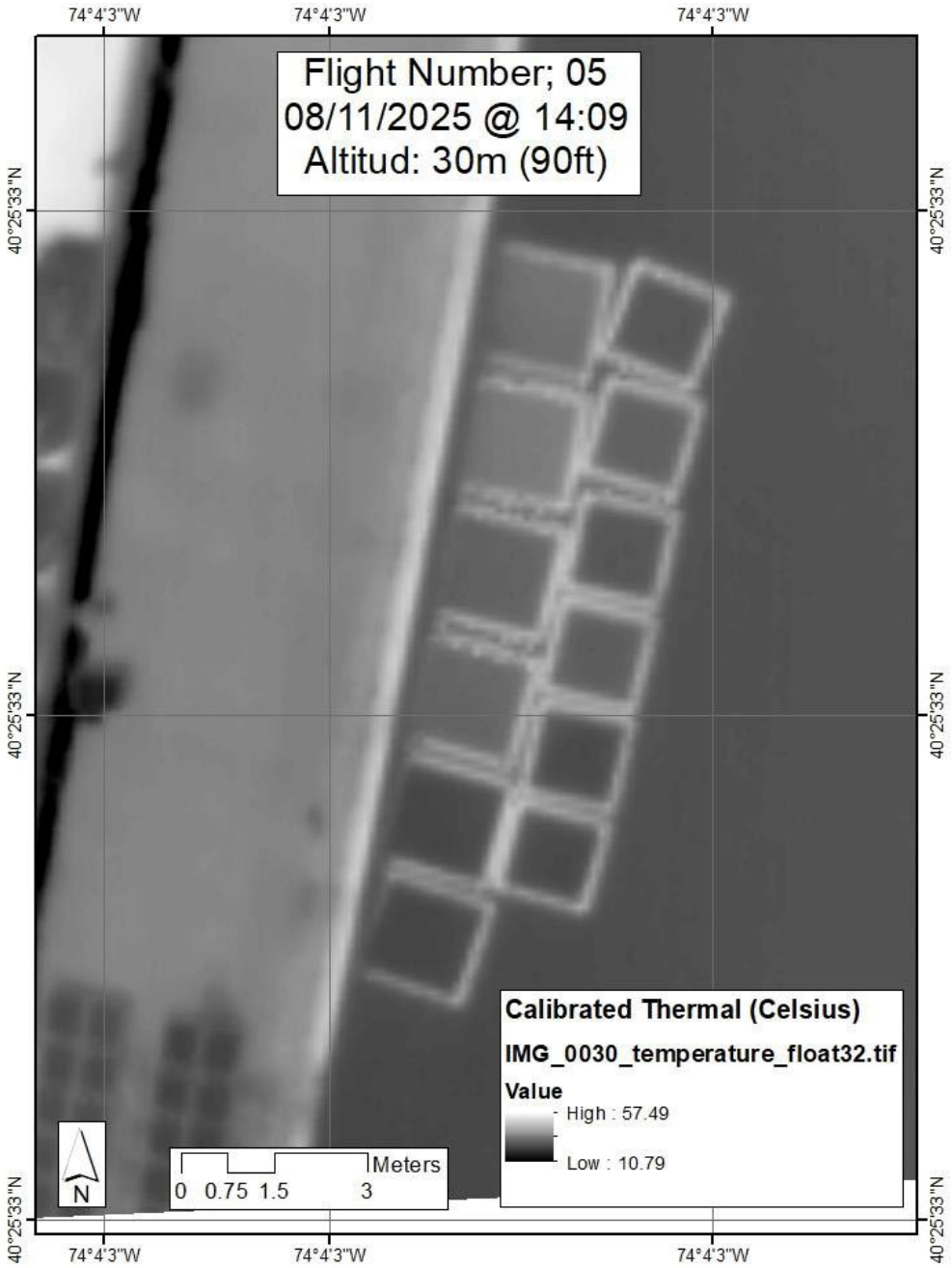

Figure 40. Thermal image of Flight 05.

After the multispectral image is collected by the UAS and the data is retrieved from the sensor's SD card, imagery is then copied to the processing computer where our algorithm is installed. Data is then selected by the algorithm to convert multispectral imagery into thickness values and to generate a map of the classified DF targets. The example shown in figure 41 was processed in 16 minutes after the data was collected. This map is generated semi-automatically by the algorithm and delivered in various formats for distribution. This map below is shown as appeared on a GIS software package (Arcmap) where the classification output is reprojected and geo-referenced.

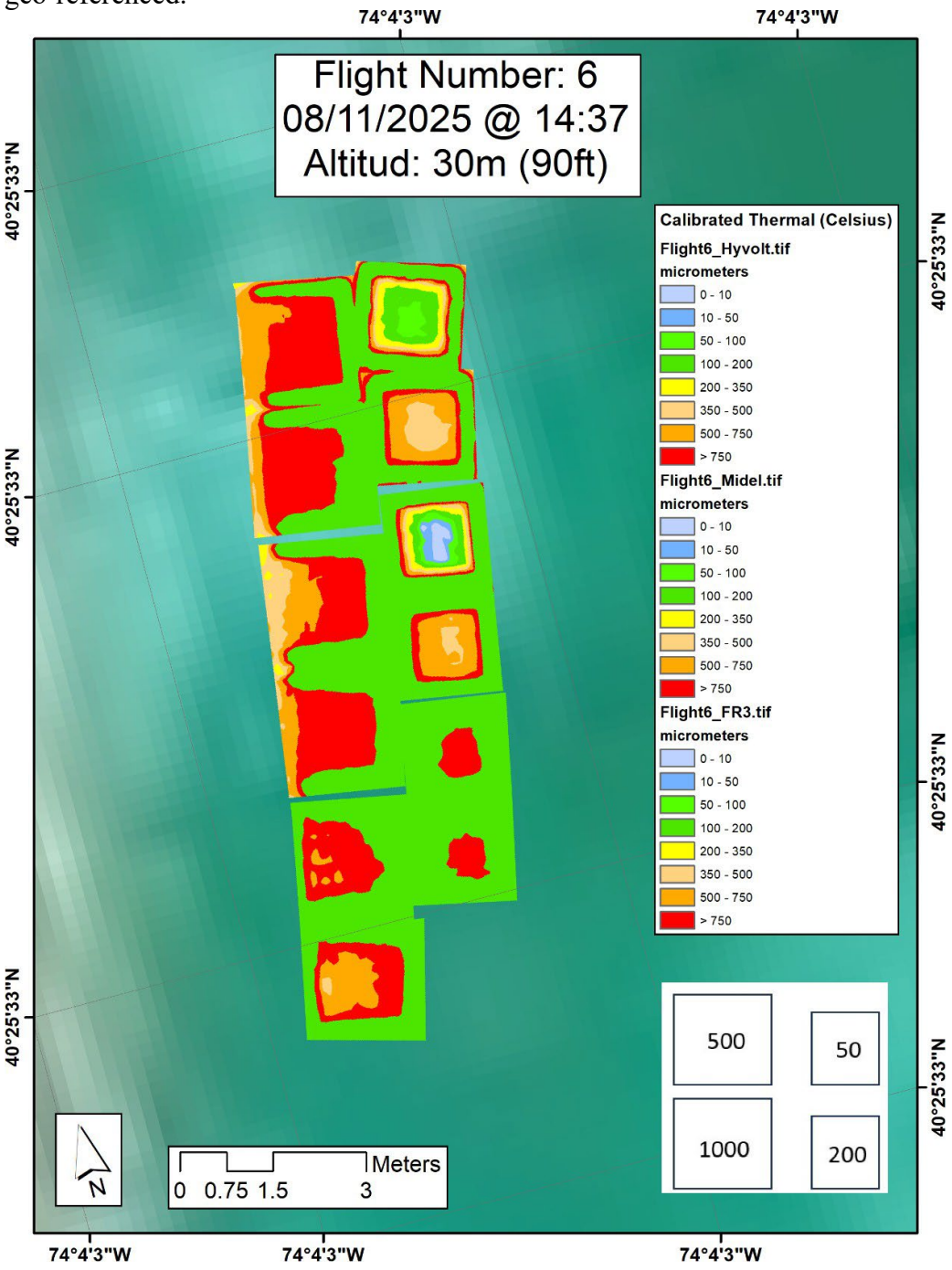

Figure 41. Near real time report generated from the DFs detected on August 11, 2025 at 14:37 hrs.

Classification outputs formats included georectified Geotiff and JPG for GIS software packages like ArcMap (ESRI) or QGIS (open source). Also, KML outputs are produced for visualization in Google Earth as displayed in Figure 42. Additional examples of Near real time classifications are added on Appendix C.

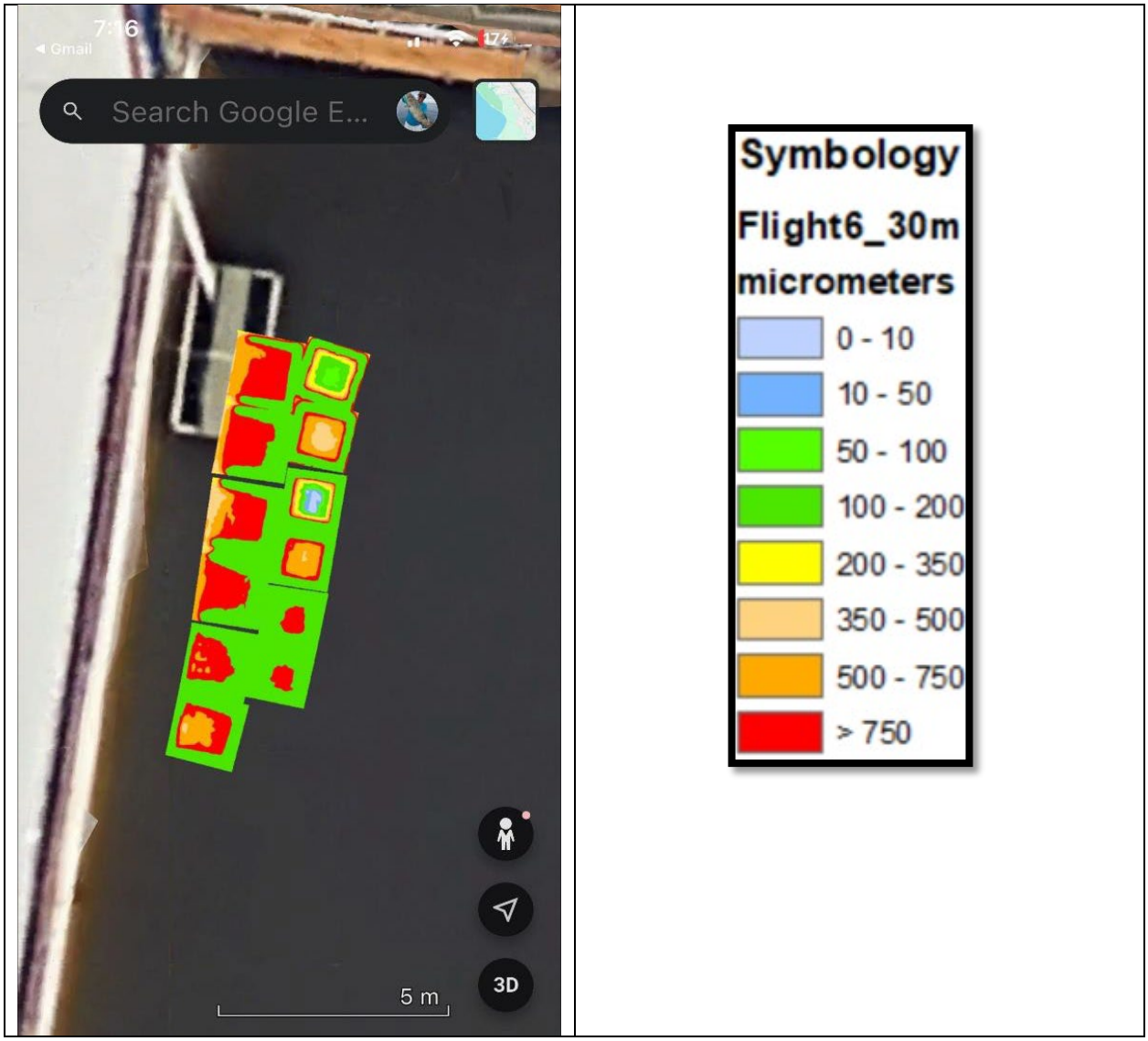

Figure 42. Near real time report generated from the DFs detected on August 11, 2025 at 14:37 hrs. for Google Earth displayed on a mobile device

18. Conclusions and Recommendations

The results of this project demonstrated that due to the physical/chemical properties of DFs, thermal and multispectral sensors can be used to detect DFs floating over water, however optical/visual sensors where not suitable to neither detect nor characterize DFs. While the Near-Infrared sensor demonstrated a remarkable capacity to detect presence/absence of DFs, the thermal sensors demonstrated their capability to characterize qualitatively and quantitatively their thickness under a range of ambient conditions.

By combining the channels RedEdge, Red, and Near-Infrared from the Altum-PT one can generate an algorithm that produces a false composite color image that shows the contrast of the floating DF more distinctively as shown on the figure below. This result confirms the capacity of a higher radiometric resolution of the multispectral sensor like the Altum-PT (superior to his predecessor RedEdge) for detecting presence/absence of DF.

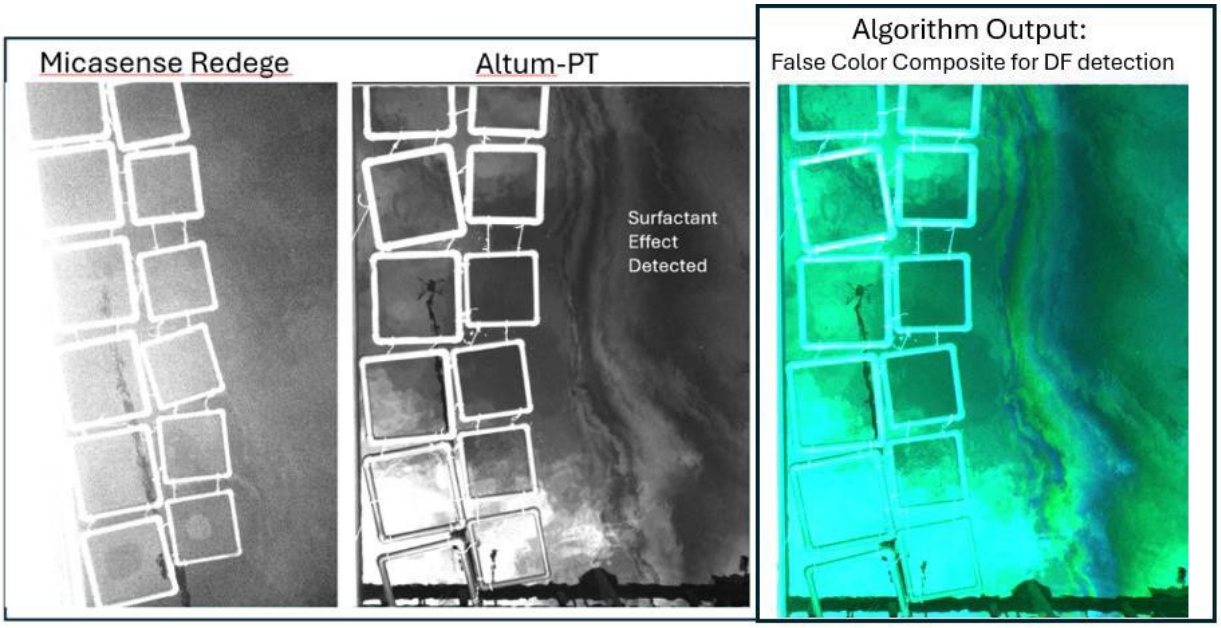

Figure 43. Near-Infrared channel from simultaneous images collected by MicaSense RedEdge (left) low resolution vs Altum-PT1 (center) high resolution. The higher spatial and radiometric resolution of the Altum allows detection of features that are under-detected by the RedEdge. The false color composite (right) enhances the contrasting of floating thin sheen of DF (undetected on any other sensors wavelength).

The positive results from the Ohmsett experiment shed light towards operationalization of remote sensing mounted on aerial sensors for emergency response operations of DFs spills. The reflectance of DFs in the near-infrared wavelength shows a contrast of .08 reflectance units higher than the clean water under day light. Due to the physical/chemical properties of DFs to store heat, detection of thicker layers of DFs could be observed even at dark after few hours after sunset using the infrared (thermal) sensor.

Measurement of temperature increases as the DF thickness increases (direct correlation) and

based on this property the development of our algorithm for rapid processing achieve a thickness classification of the DFs in the targets in near-real time. This detection is highly dependent on ambient conditions as reflectance and temperatures are affected by illumination and ambient temperature. The operationalization of detection was optimal during day light on range of background water temperature from 15°C to 35° C, however the main variable affecting detection and quantitative classification was the ambient light which is directly correlated to the sun radiation.

Key Findings.

Outputs were processed and exported for GIS and online applications (Google Earth) operated from mobile platforms (smart phone and tablet). The operationalization of our algorithm that transforms reflectance values from the multispectral sensor to DFs thicknesses produced outputs readable on portable platforms in near-real time as required on the case of an incident response. Regardless of the accuracy of the thickness classification, having a tool that could deliver tactical information for oil spill responders would be crucial for effectively mitigate the effects of a spill incident of DFs. Moreover, this tool could be a crucial asset for the assessment of a DF spill. In summary the highlight key findings of this project are:

1) DF presence/absence detection can be achieved by using the Near-infrared wavelength with a reflectance cutoff threshold of .08

2) Calibrated radiometric infrared imagery (thermal) can be used to quantitatively classify DF thickness.

3) A better understanding of the sun radiance effect on the DF has been accomplished:

    a. Hyvolt DF stores (and dissipates) more heat than Midel, and Midel more than FR3.
    b. Sun irradiance of infrared light is crucial for thickness classifications of floating spilled DFs.
    c. Because of their different heat storing capacities, different conversion equations should be used to transform temperature to thickness values (depending on the type of DF and the range of ambient temperatures).
    d. Emulsified DF reacts differently (thermally) than un-emulsified oil and its shown colder than emulsified DF. This is a factor to consider to quantify DF thickness and multispectral imagery can be used to differentiate between emulsified and non-emulsified DF.
    e. These findings are important to better interpret infrared imagery of floating DF quantitively.

4) The near-real time semi-automated algorithm has been used to generate thickness classifications of DF available on various formats readable on GIS applications and mobile platforms.
5) These findings highlight the capacity to operationalize multispectral/thermal imaging for responding to DF oil spills inshore/offshore.

19. References

Garcia-Pineda O. 2019. System and algorithm development to estimate oil thickness and emulsification. (Bureau of Safety and Environmental Enforcement Oil Spill Response Research Project # E17PC00021).

Garcia-Pineda O, Balsley A, DiPinto L, Kinner K, Panetta P. 2022. UAS Characterization of Oil in Ice – Volume I: Laboratory Results. U.S. Coast Guard Research and Development Center. https://apps.dtic.mil/sti/pdfs/AD1165443.pdf

Garrett E. Barter, Latha Sethuraman, Pietro Bortolotti, Jonathan Keller, David A. Torrey, Beyond 15 MW: A cost of energy perspective on the next generation of drivetrain technologies for offshore wind turbines, Applied Energy, Volume 344, 2023, 121272, ISSN 0306-2619, https://doi.org/10.1016/j.apenergy.2023.121272.

Kampel M, Freitas LB, Frouin RJ, Lorenzzetti JA. 2014. Automatic detection of marine surfactants by MODIS sunglint imagery: a study case of biogenic films off the southeastern coast of Brazil. In: Frouin RJ, Pan D, Murakami H, editors. *Ocean remote sensing and monitoring from space*. Proc SPIE. Bellingham (WA): SPIE; 9261:92611C. doi:10.1117/12.2073949.

Klonowski WM, Lynch MJ, Fearns PRCS, Clementson L. 2003. Hyperspectral remote sensing of Western Australian coastal waters. In: Frouin RJ, Gilbert GD, Pan D, editors. *Ocean remote sensing and imaging II*. Proc SPIE; 2003 Aug 3–8; San Diego (CA). Bellingham (WA): SPIE; 5155. doi:10.1117/12.512190.

Lyutikova MN, Ridel AV, Konovalov AA. 2023. Dielectric liquids: past, present, future (Review). *Power Technol Eng* **57**, 615–622. https://doi.org/10.1007/s10749-024-01709-x

Oil Fact Sheets for Spill Responders | response.restoration.noaa.gov. 2025. Noaagov. [accessed 2026 Jan 19]. https://response.restoration.noaa.gov/oil-and-chemical-spills/oil-fact-sheets-spill-responders.

Roslan RNR, Hanif NM, Othman MR, Wan Azmi WN, Yan XX, Ali MM, Mohamed CAR, Latif MT. 2010. Surfactants in the sea-surface microlayer and their contribution to atmospheric aerosols around coastal areas of the Malaysian peninsula. *Mar Pollut Bull*. 60(9):1584–1590. doi:10.1016/j.marpolbul.2010.04.004.

U.S. Department of Energy. How Do Wind Turbines Work? Office of Energy Efficiency and Renewable Energy. https://www.energy.gov/eere/wind/how-do-wind-turbines-work.

20. Appendix A: Technical Summary

REPORT TITLE: Dielectric Fluids Remote Sensing Testing

CONTRACT NUMBER(S): 140E0124P0011

FISCAL YEARS(S) OF PROJECT FUNDING: FY2025

CUMULATIVE PROJECT COST: $226,500.00

COMPLETION DATE OF REPORT: 11 November 20225

BSEE COR(S): Jay Cho

BSEE CO(S): Catherine Robertson

PROJECT MANAGER(S): Diana Garcia

AFFILIATION OF PROJECT MANAGER: Water Mapping, LLC

ADDRESS: 1047 Aquamarine dr, Gulf Breeze, FL

PRINCIPAL INVESTIGATOR(S): Oscar Garcia, PhD

KEY WORDS: Dielectric Fluid, Remote Sensing, Oil, Multispectral.

21. Appendix B: Temperature data collected

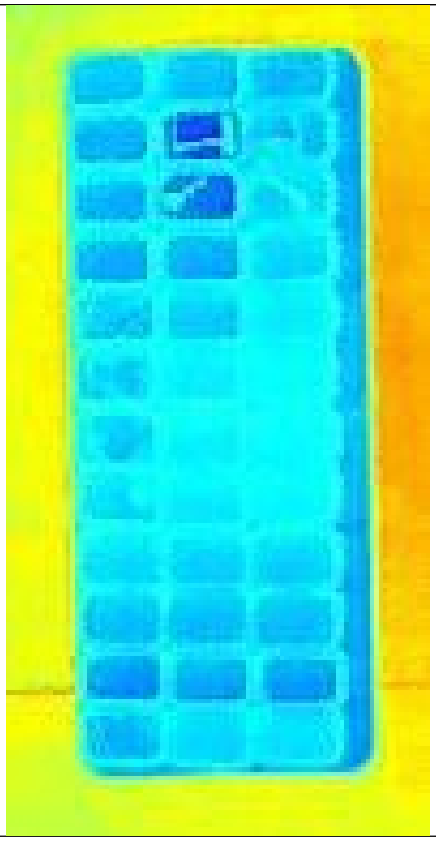

Image	DJI_20240815064014_0002_T		
Hour	06:40:14		
Water Temp	68°F		
	FR3 (°F)	MIDEL (°F)	HYVOLT (°F)
0	68.2	68.4	68.4
10	67.6	67.3	68.2
50	67.5	66.6	69.3
100	67.5	67.5	68.5
200	67.5	68.2	69.3
500	67.6	69.1	69.3
750	67.6	68.9	69.3
1000	68.4	68.9	69.4
3000	68.4	68.4	68.9
5000	68.2	68.2	68.5
E1	67.5	68.2	68
E2	68	69.3	69.3

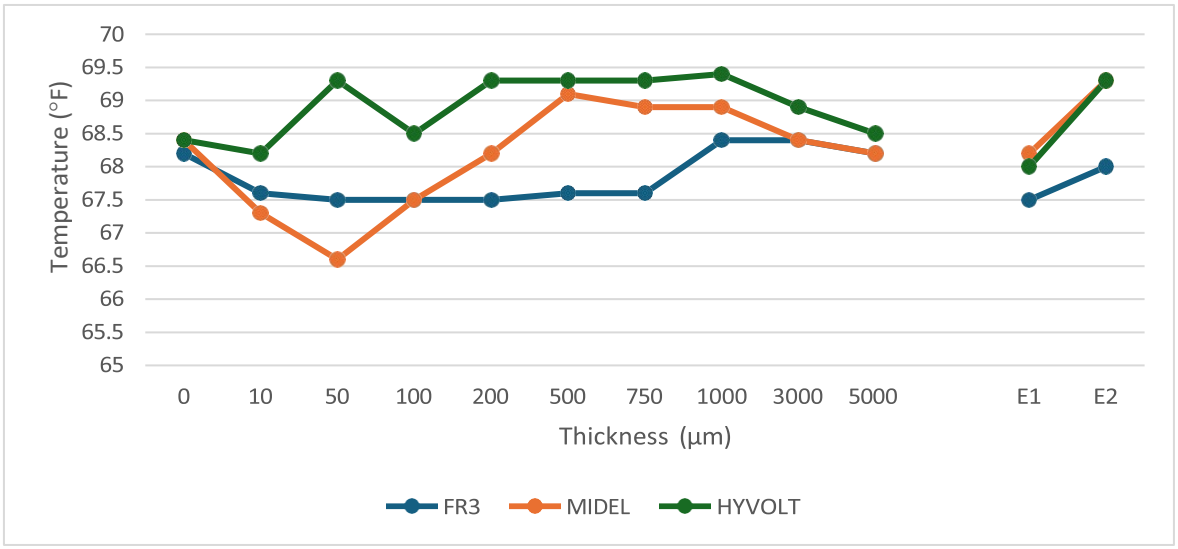

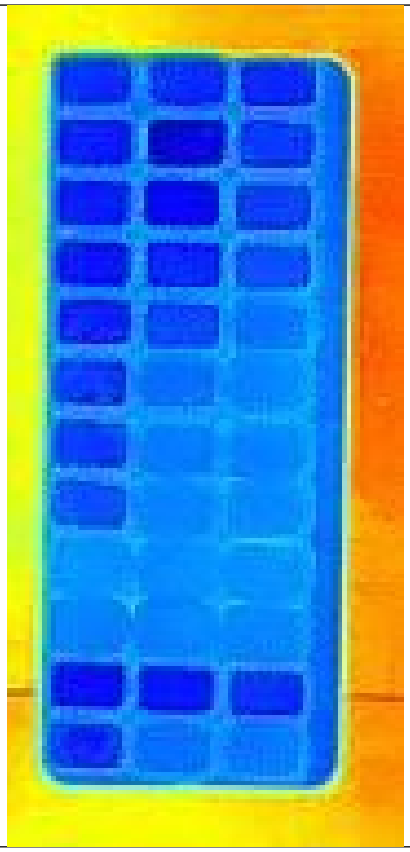

Image	DJI_20240814211752_0002_T		
Hour	21:17:52		
Water Temp	69°F		
	FR3 (°F)	MIDEL (°F)	HYVOLT (°F)
0	68.9	69.1	69.1
10	68.4	66.7	69.4
50	68.4	67.6	69.3
100	68.4	68.9	70
200	68.5	69.3	70.7
500	69.3	70.7	71.1
750	68.9	70.9	71.1
1000	68.8	70.9	71.1
3000	71.2	71.2	71.2
5000	71.1	71.2	71.2
E1	68.4	68.5	69.3
E2	68.9	71.1	71.2

Temperature Vs Thickness (Water @ 69°F)

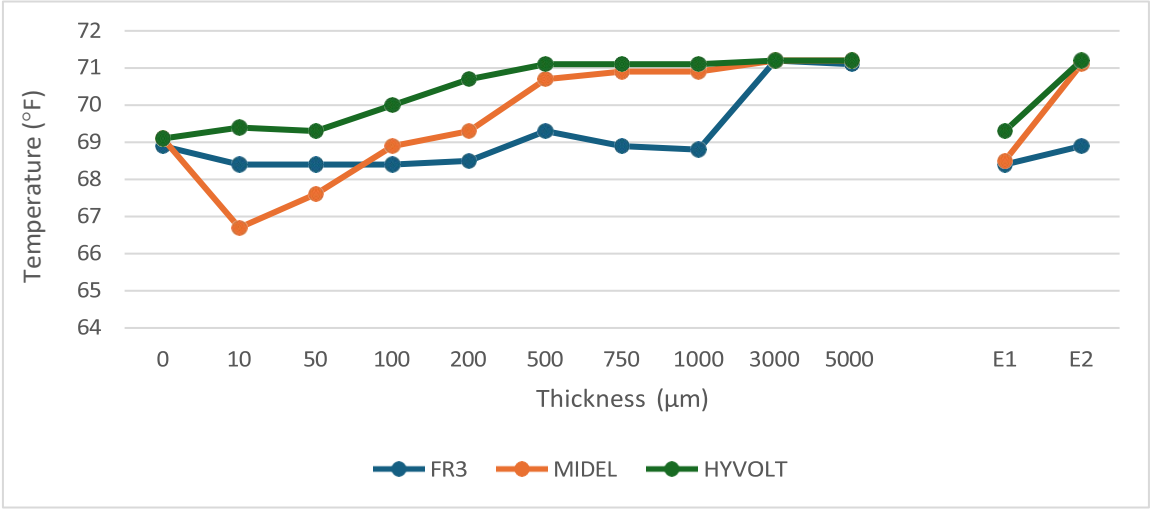

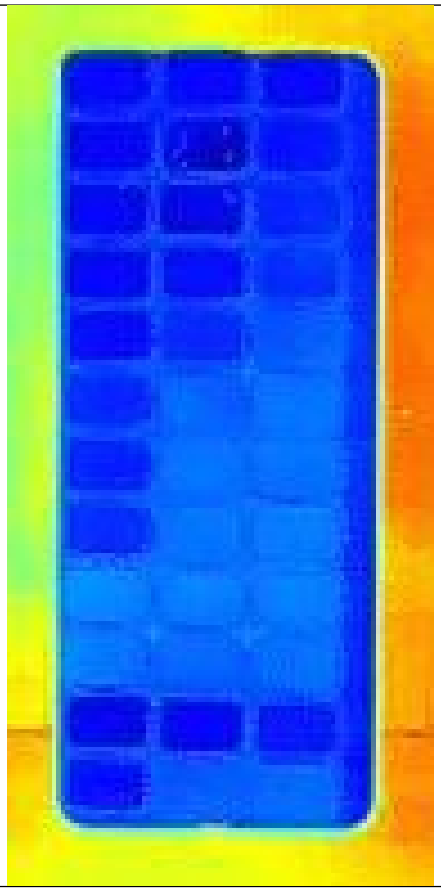

Image	DJI_20240814202425_0001_T		
Time	20:24:25		
Water Temp	69°F		
	FR3 (°F)	MIDEL (°F)	HYVOLT (°F)
0	68.9	69.1	69.1
10	68.4	66.6	69.8
50	68.4	68.4	70.2
100	68.4	69.3	70.3
200	68.5	70.2	71.1
500	69.8	71.1	71.8
750	69.4	71.8	71.8
1000	70.2	71.8	72
3000	72	72.1	72
5000	71.8	71.2	71.8
E1	68.4	68.5	70.2
E2	69.1	71.6	72

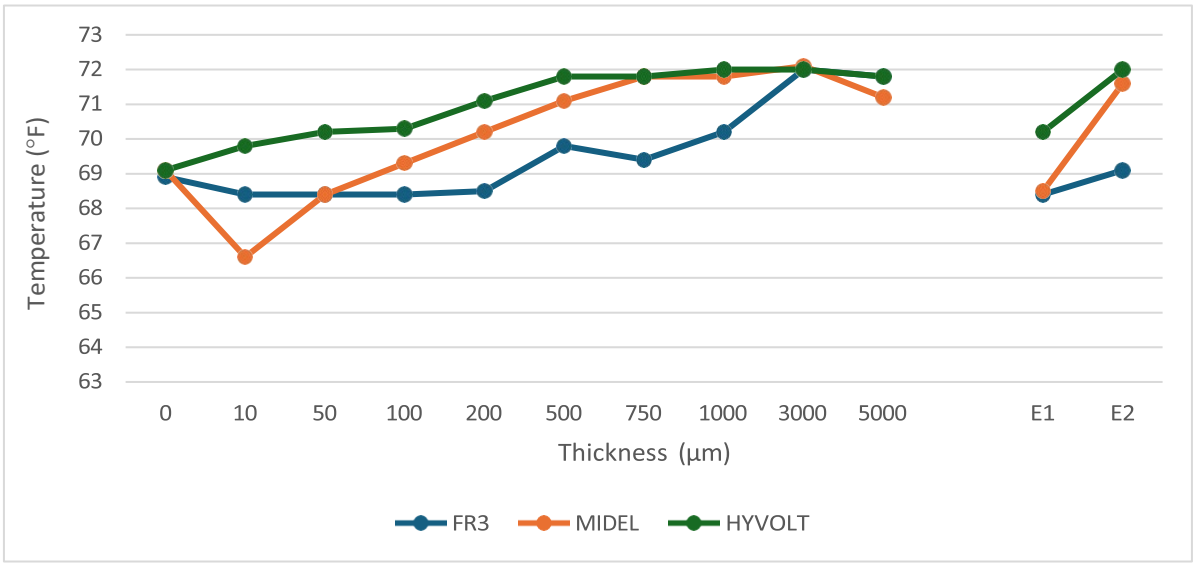

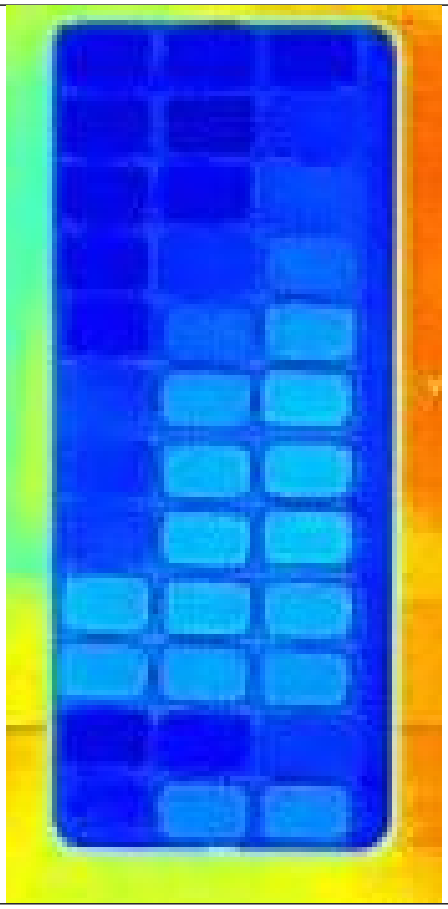

Image	DJI_20240814194758_0002_T		
Time	19:47:58		
Water Temp	69°F		
	FR3 (°F)	MIDEL (°F)	HYVOLT (°F)
0	69.4	69.8	69.8
10	69.3	69.1	71.8
50	69.3	70	72.1
100	69.3	71.8	72.9
200	70.2	72.7	73.9
500	71.6	73.9	74.7
750	71.2	74.3	74.7
1000	72	74.7	74.7
3000	74.5	74.7	74.7
5000	73.9	74.3	74.5
E1	69.4	70.7	72.1
E2	71.6	73.9	73.9

Temperature Vs Thickness (Water @ 69°F)

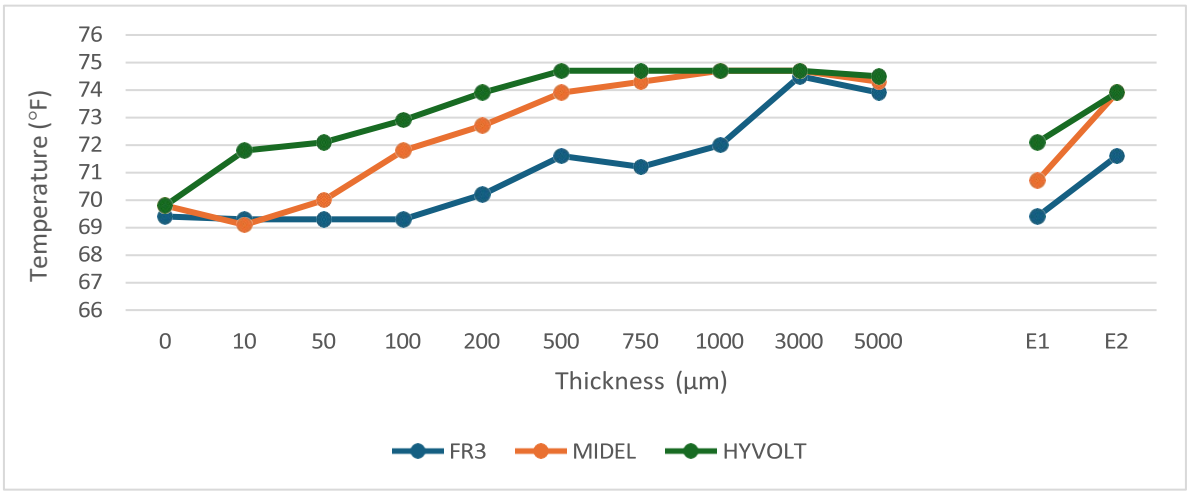

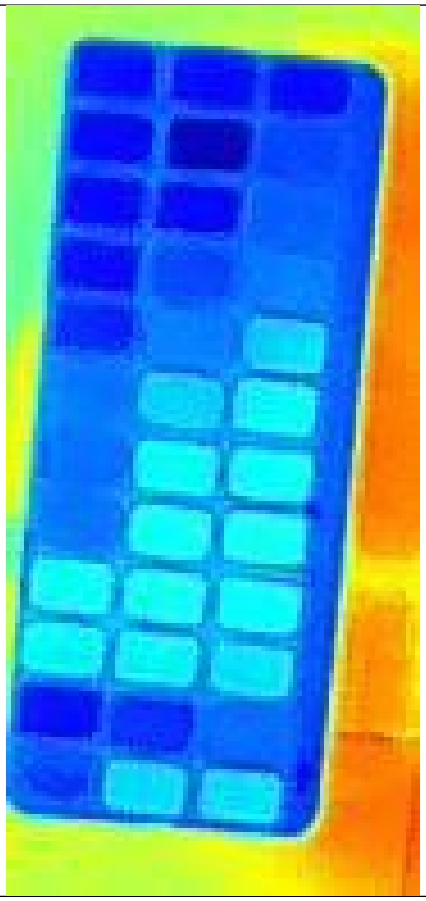

Image	DJI_20240814190430_0001_T		
Time	19:04:30		
Water Temp	72°F		
	FR3 (°F)	MIDEL (°F)	HYVOLT (°F)
0	72.1	72.5	72.5
10	72	70.9	74.7
50	72	72.1	74.8
100	72.1	73.9	76.1
200	72.9	75.4	77.4
500	74.7	77.2	78.3
750	74.7	78.1	78.4
1000	75.2	78.4	79
3000	78.3	78.8	78.4
5000	77.9	78.3	77.9
E1	72.9	73.8	75.7
E2	74.3	77.9	78.3

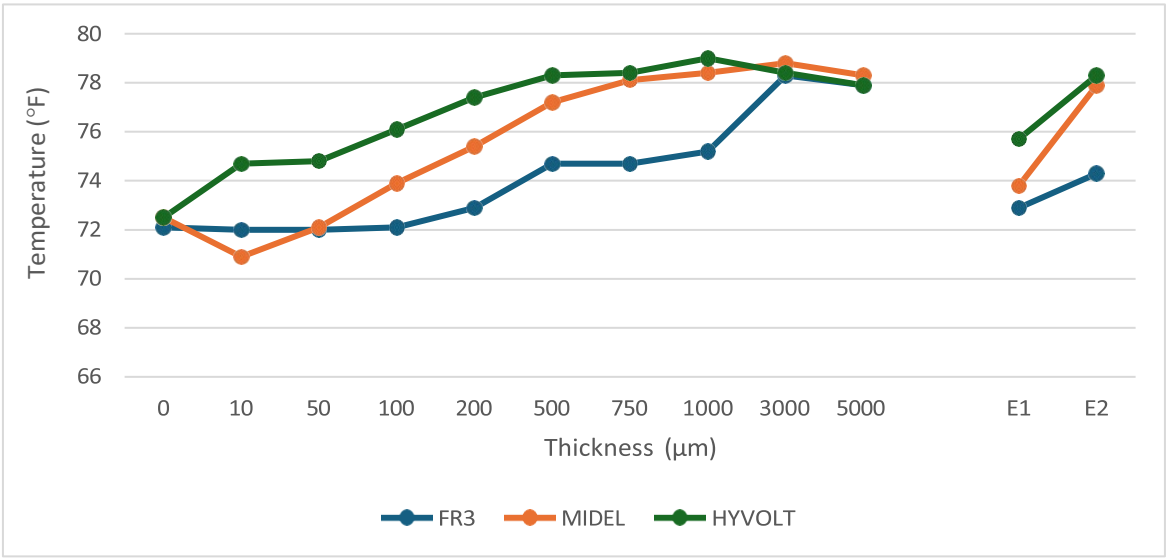

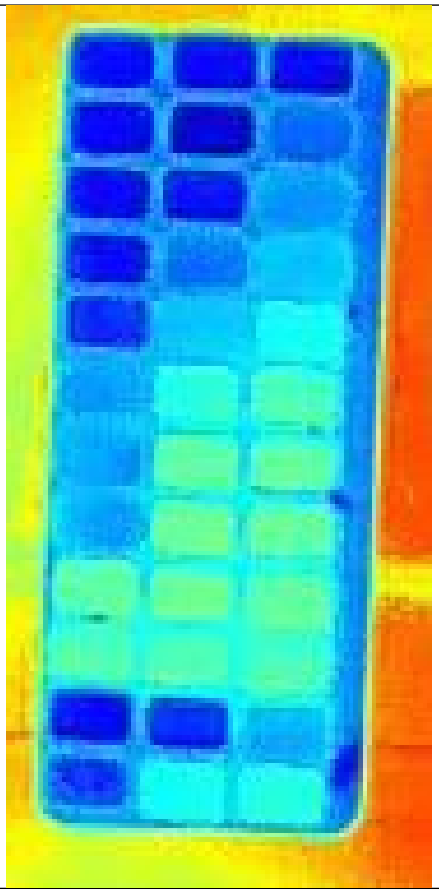

Image	DJI_20240814181117_0001_T		
Time	18:11:17		
Water Temp	73°F		
	FR3 (°F)	MIDEL (°F)	HYVOLT (°F)
0	73	73	72.9
10	72.9	71.6	75.6
50	73	73.6	76.6
100	73	75.6	77.5
200	73.9	77.5	79.3
500	76.6	79.7	80.6
750	76.6	81	81
1000	76.5	81	81
3000	80.8	81.1	81
5000	80.6	80.6	80.6
E1	73	74.3	77.2
E2	73.9	79.3	79.9

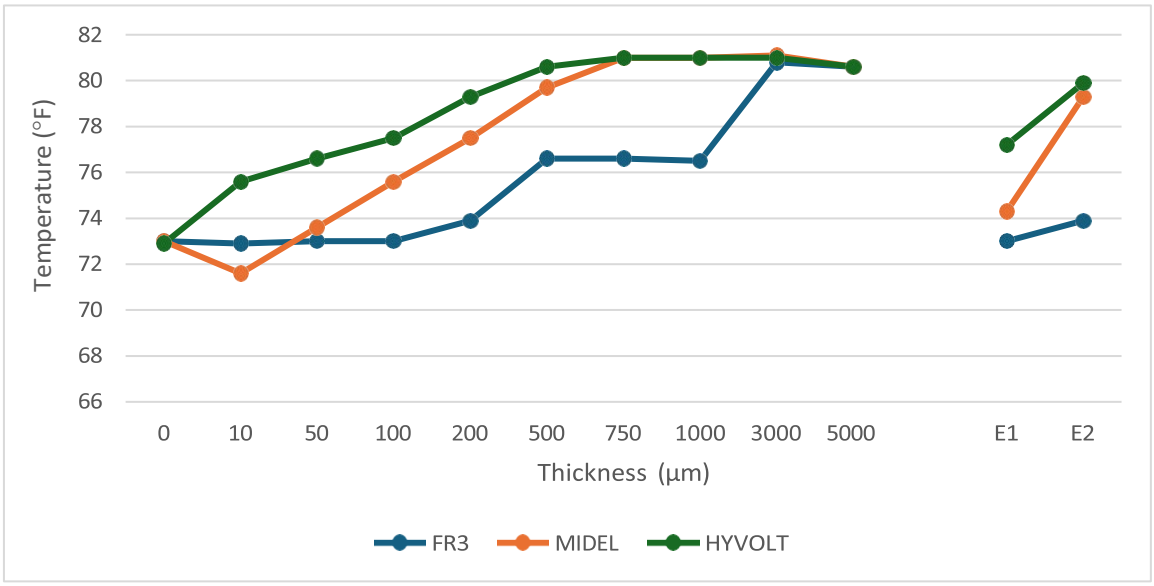

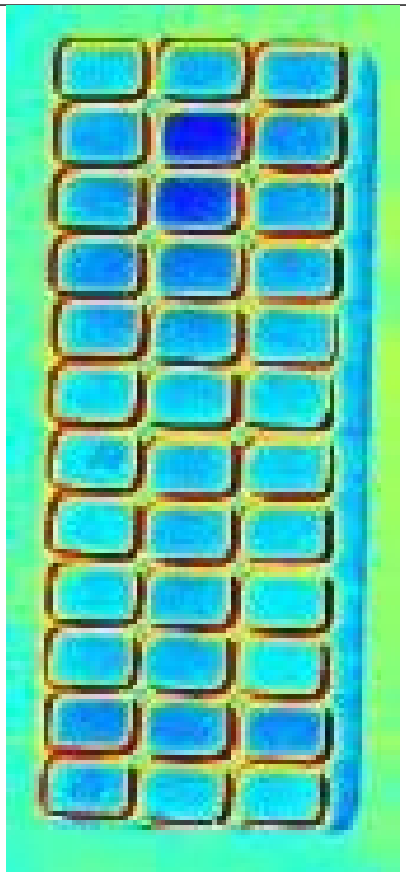

Image	DJI_20240815074743_0002_T		
Time	07:47:43		
Water Temp	78°F		
	FR3 (°F)	MIDEL (°F)	HYVOLT (°F)
0	78.3	77.9	78.1
10	77.4	74.8	77.4
50	77.4	75.6	78.3
100	77	76.6	78.1
200	78.1	77.4	78.3
500	78.4	78.8	78.4
750	78.1	78.3	78.4
1000	79	78.3	78.8
3000	78.4	78.3	78.8
5000	78.3	78.1	79.2
E1	77	77.4	77.5
E2	77.5	78.4	79.2

Temperature Vs Thickness (Water @ 78°F)

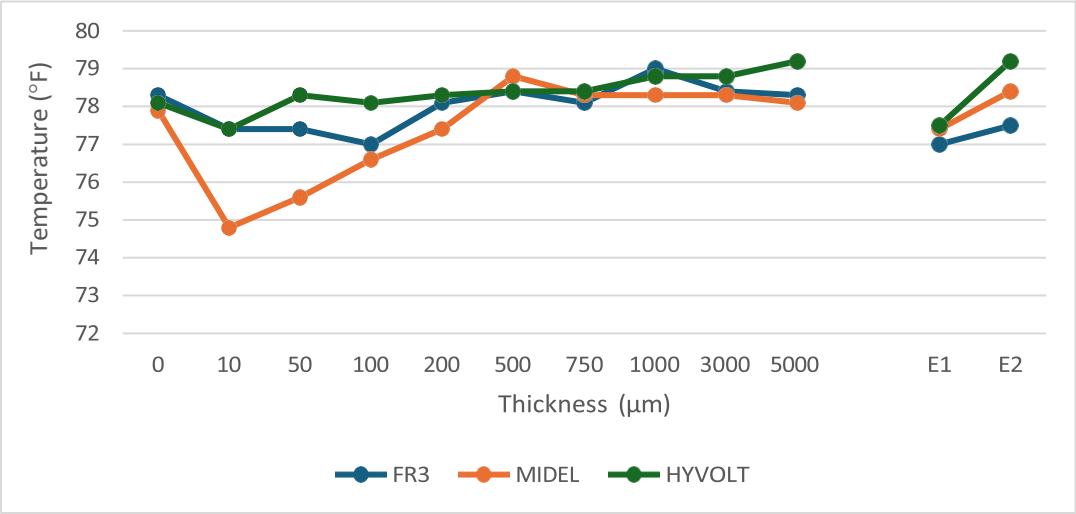

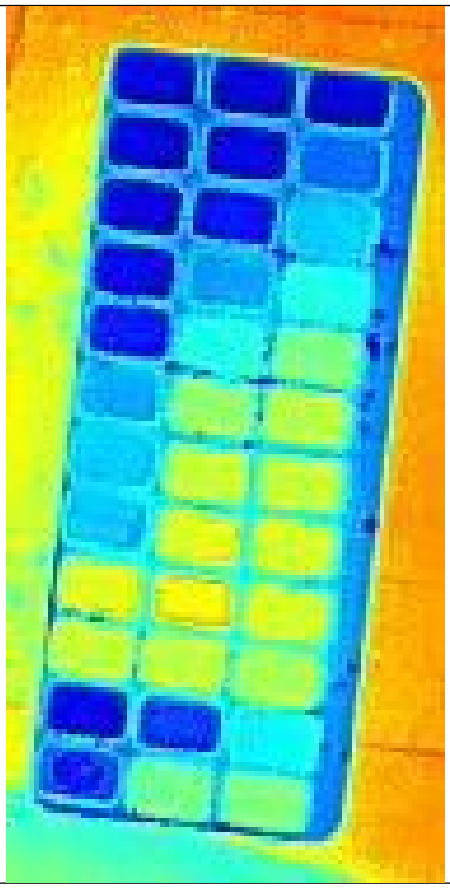

Image	DJI_20240814170231_0002_T		
Time	17:02:31		
Water Temp	76°F		
	FR3 (°F)	MIDEL (°F)	HYVOLT (°F)
0	76.5	76.3	76.5
10	76.1	76.5	81
50	76.5	78.3	83.8
100	76.6	82.4	86
200	78.1	85.5	88.2
500	81.9	88.9	89.8
750	83.3	90	90
1000	83.3	90.9	90.1
3000	90.9	91.6	90.1
5000	89.6	89.8	89.1
E1	76.5	79.7	84.6
E2	78.4	88.2	88.2

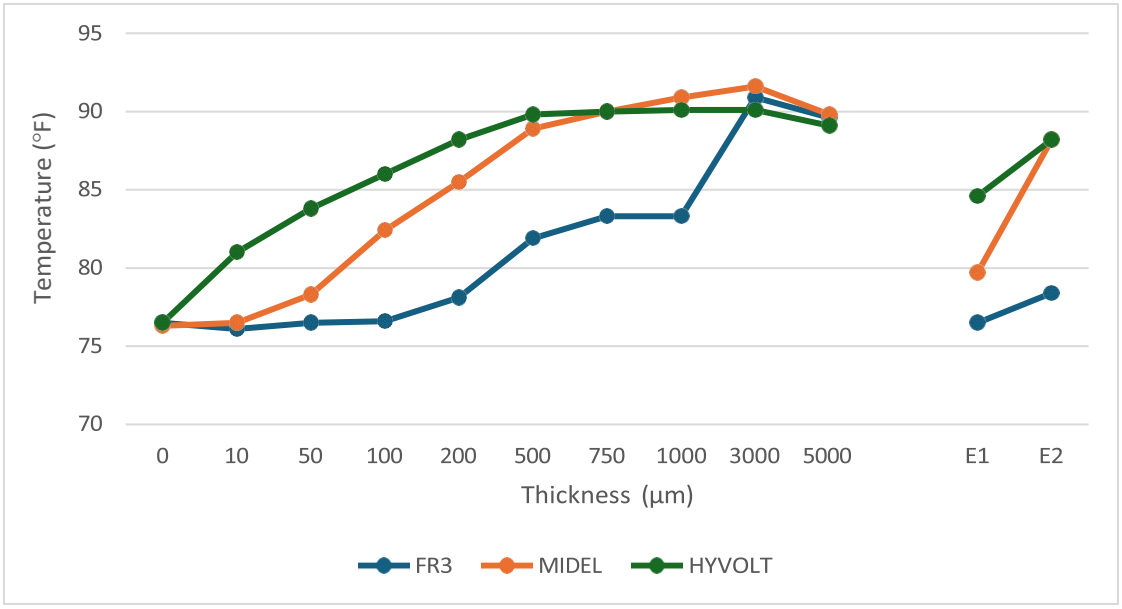

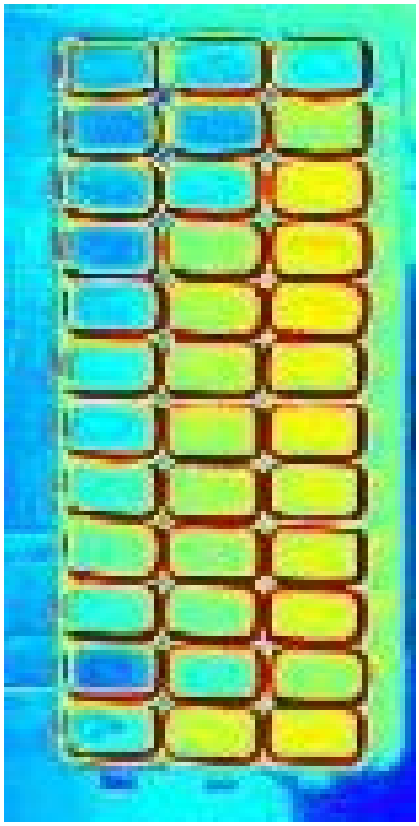

Image	DJI_20240815094311_0002_T		
Time	09:43:11		
Water Temp	89°F		
	FR3 (°F)	MIDEL (°F)	HYVOLT (°F)
0	88.2	88.7	89.6
10	87.1	87.4	94.5
50	88	89.2	97.3
100	87.1	94.3	98.8
200	89.1	95.4	98.6
500	90	95.9	97.9
750	90	95.4	97.9
1000	91.4	95.2	97.2
3000	92.5	93.7	97
5000	90.9	92.8	96.8
E1	86.4	90.9	94.1
E2	88.9	95.2	97.3
E3	91.8	94.5	97

Temperature Vs Thickness (Water @ 89°F)

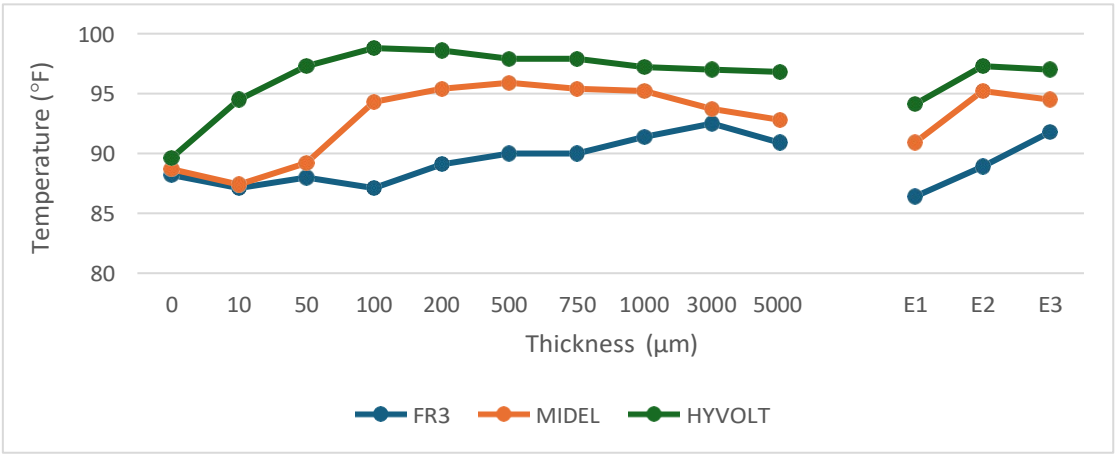

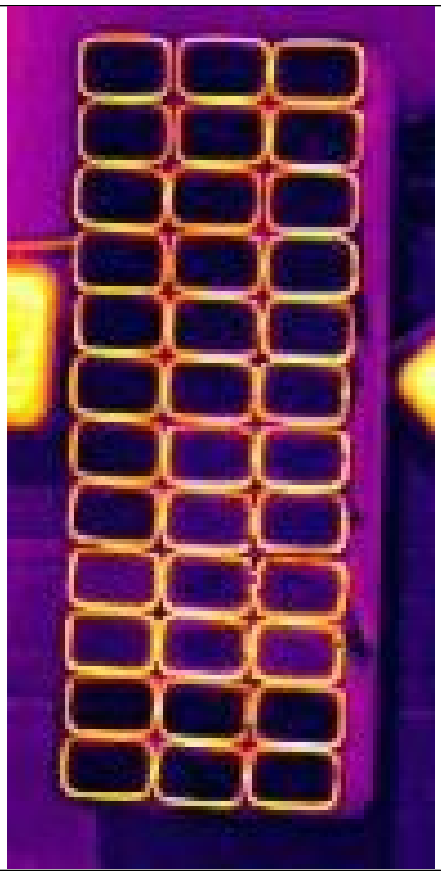

Image	DJI_20240814234719_0004_T		
Time	23:47:19		
Water Temp	87°F		
	FR3 (°F)	MIDEL (°F)	HYVOLT (°F)
0	87.1	87.3	88.2
10	87.1	87.3	87.3
50	87.3	87.3	88.2
100	87.4	88.3	88.7
200	87.8	90.1	91.9
500	89.2	91.8	93.4
750	90	95.9	95.4
1000	91.8	97	95.2
3000	98.8	95.2	97.2
5000	96.4	95.4	98.8
E1	86.9	87.3	87.1
E2	86.9	86.4	87.3

Temperature Vs Thickness (Water @ 87°F)

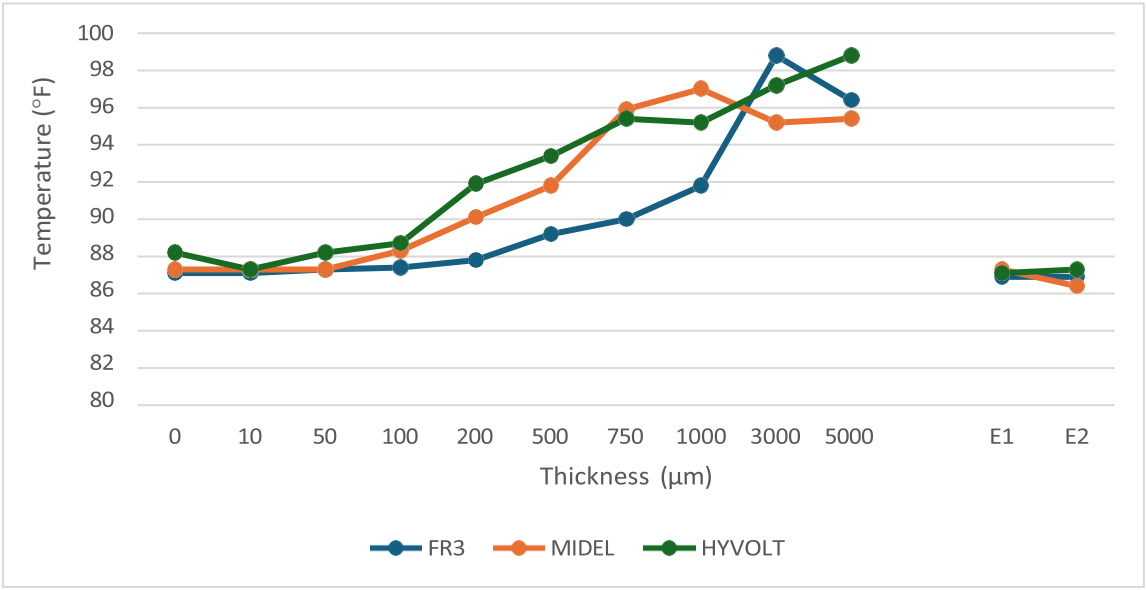

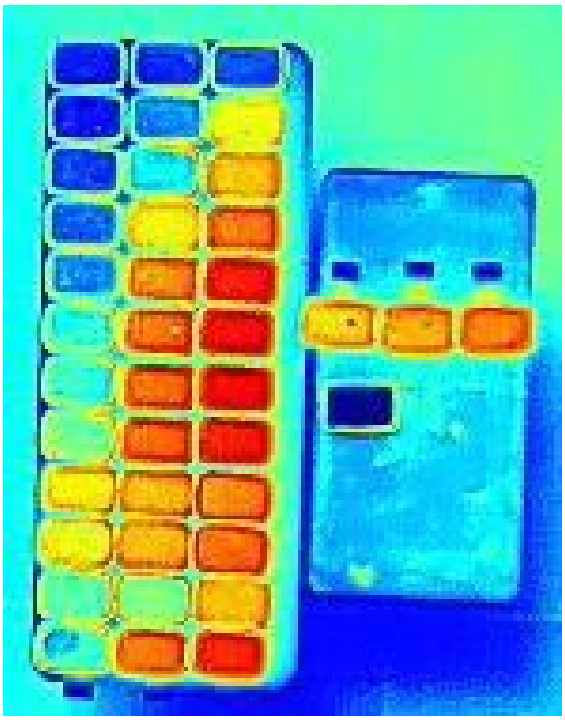

Image	DJI_20240815112231_0002_T		
Time	11:22:31		
Water Temp	93°F		
	FR3 (°F)	MIDEL (°F)	HYVOLT (°F)
0	92.8	93.4	95
10	92.7	96.8	108
50	94.3	99.7	114.3
100	95.4	111.4	118.8
200	96.8	117.5	122.5
500	101.5	119.5	123.3
750	102.6	119.5	124.2
1000	104.2	120.2	123.3
3000	114.1	116.8	118.8
5000	112.6	116.8	119.7
E1	104	105.8	116.1
E2	101.7	119.3	122.4
E3	113.5	115.2	116.2

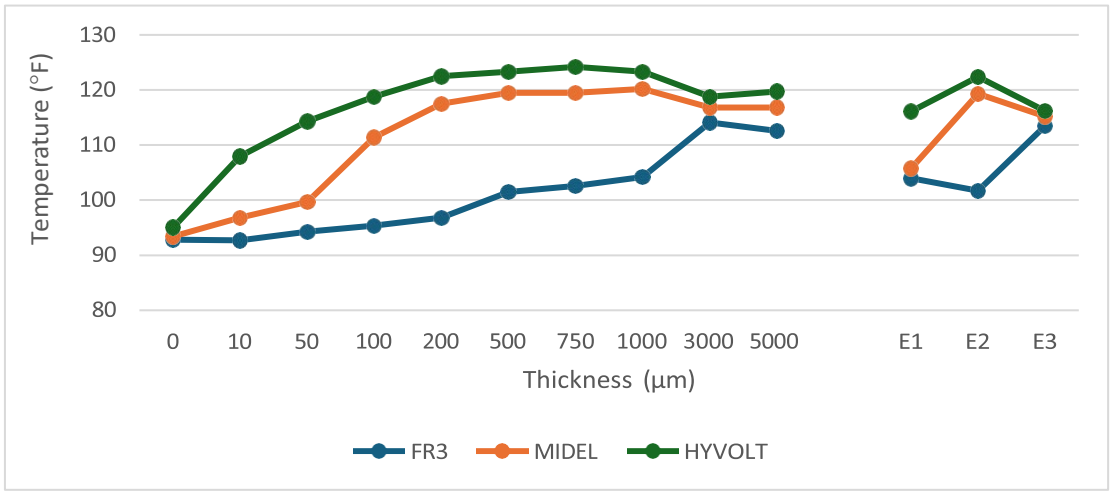

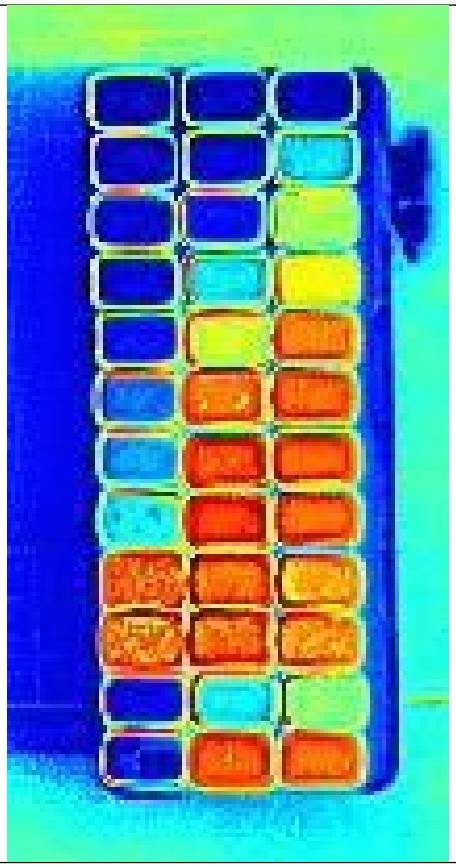

Image	DJI_20240814141329_0002_T		
Time	14:13:29		
Water Temp	97°F		
	FR3 (°F)	MIDEL (°F)	HYVOLT (°F)
0	98.8	97.7	97.7
10	99.1	100	112.3
50	99.9	103.1	118.6
100	100.8	112.3	121.1
200	102.7	120.7	127.4
500	107.8	128.8	130.5
750	109.6	134.6	131.9
1000	112.5	136.8	131.2
3000	133	133.2	127
5000	131.2	133.2	127.8
E1	101.8	113.5	118.6
E2	101.3	133.3	131.4

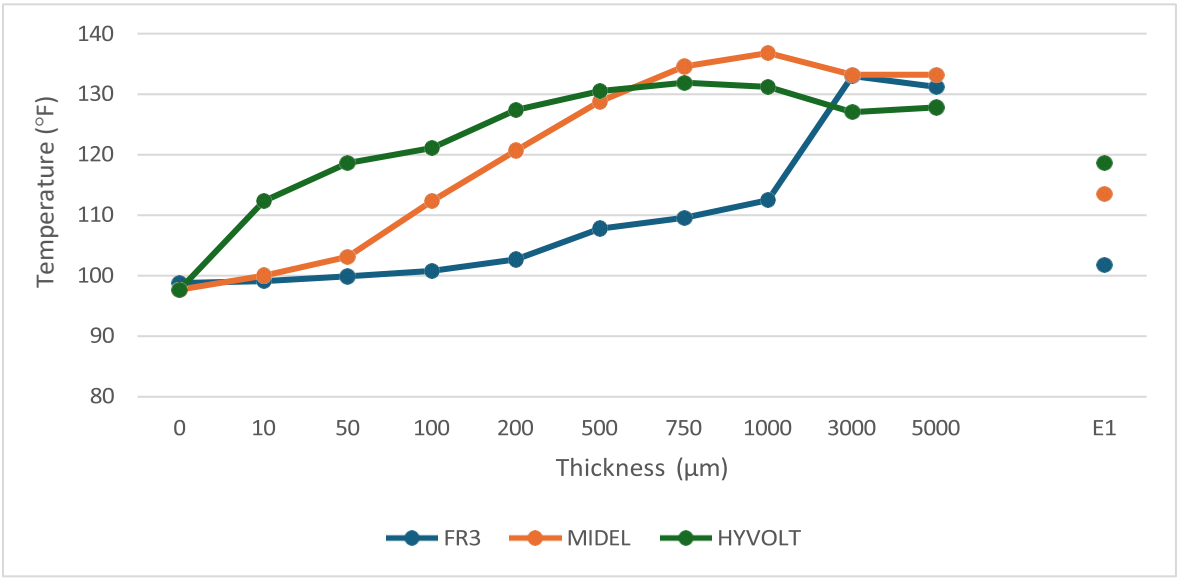

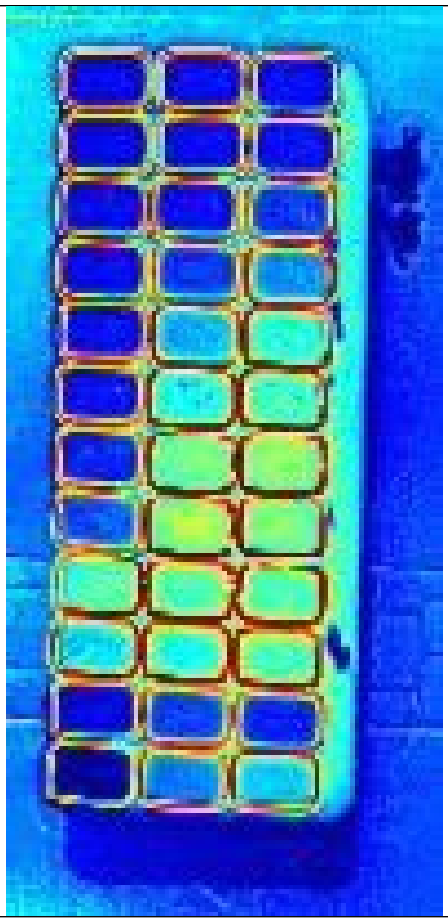

Image	DJI_20240815001052_0005_T		
Time	00:10:52		
Water Temp	102°F		
	FR3 (°F)	MIDEL (°F)	HYVOLT (°F)
0	101.7	102.2	102.2
10	101.7	101.7	102.6
50	101.8	102.6	106.2
100	102.2	106.3	109.8
200	103.1	111.2	114.3
500	104.2	113.9	115.7
750	105.3	117.7	118.4
1000	108.5	119.5	117.5
3000	116.1	116.1	115.9
5000	112.5	113.9	115.3
E1	100	107.1	104.4
E2	93.6	109.4	111.6

Temperature Vs Thickness (Water @ 102°F)

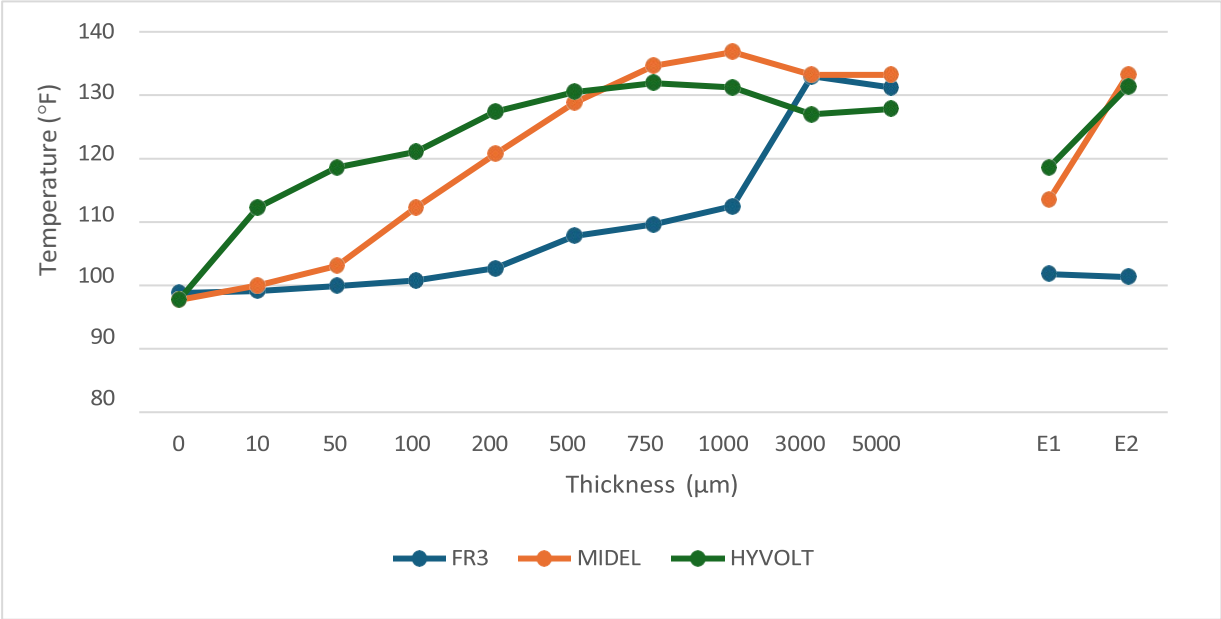

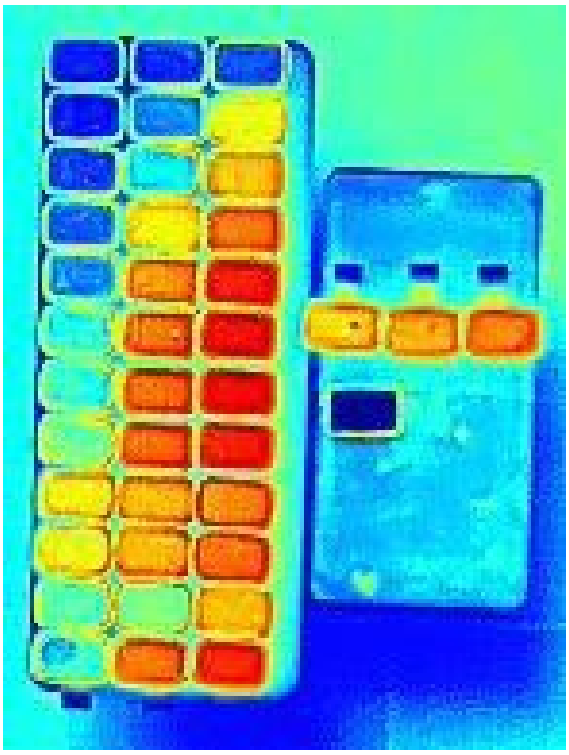

Image	DJI_20240815124010_0001_T		
Time	12:40:10		
Water Temp	102°F		
	FR3 (°F)	MIDEL (°F)	HYVOLT (°F)
0	101.7	101.7	103.3
10	101.3	103.5	115.7
50	104.4	108.9	123.8
100	105.3	123.4	129.6
200	107.1	133.2	136.8
500	115	135.1	140
750	114.1	136.8	141.1
1000	117	137.8	140.4
3000	129.6	134.1	136.9
5000	128.8	135	137.7
E1	114.4	115.9	127.4
E2	124.3	135.7	138.6
E3	126.5	129.7	130.5

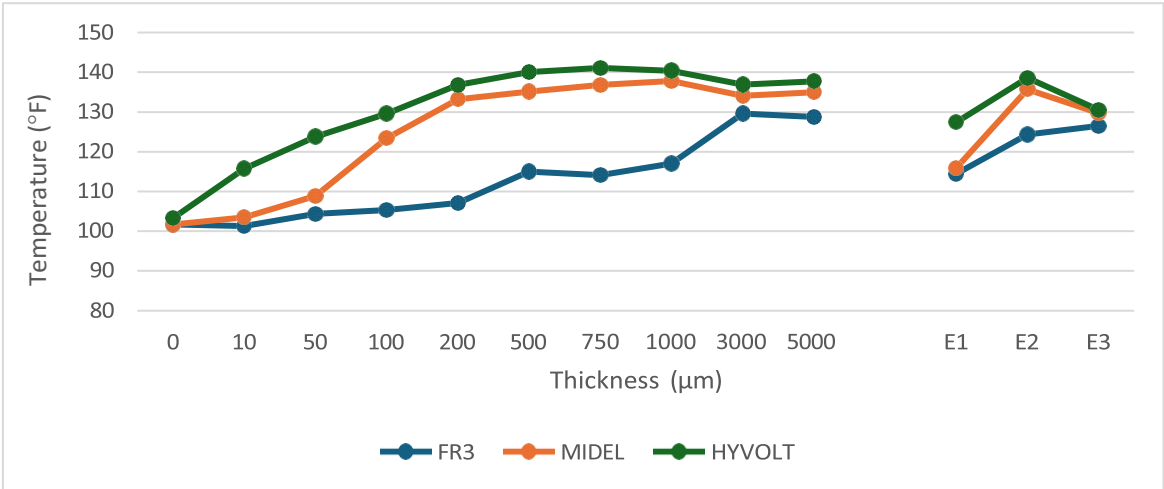

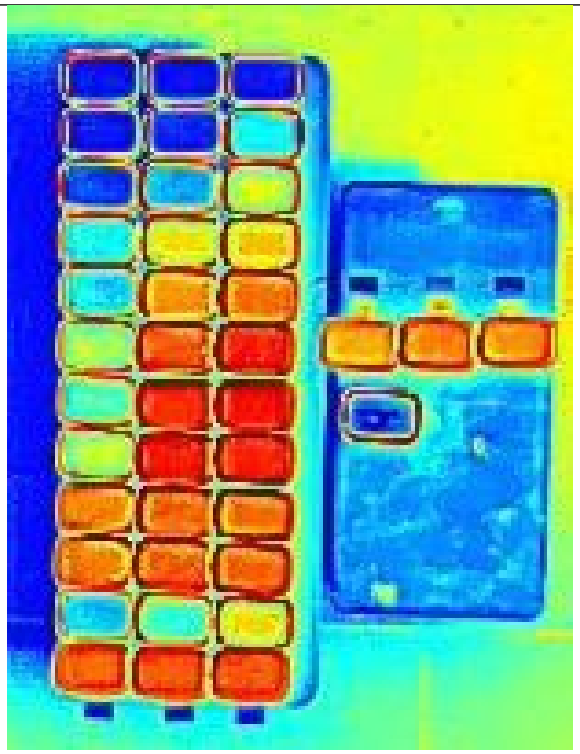

Image	DJI_20240815143156_0001_T		
Time	14:31:56		
Water Temp	102°F		
	FR3 (°F)	MIDEL (°F)	HYVOLT (°F)
0	102.6	102.6	100.9
10	102.7	103.6	112.6
50	105.3	109.8	121.5
100	133.4	126	128.5
200	111.6	135.7	138.4
500	119.3	141.3	143.8
750	117	143.6	144.9
1000	121.1	145	144.1
3000	137.8	140.9	139.5
5000	138.6	141.1	140.4
E1	111.2	115.3	126.5
E2	139.5	104.9	140.2
E3	130.3	134.1	131.9

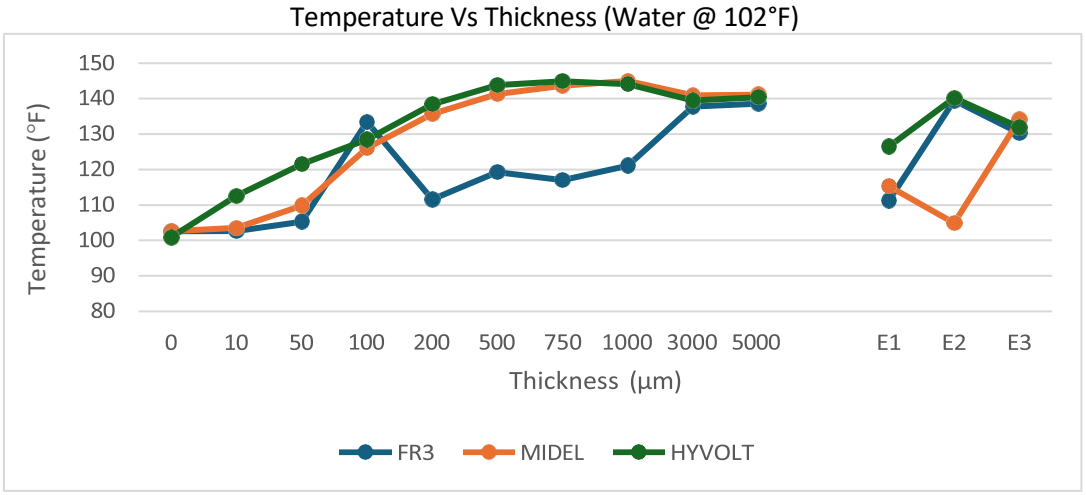

22. Appendix C: Thermal Imagery

Image Name: 20240919_095701_R

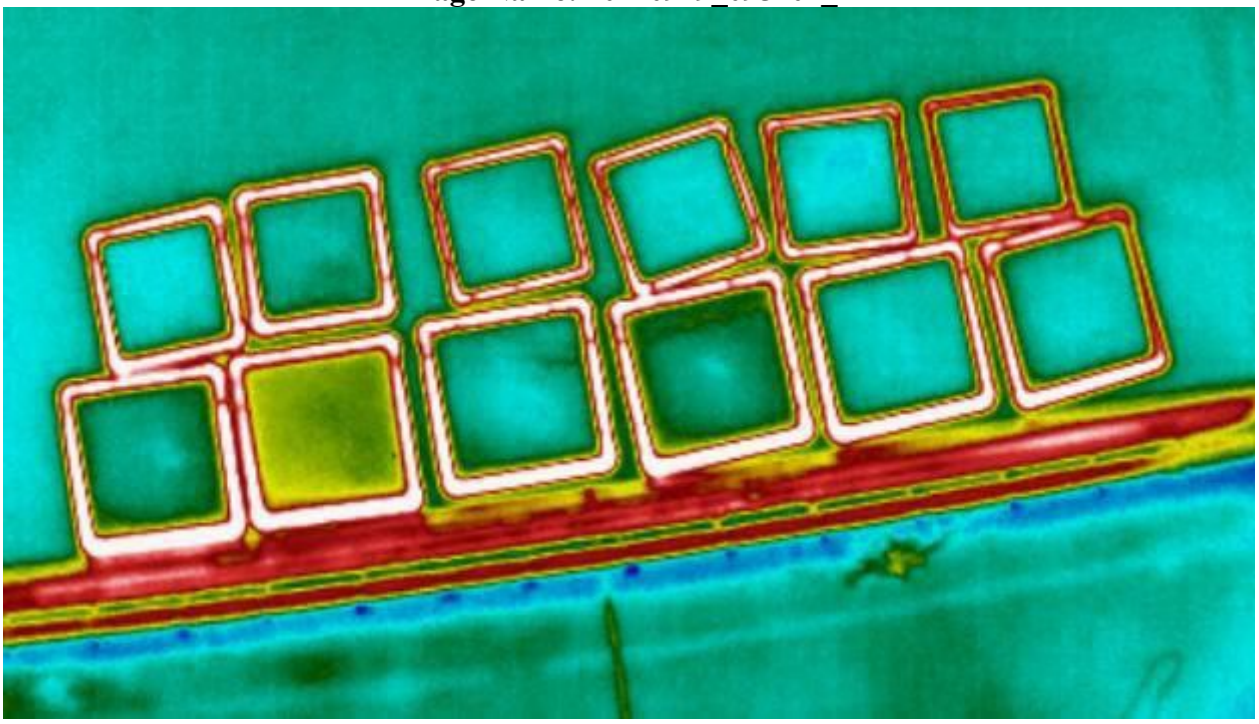

	Thickness (µm)	MAX (°C)	MIN (°C)	AVG (°C)
FR3	50	23.8	22	22.6
FR3	200	23.5	22.7	23
FR3	500	23.6	22.5	22.9
FR3	1000	24	22.4	22.9

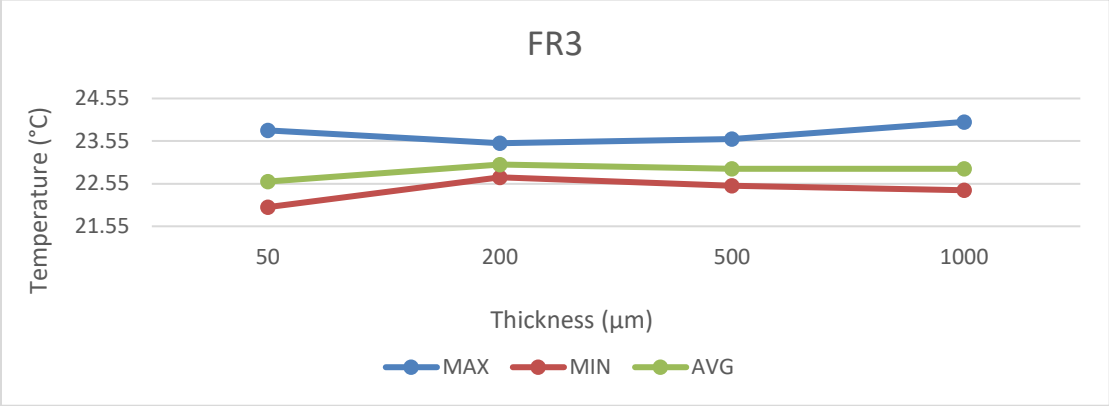

	Thickness (µm)	MAX (°C)	MIN (°C)	AVG (°C)
MIDEL	50	23.6	22.5	23
MIDEL	200	23.5	22.3	22.7
MIDEL	500	24.3	22.4	23.1
MIDEL	1000	26.1	22.7	23.8

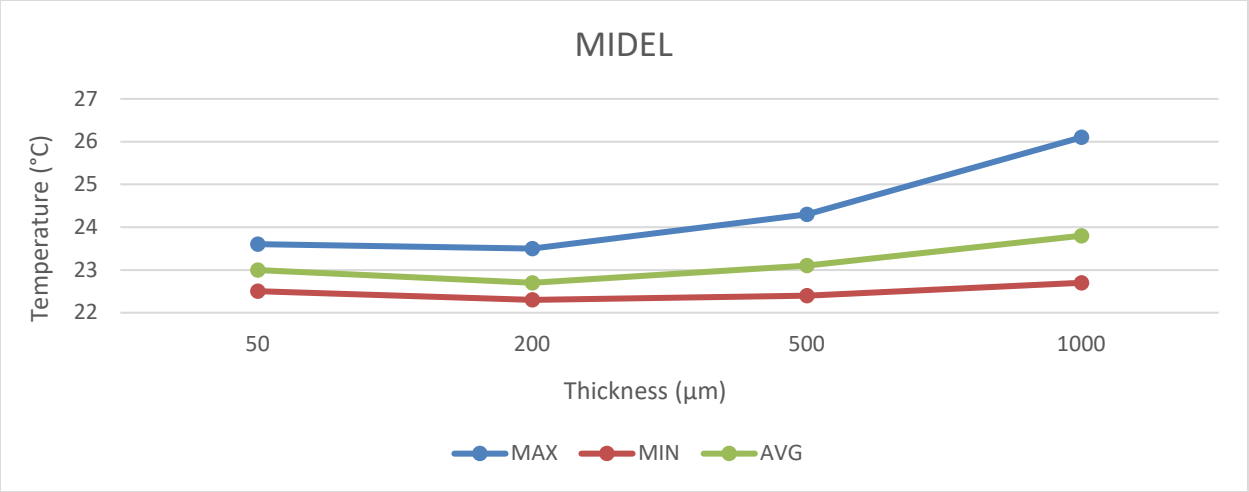

	Thickness (µm)	MAX (°C)	MIN (°C)	AVG (°C)
HYVOLT	50	23.2	22.2	22.6
HYVOLT	200	24	22.8	23.3
HYVOLT	500	24.2	22.8	23.5
HYVOLT	1000	27.7	25.2	25.9

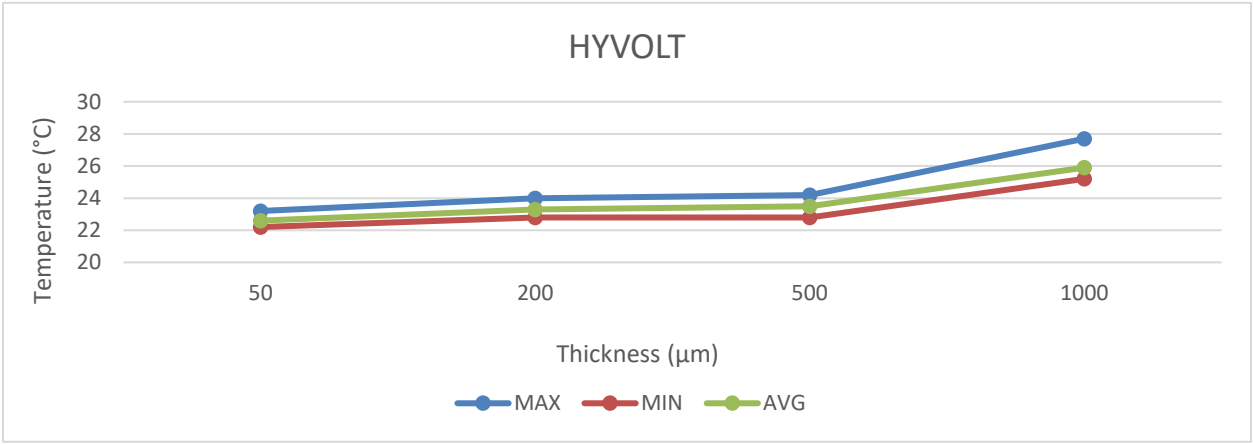

Image Name: 20240919_102009_R

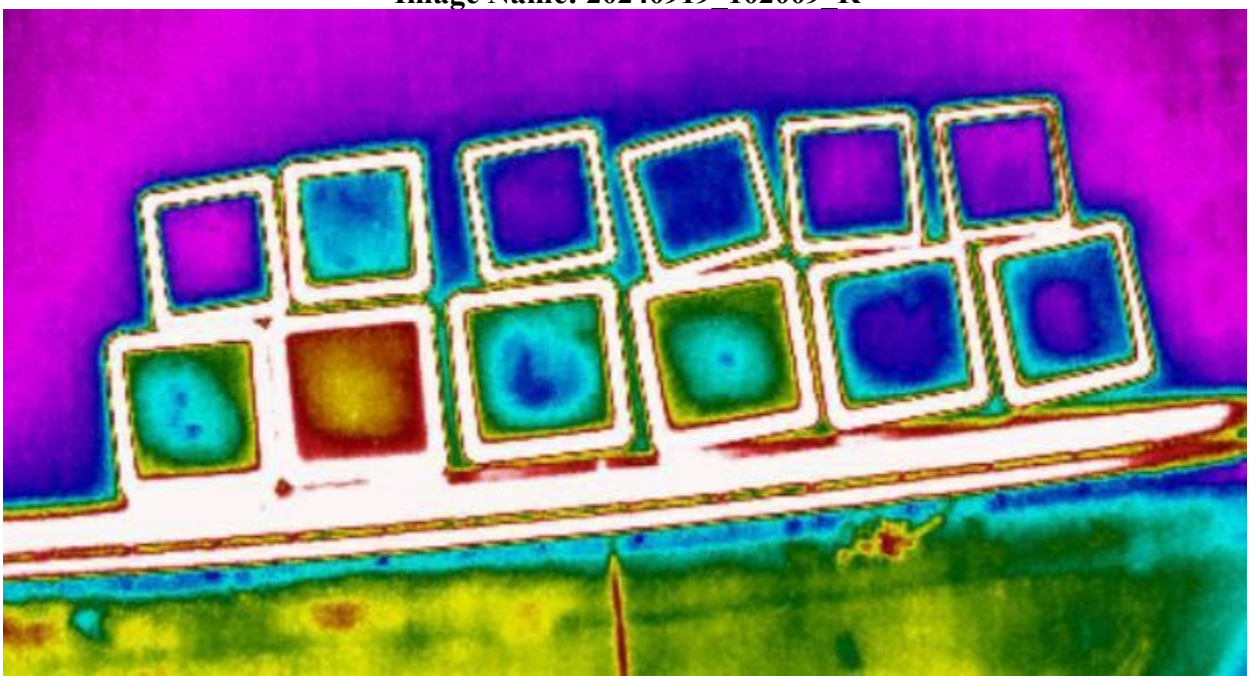

	Thickness (µm)	MAX (°C)	MIN (°C)	AVG (°C)
FR3	50	22.7	21.8	22.2
FR3	200	22.7	21.8	22.2
FR3	500	24.4	22.4	22.9
FR3	1000	24.7	22.1	23

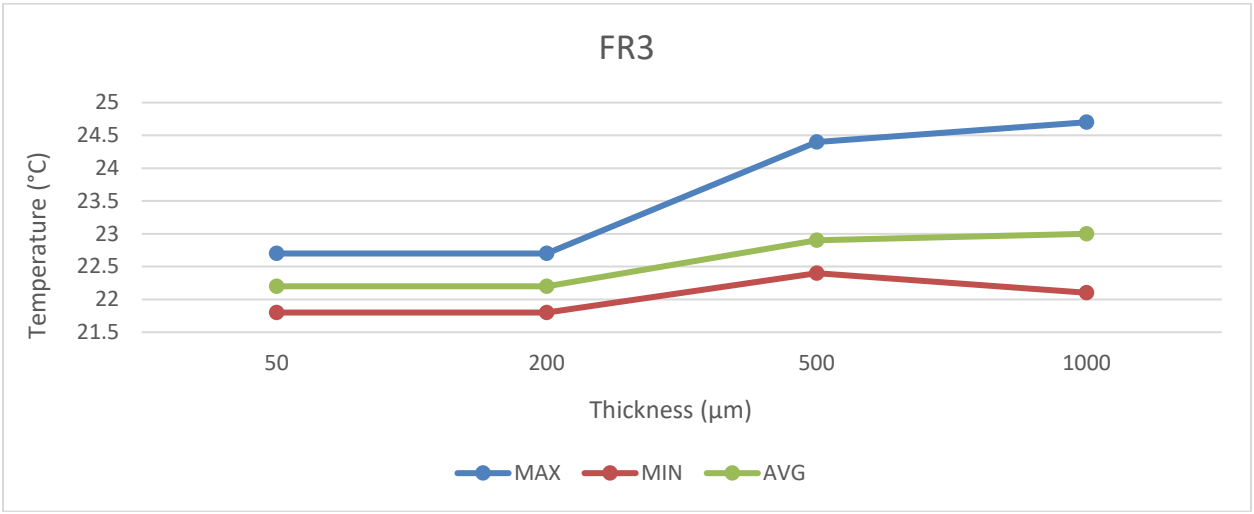

	Thickness (µm)	MAX (°C)	MIN (°C)	AVG (°C)
MIDEL	50	23.3	22.2	22.6
MIDEL	200	23.8	22.7	23
MIDEL	500	25.5	22.8	24.1
MIDEL	1000	26.1	23.6	24.9

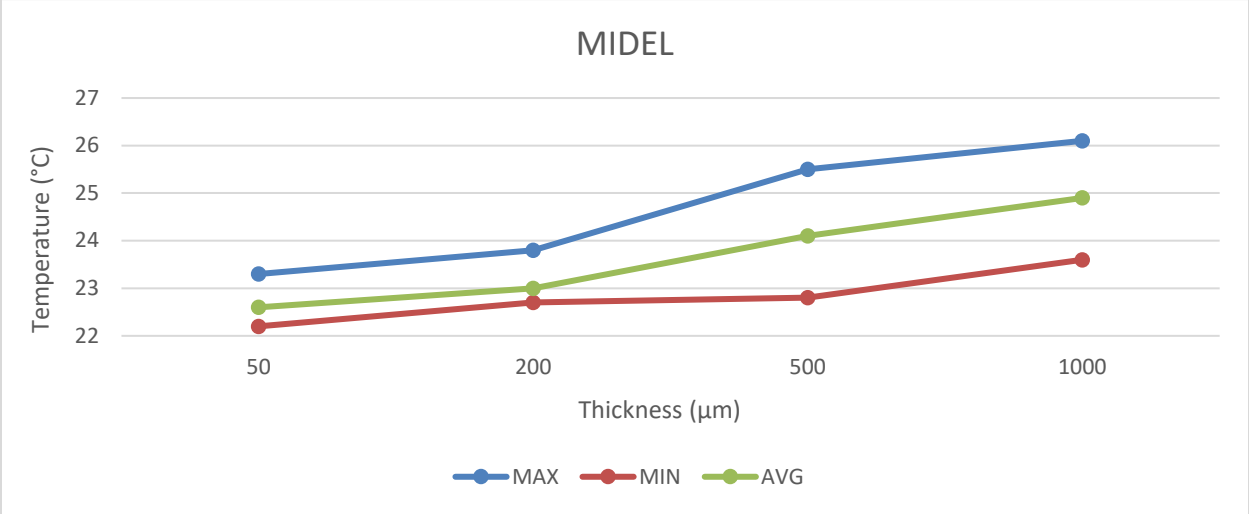

	Thickness (µm)	MAX (°C)	MIN (°C)	AVG (°C)
HYVOLT	50	22.5	20.2	21.9
HYVOLT	200	24.4	23	23.7
HYVOLT	500	26.3	23.1	24.6
HYVOLT	1000	28.7	26.7	27.6

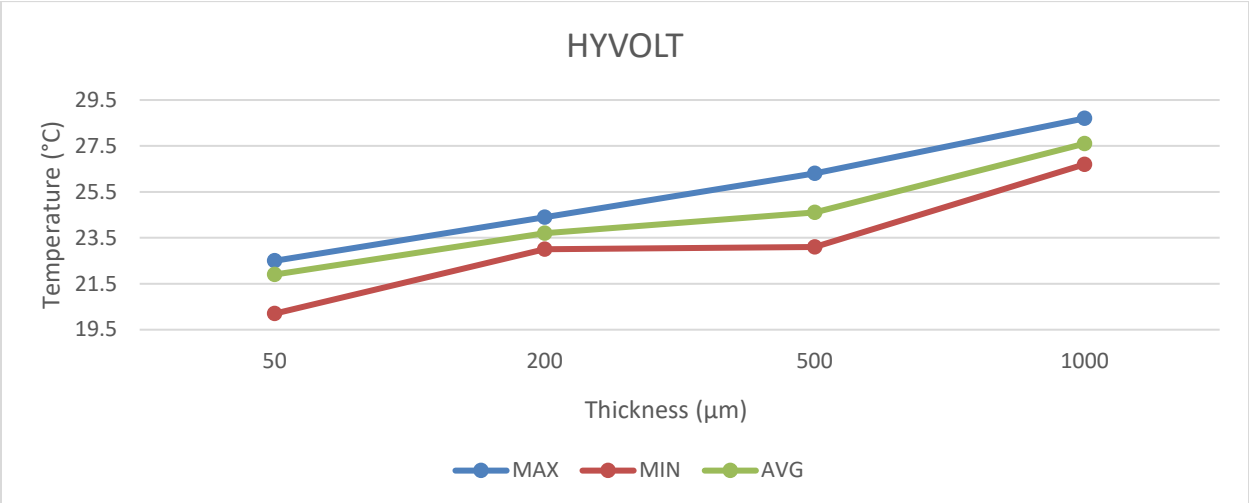

Image Name: 20240919_112009_R

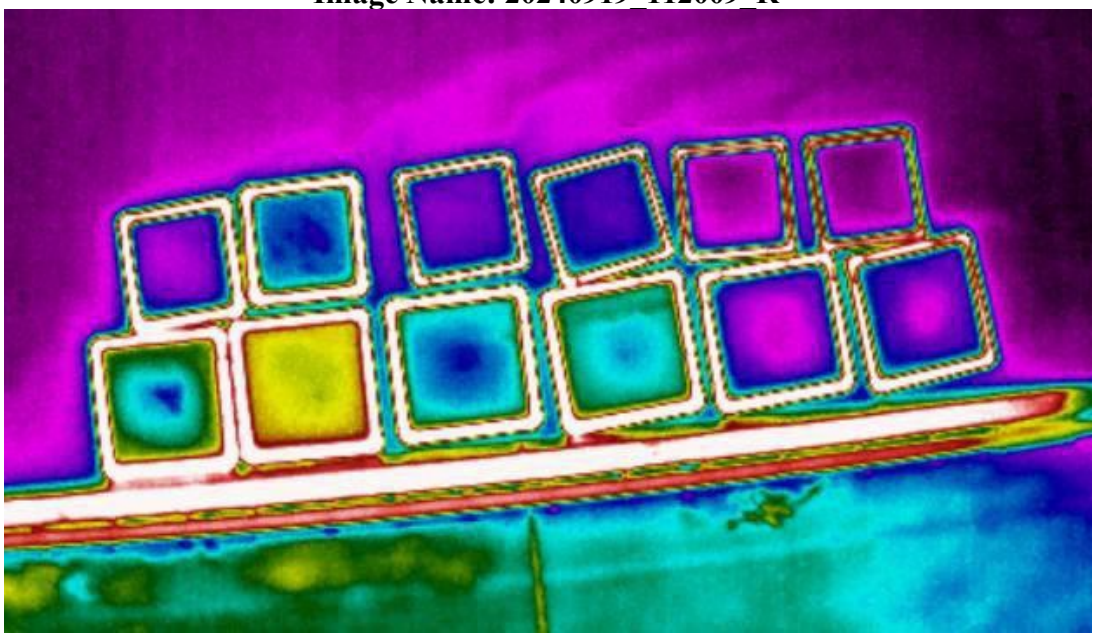

	Thickness (µm)	MAX (°C)	MIN (°C)	AVG (°C)
FR3	50	26.8	25	25.7
FR3	200	26	24.9	25.4
FR3	500	27.9	25.8	26.6
FR3	1000	28.1	25.8	27

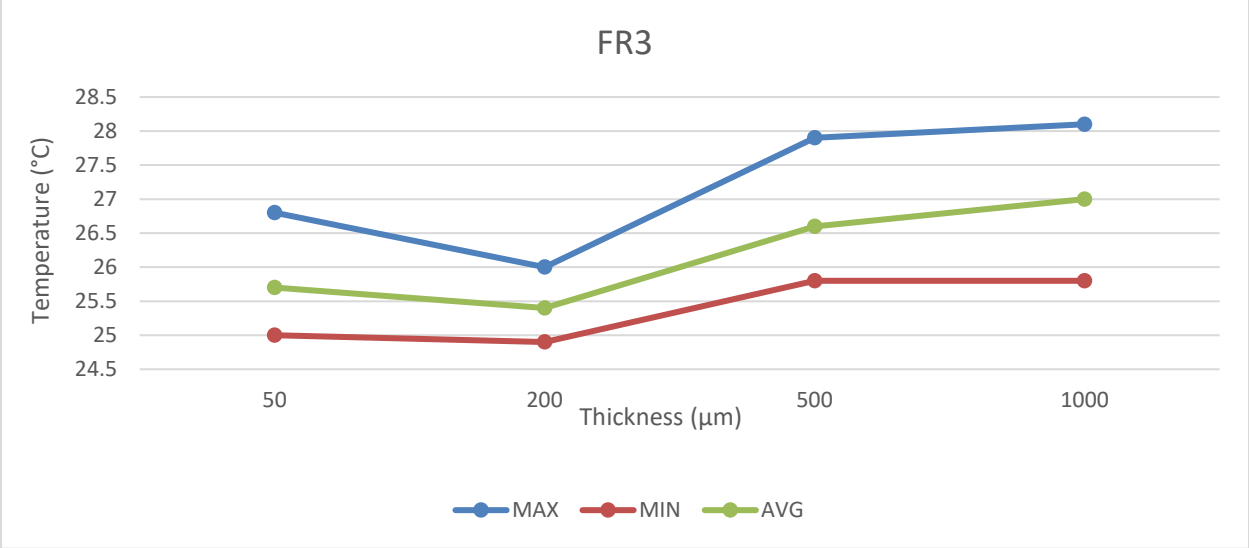

	Thickness (µm)	MAX (°C)	MIN (°C)	AVG (°C)
MIDEL	50	27.8	26.7	27.2
MIDEL	200	28.1	27.1	27.5
MIDEL	500	30.5	27.9	29.1
MIDEL	1000	31.6	28.9	30.1

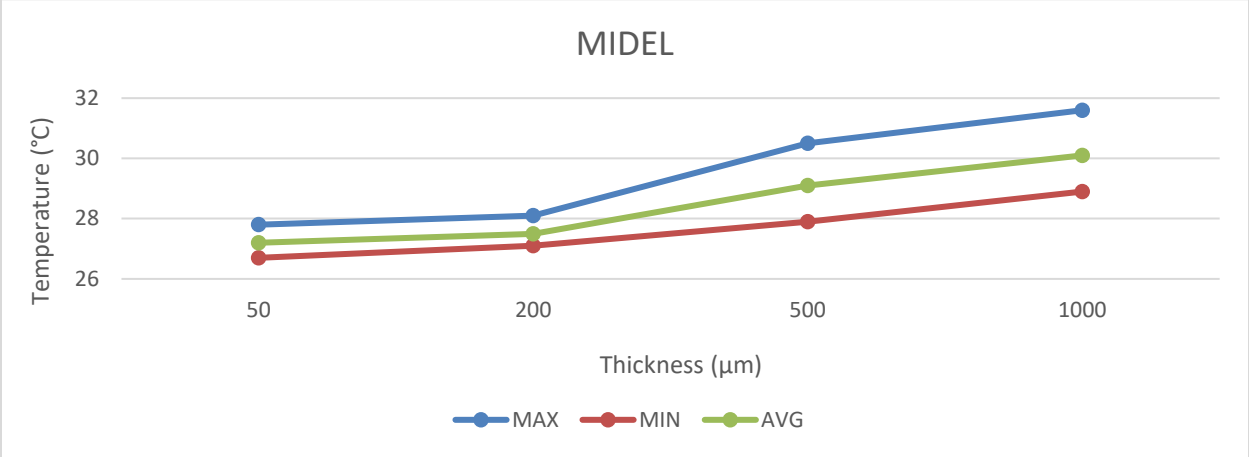

	Thickness (µm)	MAX (°C)	MIN (°C)	AVG (°C)
HYVOLT	50	27.8	26.2	26.8
HYVOLT	200	30.4	27.6	28.6
HYVOLT	500	32.4	27.8	30.4
HYVOLT	1000	34.5	33	33.6

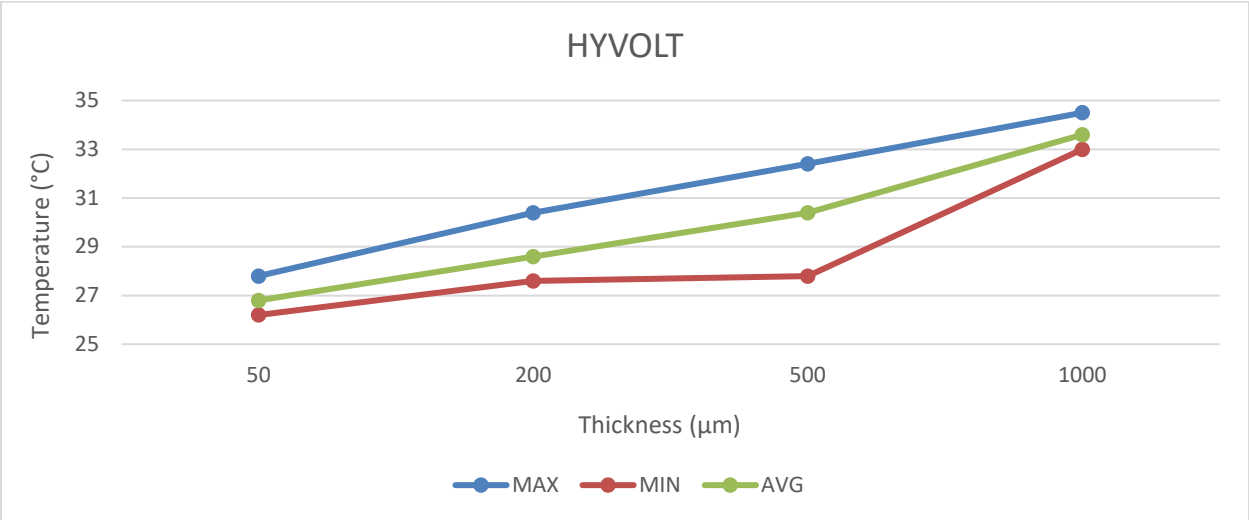

Image Name: 20240919_120209_R

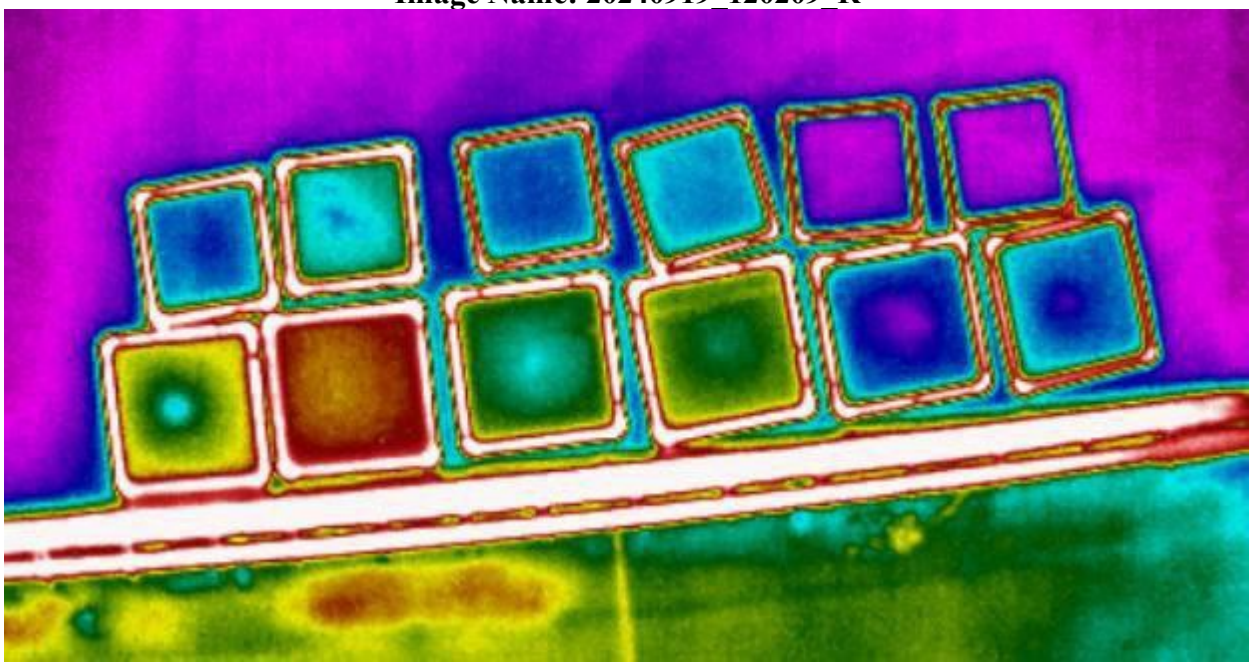

	Thickness (µm)	MAX (°C)	MIN (°C)	AVG (°C)
FR3	50	27.8	27	27.4
FR3	200	27.7	27	27.3
FR3	500	29.2	27.4	28.3
FR3	1000	29.6	27.9	28.8

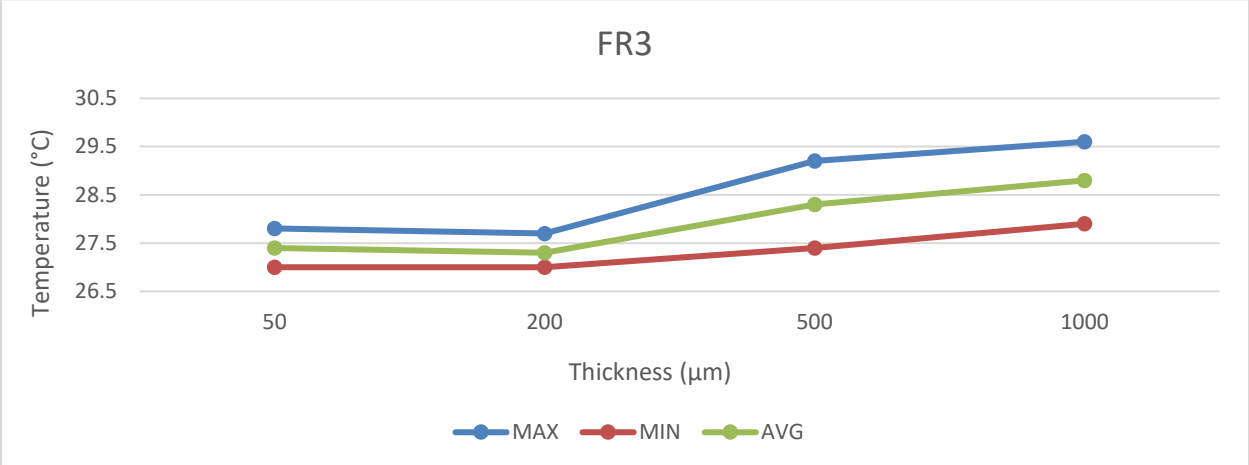

	Thickness (µm)	MAX (°C)	MIN (°C)	AVG (°C)
MIDEL	50	29.7	28.5	28.8
MIDEL	200	29.7	28.9	29.2
MIDEL	500	31.3	29.6	30.5
MIDEL	1000	32.3	30.4	31.1

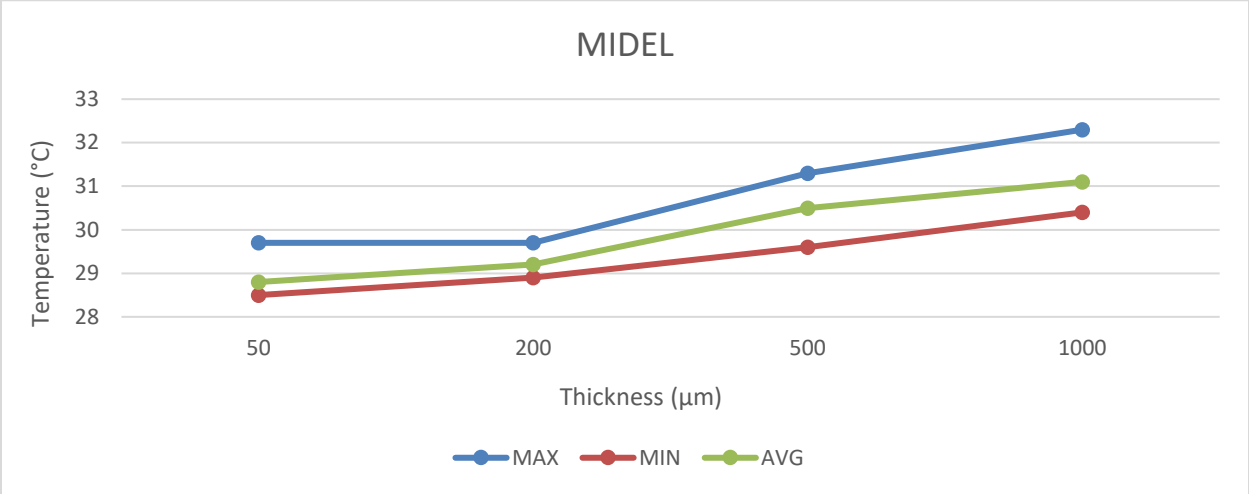

	Thickness (µm)	MAX (°C)	MIN (°C)	AVG (°C)
HYVOLT	50	29.3	27.6	28.8
HYVOLT	200	30.3	29	29.7
HYVOLT	500	32.6	29.4	31.4
HYVOLT	1000	33.8	32.7	33.2

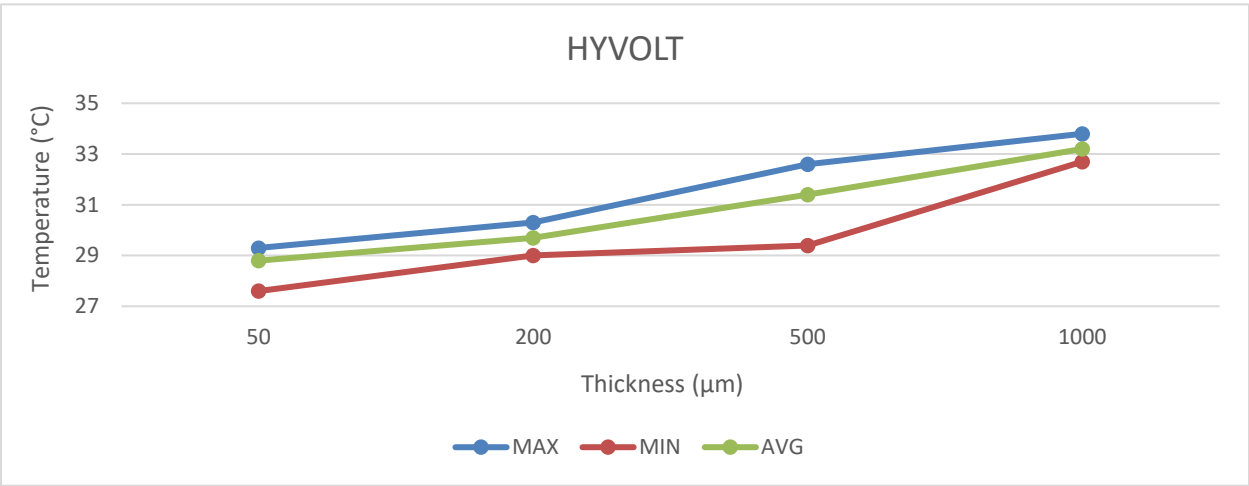

23. Appendix D:

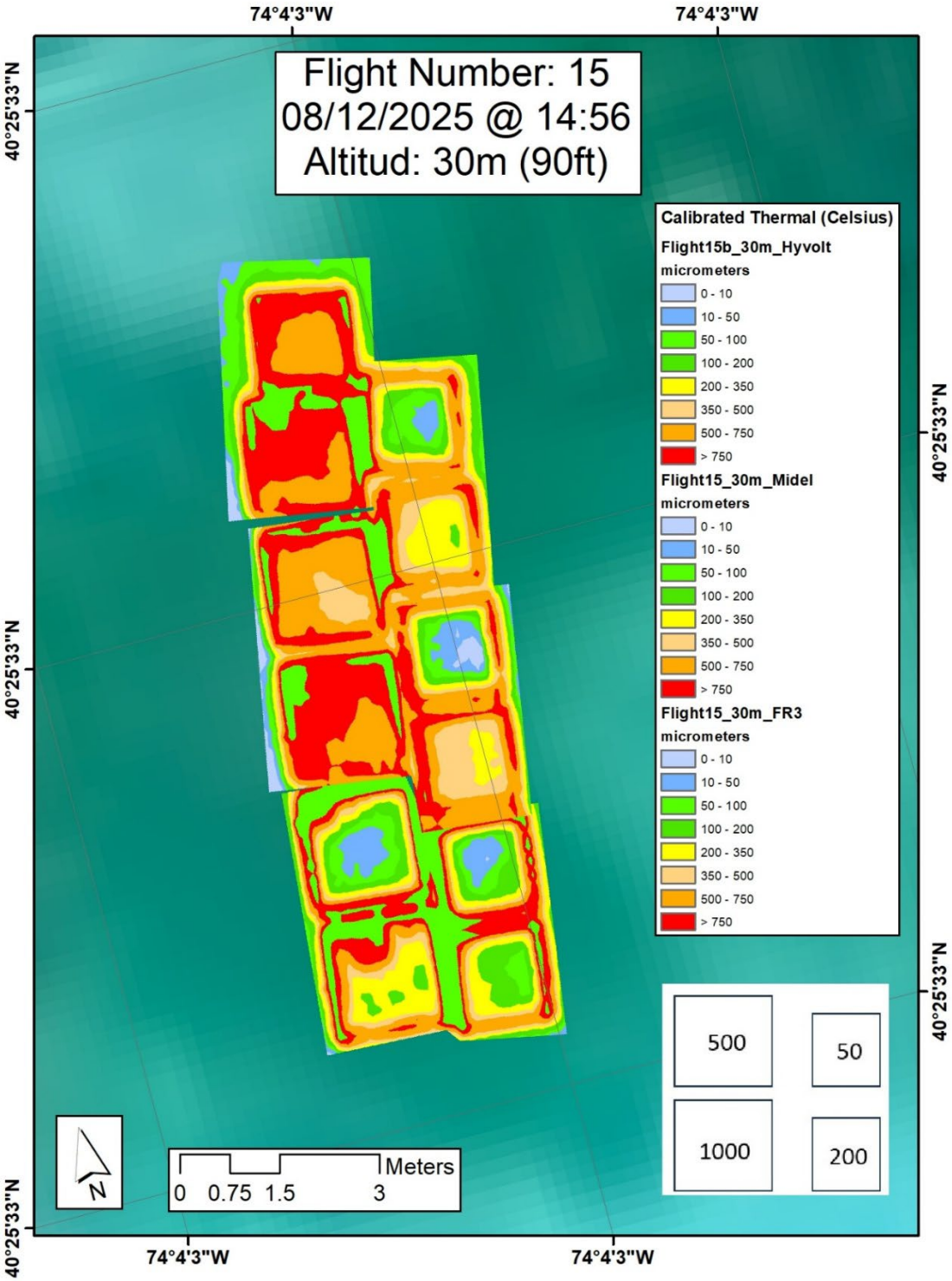

Near real time report generated from the DFs detected on August 12, 2025 at 14:56 hrs.

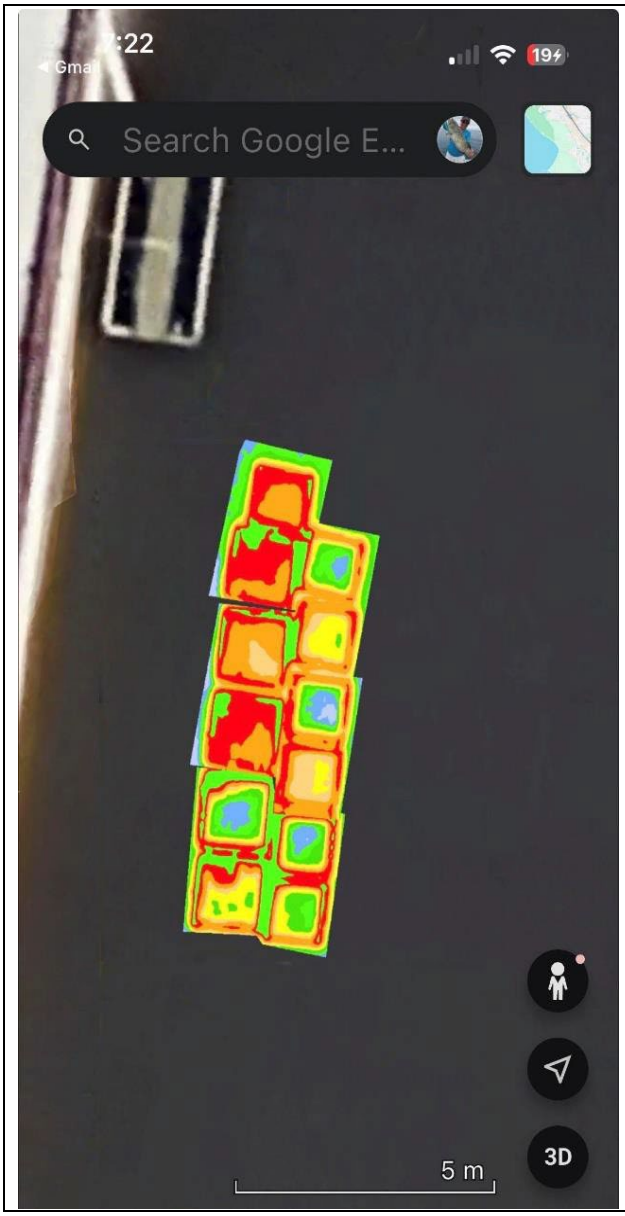

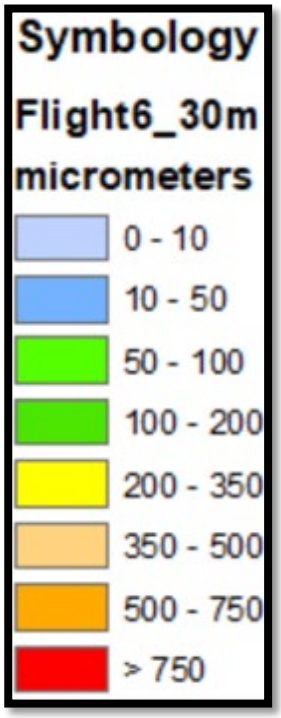

Near real time report generated from the DFs detected on August 12, 2025 at 14:56 hrs. for Google Earth displayed on a mobile device.

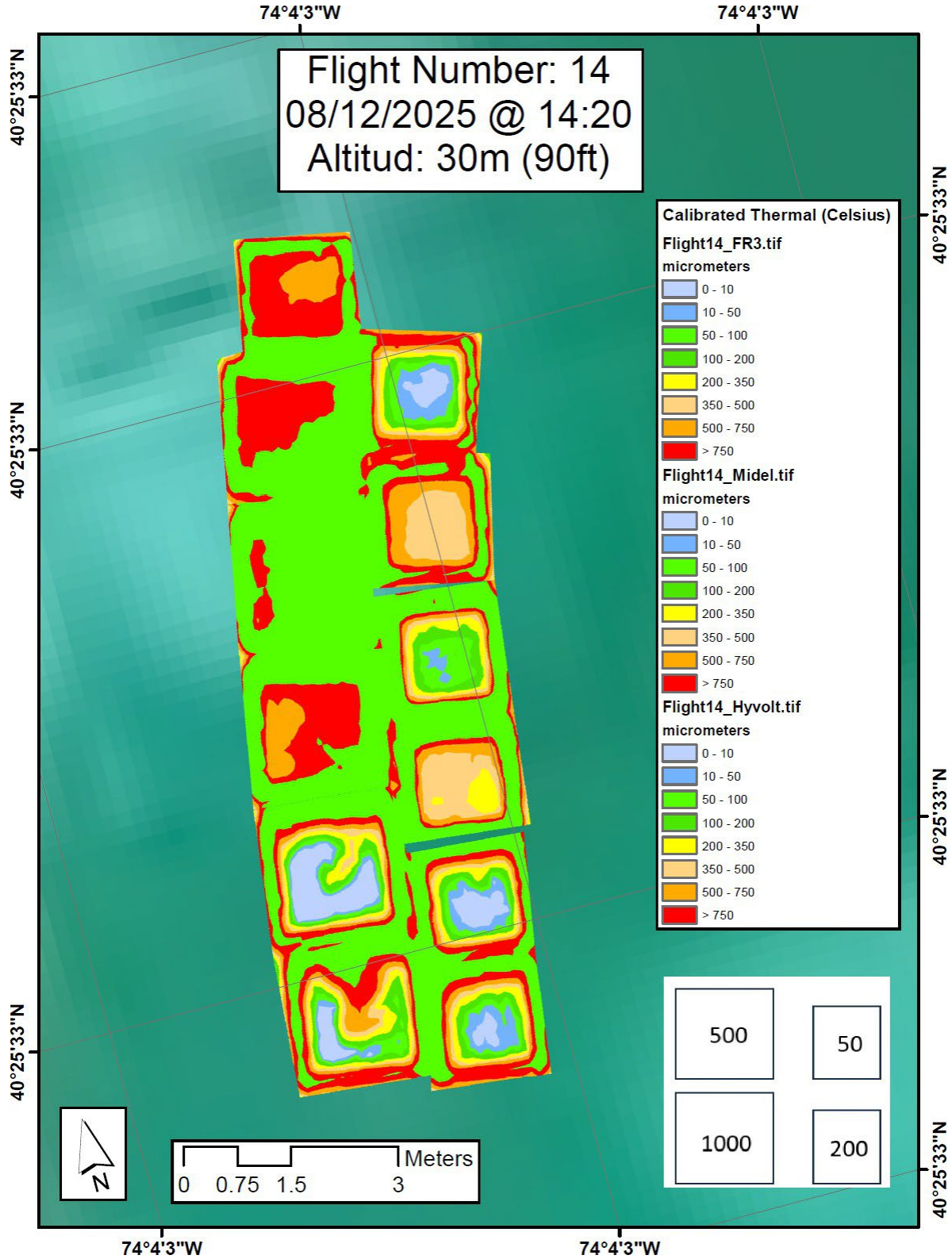

Near real time report generated from the DFs detected on August 12, 2025 at 14:20 hrs.

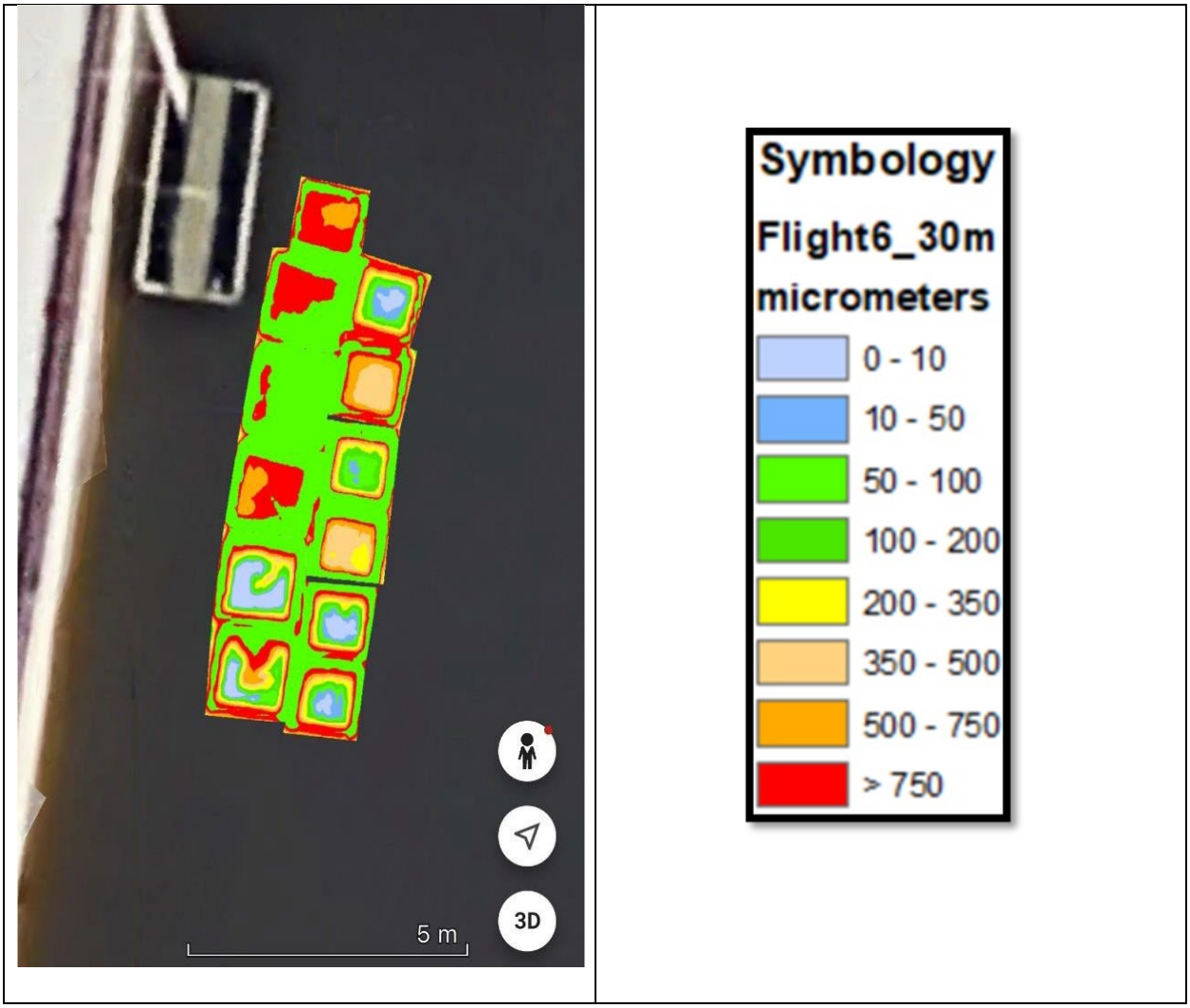

Near real time report generated from the DFs detected on August 12, 2025 at 14:20 for Google Earth displayed on a mobile device.

24. Abbreviations and Acronyms

BOEM	Bureau of Ocean Energy Management
BSEE	Bureau of Safety and Environmental Enforcement
CO	Contracting Officer.
COR	Contracting Officer's Representative
CREEL	The Cold Regions Research and Engineering Laboratory
DF	Dielectric Fluid
DOI	Department of the Interior
ITC	Investment Tax Credit
OHMSETT	Oil and Hazardous Materials Simulated Environmental Test Tank
OSPD	Oil Spill Preparedness Division
OSRR	Oil Spill Response Research
PTC	Production Tax Credit
WM	Water Mapping

Department of the Interior (DOI)
The Department of the Interior protects and manages the Nation's natural resources and cultural heritage; provides scientific and other information about those resources; and honors the Nation's trust responsibilities or special commitments to American Indians, Alaska Natives, and affiliated island communities.

Bureau of Safety and Environmental Enforcement (BSEE)
The mission of the Bureau of Safety and Environmental Enforcement works to promote safety, protect the environment, and conserve resources offshore through vigorous regulatory oversight and enforcement.

BSEE Oil Spill Preparedness Program
BSEE administers a robust Oil Spill Preparedness Program through its Oil Spill Preparedness Division (OSPD) to ensure owners and operators of offshore facilities are ready to mitigate and respond to substantial threats of actual oil spills that may result from their activities. The Program draws its mandate and purpose from the Federal Water Pollution Control Act of October 18, 1972, as amended, and the Oil Pollution Act of 1990 (October 18, 1991). It is framed by the regulations in 30 CFR Part 254 – Oil Spill Response Requirements for Facilities Located Seaward of the Coastline, and 40 CFR Part 300 – National Oil and Hazardous Substances Pollution Contingency Plan. Acknowledging these authorities and their associated responsibilities, BSEE established the program with three primary and interdependent roles:

- Preparedness Verification,
- Oil Spill Response Research, and
- Management of Ohmsett - the National Oil Spill Response Research and Renewable Energy Test Facility.

The research conducted for this Program aims to improve oil spill response and preparedness by advancing the state of the science and the technologies needed for these emergencies. The research supports the Bureau's needs while ensuring the highest level of scientific integrity by adhering to BSEE's peer review protocols. The proposal, selection, research, review, collaboration, production, and dissemination of OSPD's technical reports and studies follows the appropriate requirements and guidance such as the Federal Acquisition Regulation and the Department of Interior's policies on scientific and scholarly conduct.